N-HETEROCYCLIC CARBENE METAL COMPLEXES:

SYNTHESIS, KINETICS, REACTIVITY, AND RECYCLING WITH POLYMERS

A Dissertation

by

HAW-LIH SU

Submitted to the Office of Graduate Studies of
Texas A&M University
in partial fulfillment of the requirements for the degree of

DOCTOR OF PHILOSOPHY

August 2011

Major Subject: Chemistry

N-Heterocyclic Carbene Metal Complexes:

Synthesis, Kinetics, Reactivity, and Recycling with Polymers

N-HETEREOCYCLIC CARBENE METAL COMPLEXES:

SYNTHESIS, KINETICS, REACTIVITY, AND RECYCLING WITH POLYMERS

A Dissertation

by

HAW-LIH SU

Submitted to the Office of Graduate Studies of
Texas A&M University
in partial fulfillment of the requirements for the degree of

DOCTOR OF PHILOSOPHY

Approved by:

Chair of Committee,	David E. Bergbreiter
Committee Members,	Daniel A. Singleton
	Brian T. Connell
	Melissa A. Grunlan
Head of Department,	David H. Russell

August 2011

Major Subject: Chemistry

ABSTRACT

N-Heterocyclic Carbene Metal Complexes:

Synthesis, Kinetics, Reactivity, and Recycling with Polymers.

(August 2011)

Haw-Lih Su, B.S.; M. S., National Tsing Hua University, Taiwan

Chair of Advisory Committee: Dr. David E. Bergbreiter

N-Heterocyclic carbenes (NHCs) are good ligands to most transition metals forming stable complexes. Many of the NHC-metal complexes are now widely used catalysts. However, the usage of these catalysts encounters the general problems associated with homogeneous catalysis: the purification of the catalysis reaction products is often time-consuming and generates large amounts of waste. Moreover, the toxic or expensive catalysts are difficult to be separated, recycled, and reused. Chapters II and III of this dissertation focus on addressing these problems through the development of an easier and "greener" process to improve the usage of some NHC-metal complexes. Polymer-supported catalysts and polymer-supported sequestrants were prepared and used to facilitate the separation/recycling of catalysts and the purification of products. These polymer-supported ligands, catalysts, and sequestrants showed comparable reactivity to their low molecular weight counterparts and had different solubility properties due to the nature of polymers. Using these materials with the corresponding operations provides simple methods to separate deeply colored, metal-

containing by-products from the reaction mixtures.

Chapter IV of this dissertation aims at solving a fundamental question about the nature of NHC-silver(I) complexes. The NHC-silver(I) complex is an important synthetic intermediate as it can be used to prepare other NHC-metal complexes through transmetallation. The carbene carbon of an NHC-silver(I) complex in ^{13}C NMR spectra was usually reported as a doublet of doublets or as a singlet in different cases. This phenomenon was explained with a ligand exchange mechanism proposed twelve years ago. However, few reports are available in the literature about the mechanism of the NHC ligand exchange processes at silver. In order to facilitate the study of the solution behaviors of NHC-silver(I) complexes, ^{13}C-labeled NHC-silver(I) complexes were prepared and studied using variable temperature ^{13}C NMR spectroscopy. This study could be useful for future applications of ligand transferring from silver to other metals for the preparation of NHC-metal complexes.

DEDICATION

To my family and the ones who have loved and supported me over the years

ACKNOWLEDGEMENTS

First at all, I would like to express my deepest gratitude to my advisor, Professor Bergbreiter, for his zeal of being a great teacher in chemistry, in research, and in English. His unique teaching style not only guided me to be a researcher but also led me to be a good teacher in the future.

Second, I would like to acknowledge Professor Bazzi for his generous support in funding and for purchasing many expensive chemicals. I thank Professor Singleton, Professor Connell, and Professor Grunlan for serving as my committee members. I also thank Professor Akbulut and Professor Cremer for serving as substituation committee members for my oral exam and seminer, respectively.

I gratefully acknowledge support from the Qatar National Research Fund, National Science Foundation, and the Robert A. Welch Foundation for my research and traveling expense to conferences.

My gratitude also goes to the members in Bergbreiter's group. First, I would like to thank Film, Tian, and Shawn for sharing their experience and for their guidance in my early years. I appreciate the long discussions in chemistry and on life experience with Jeff and Felix in my later years. I want to thank Jill for taking care of various business tasks in the lab. Without their help and suggestions, things would have been much more difficult. I would also like to thank Osburn, Shayna, Patrick, Denisse, Hui, Sushi, Kristine, Chris, Ainsley, Brandon, Nilusha, Tatyana, Ilse, Grit, Alex and my mentees,

Sally and Ohm, for their help during the period of my graduate study at Texas A&M University.

I acknowledge the Department of Chemistry and Texas A&M University for accepting me as a graduate student, providing courses by many excellent teachers and supporting the instruments for my research work. I appreciate the help and guidance from Dr. Pérez and Dr. Reibenspies for theoretical calculation and solving crystal structures, respectively. I also want to express my thanks to the department and school faculty and staff for making my time at A&M a great experience. Especially, I would like to thank Joe, Julie and Sandy for helping me deal with the paperwork and guidance I received when I was a new graduate student.

I would also like to thank all my friends in the Department of Chemistry, Taiwanese Student Association, and College Station Chinese Church for experience sharing and help. I also thank my friends in Taiwan for supports. I especially thank the help from Professor Han, Professor Chang, Professor Liu, Professor Lu, Mark, Albert, Alison, Ike, Jenny, Wei-Ssu, Sheng-Jui, Yu-Chieh, and Jimmy.

Finally, I would like to express gratitude to Min-Fang for her love and sharing her life with me. She is the most valuable treasure I have in College Station.

NOMENCLATURE

ΔG	Gibbs free energy difference
ΔH	enthalpy difference
ΔS	entropy difference
Ac	acetyl
ADMET	acyclic diene metathesis
Ag	silver
aq	aqueous
Ar	aryl
Bn	benzyl
bp	boiling point
cal	calorie(s)
CM	cross metathesis
Cp	cyclopentadienyl
CuAAC	Cu(I)-catalyzed [3+2] azide-alkyne cycloaddition
CW	continuous-wave
Cy	cyclohexyl
d	days
DCM	dichloromethane
DFT	density function theory
DMA	*N*, *N'*-dimethylacetamide

DME	1,2-dimethoxyethane
DMF	*N*, *N'*-dimethylformamide
DMSO	dimethylsulfoxide
ECP	Effective core potential
Et	ethyl
eq.	equation
equiv.	equivalent
FT	Fourier transform
H	hours
HOMO	highest occupied molecular orbital
Hünig's base	diisopropylethylamine
ICP-MS	inductively coupled plasma mass spectroscopy
Im	imidazole
IMes	*N*,*N*'-dimesitylimidazolylidene
IPA	isopropyl alcohol
^{i}Pr	isopropyl
IPr	*N*,*N*'-bis((2,6-diisopropyl)phenyl)imidazolylidene
IR	infrared spectroscopy
k	rate constant
k_b	Boltzmann constant
KHMDS	potassium bis(trimethylsilyl)amide
LANL2DZ	Los Alamos National Laboratory double-ζ

Me	methyl
Mes	mesityl (2,4,6-trimethylphenyl)
mL	milliliters
mp	melting point
Ms	mesyl (methanesulfonyl)
MS	molecular sieves
MW	microwave
n	normal (unbranched alkyl chain)
NHC	*N*-heterocyclic carbene
NMR	nuclear magnetic resonance
p	para
Ph	phenyl
PIB	polyisobutylene
PE	polyethylene
Pd	palladium
Ph	phenyl
phen	9.10-phenathroline
PTSA	*p*-toluenesulfonic acid
R	alkyl
RCM	ring-closing metathesis
ROMP	ring-opening metathesis polymerization
Ru	ruthenium

SPE	single point energy
^{t}Bu	tetrabutyl
T	temperature
TBA	tetra-*n*-butylammonium
TEA	triethylamine
THF	tetrahydrofuran
TS	transition state
UV	ultraviolet
VT	variable temperature

TABLE OF CONTENTS

CHAPTER Page

LIST OF FIGURES

FIGURE Page

FIGURE Page

FIGURE Page

LIST OF TABLES

CHAPTER I

INTRODUCTION

N-Heterocyclic carbenes (NHCs) are a class of organic compounds receiving increasing interests from scientists in many fields of chemistry since 1990s. They have been widely used as ligands in organometallic complexes,[1,2,3] as organocatalysts in synthetic chemistry,[4,5] as reducing agents[6] and are key intermediates in biological reactions. NHCs are important in these diverse fields because of their unique properties.

Structures and Electronic Configurations of Carbenes

To understand the chemistry of NHCs, it is helpful compare the properties of NHCs with other carbenes. A carbene is an organic molecule containing a neutral divalent carbon; the carbon is bonded to two other groups/atoms covalently and bears two nonbonding electrons.[7] Based on their ground-state electron configurations, carbenes are classified into two categories: singlet carbenes and triplet carbenes.[8] A triplet carbene contains two unpaired electrons in two different orbitals and can be considered as a diradical species with the two radical on the same carbon. A singlet carbene contains antiparallel electrons in the same orbital and has an unfilled valence orbital. Because of this electron pair, a singlet carbene can behave as a nucleophile. At the same time, because of the empty orbital, a singlet carbene also has the character of an electron-deficient species and can behave as an electron acceptor or as an

---

This dissertation follows the style of *Journal of the American Chemical Society.*

electrophile. Although singlet carbene carbons are actually electronically neutral, they are sometimes considered as species possessing positive charge and negative charge at the same time. Their description as zwitterions emphasizes their special property of having nucleophilic character and electrophilic character at the same time. Because the electron configurations determine the carbenes' chemical properties, it is important to realize and to predict the factors that affect the ground-state electron configuration of a carbene.

The ground-state electron configuration of a carbene is determined by the molecular geometry and the substituent groups of the carbene carbon. Figure 1 illustrates the energy diagrams of a crabene in a linear structure and a bent geometry.[9] In a linear carbene, the carbene carbon is considered to have sp hybridization bonding to the two groups/atoms and leaving two degenerate p-orbitals. In this case, Hund's rules predict a triplet ground state and the two electrons with parallel spins would occupy in the degenerate p-orbitals. When the carbene center is nonlinear (sp^2 hybridized), the unfilled two orbitals become different because of symmetry breaking. The orbital parallel to the plane defined by the three atoms is called the σ-orbital and has lower energy because of the stabilization due to the s-character from the hybridization. The orbital perpendicular to the plane is designated as the p_π-orbital and has energy identical to a p-orbital. In this case, the lowest energy electron configuration is determined by the energy difference between the σ-orbital and p_π-orbital. When the energy gap between σ-orbital and p_π-orbital is large, an electron pair occupies the lower energy σ-orbital and the carbene is a singlet carbine (Figure 2(a)). When the energy gap is smaller than the

pairing energy of the two electrons, the carbene is a triplet carbene in ground state (Figure 2(b)).

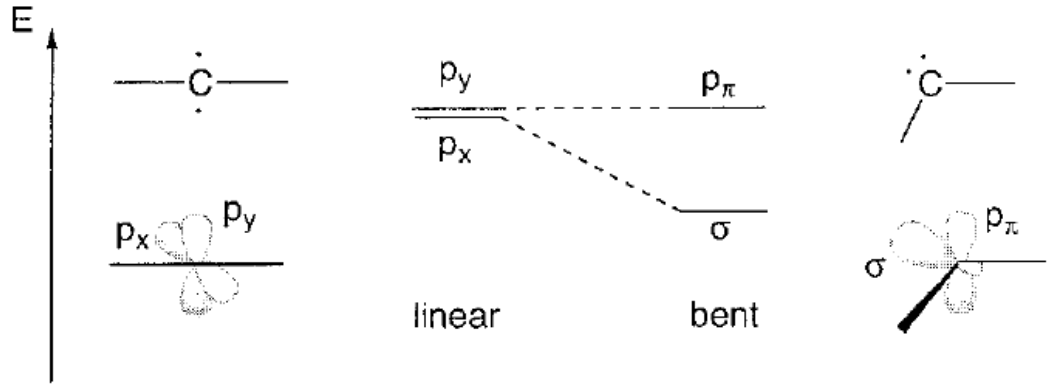

Figure 1. Simplified energy diagrams of linear and nonlinear carbenes.[9]

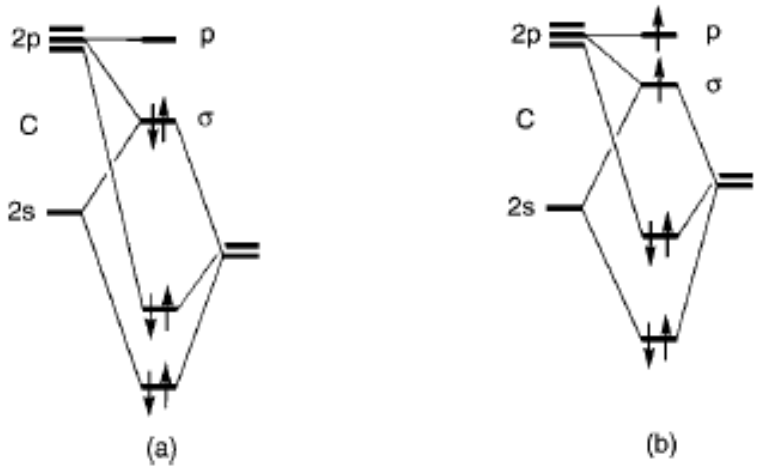

Figure 2. Energy diagrams of nonlinear carbenes with (a) large and (b) small energy gap between σ-orbital and p_π-orbital.[9]

The energy difference between the σ-orbital and p_π-orbital is influenced by the bond angle of the three atoms of the carbene. As shown in Figure 1, when the bond angle is bigger, the molecular geometry is similar to the linear structure. In this case, the s-character in the σ-orbital decreases and the σ-orbital acquires less stabilization. Therefore, the energy gap between the σ-orbital and p_π-orbital decreases and the triplet carbene becomes favored. Figure 3 shows the relative energies of singlet and triplet methylene for various HCH angles from the results of computational calculation using a B3LYP/TZ2P basis set.[10] The calculation shows that when the HCH angle is smaller than 103°, a singlet electron configuration is favored. When the HCH angle is bigger than 104°, a triplet electron configuration is favored. The global energy minimum occurs at the bond angle of *ca*. 135°.

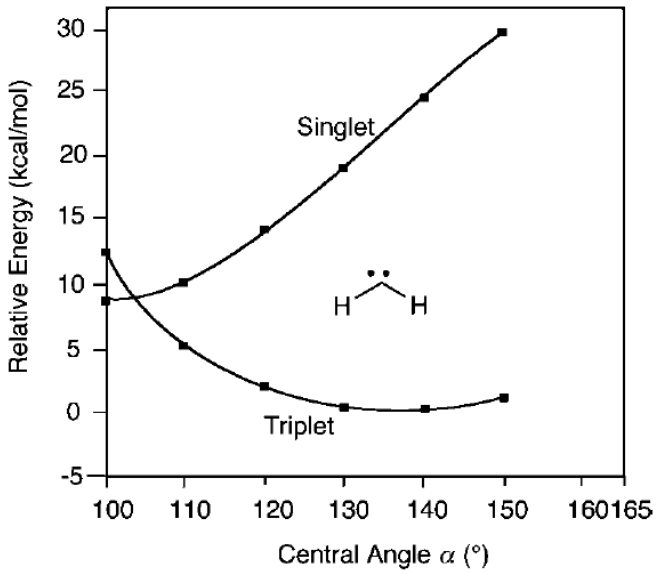

Figure 3. Computational results of the relative energies of singlet and triplet methylene with respect to the central bond angle.[10]

The inductive effects mainly affect the σ-orbital. It has been recognized that carbenes with σ-electron-withdrawing substituents favor the singlet state. This effect can be rationalized on the basis of perturbation orbital diagrams: the σ-electron-withdrawing substituents inductively stabilize the carbene's σ-orbital by increasing its s-character and leave the p_π-orbital unchanged (Figure 2).

The substituents causing the resonance effect, which is more often called the mesomeric effect, affect the p_π-orbital and can be classified into three types: X (π-electron-donating groups, such as $–NR_2$, -OR, -SR, and halides), Z (*π*-electron-withdrawing groups, such as –COR, -CN, $-BR_2$, -SOR, $-SO_2R$, -NO, and $–NO_2$), and C (conjugating croups, such as alkenes, alkynes, and aryl groups).[9] As shown in Figure 4(a), an X substituent interacts with the p_π-orbital and increases the energy of p_π-orbital. Therefore, the energy gap between σ-orbital and p_π-orbital increases and induces the ground state of the X-substituted carbene singlet. Z and C substituents have an empty p or π* orbital, which interacts with p_π-orbital and decreases the energy of p_π-orbital. The energy difference between σ-orbital and p_π-orbital thus decreases and a triplet carbene is expected. (Figure 4(b)(c))

There is another way to understand the resonance effect. Assuming the carbene is a singlet carbene, the empty p_π-orbital will be stabilized with a π-electron-donating group and destabilized with a *π*-electron-withdrawing group. However, since a conjugating substituent will stabilize both the empty p_π-orbital and the radical, this method does not predict the electronic structure with all classes of substituents.

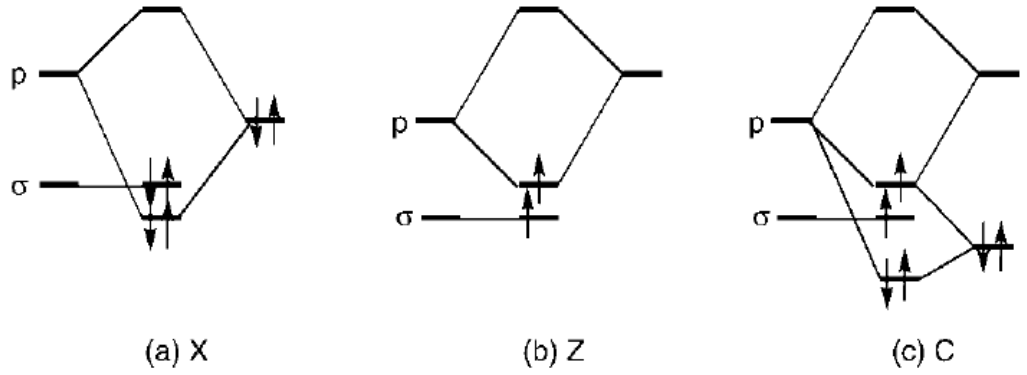

Figure 4. Pertubation energy diagrams of carbene illustrate the resonance effect of the substituents: a carbene p_π-orbital interacts with (a) a π-electron-donating group, (b) a π-electron-withdrawing groups, and (c) a conjugating croup.[9]

Steric groups stabilize all kinds of carbenes kinetically but steric effects are relatively less important in determining electron configuration than the inductive effects and resonance effects. However, when the electronic effects are negligible, the steric effect may become the main factor determining ground-state spin multiplicity. Sterically bulky groups affect the energy gap between the σ-orbital and p_π-orbital mainly through hyperconjugation and carbene bond angle broadening. Like conjugating groups, hyperconjugation also decreases the energy gap between σ-orbital and p_π-orbital. The broadening of the carbene bond angle is the result of the steric hindrance of the bulky groups. The bond angle broadening makes the geometry more linear and the energy difference between σ-orbital and p_π-orbital therefore decreases. Both hyperconjugation and the carbene bond angle broadening causes the decrease of energy gap between σ-orbital and p_π-orbital and a triplet ground-state electron configuration becomes favored.

This can be demonstrated by the fact that dimethylcarbene has a singlet ground state with a 111^{o} carbene bond angle while di(*tert*-butyl)carbene is triplet with a 143° carbene bond angle.[10]

Many NHCs are diamino carbenes. In terms of their inductive effects, nitrogen has higher electronegativity making amino groups σ-electron-withdrawing substituents that destabilize the σ-orbital. When considering their resonance effects, amino substituents are π-electron-donating groups that destabilize the p_{π}-orbital. Both effects increase the energy difference between the σ-orbital and p_{π}-orbital so these NHCs are singlet carbenes. The energies calculated for a series of diamino carbenes using *ab initio* quantum calculations are summarized in Figure 5.[11,12] From the results, it can be seen that the inductive effect and resonance effect provides 20 and 67 kcal/mol stabilization energies, respectively. The presence of a five-member ring makes the carbene bond angle smaller and further increases the σ-p_{π} energy gap to provide an additional 6 kcal/mol of stabilization energy. If the five-member ring contains unsaturated double bond, the heterocycle has 6 π-electrons and gains another 20 kcal/mol of aromatic stabilization energy. These stabilization energies lead to NHCs that exist as stable singlet carbenes with large σ-p_{π} energy differences, *i.e.* large HOMO-LUMO energy gaps.

Based on the above discussion, the two electrons of a NHC should be on the σ-orbital which located in the molecular plane with an empty p_{π}-orbital perpendicular to the plane. This hypothesis is consistent with the experimental data: perdeuterio-1,3,4,5-tetramethylimidazol-2-ylidene was isolated by Arduengo *et al.* and analyzed using

neutron and X-ray diffraction.[13] The electron distribution of the carbene was very closely matched by density functional theory (DFT) calculation results: on the molecular plane, it is clear to see that the electron density of the carbene carbon is in the direction away from all other bonded atoms (Figure 6(a)); the out-of-plane electron density mainly localizes on nitrogen atoms and the distribution on carbene carbon is negligible (Figure 6(b)).[13]

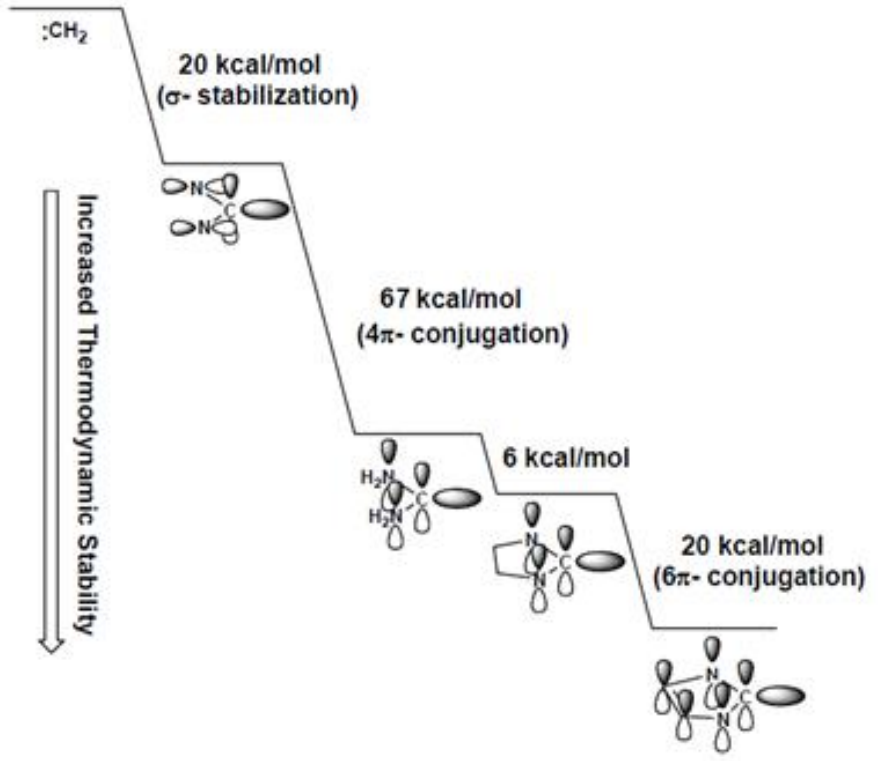

Figure 5. Summarized *ab initio* calculation results: the diamino carbenes gain significant thermodynamic stabilization from electronic effects; when the diamino carbene is part of five-member ring or aromatic structure, even more stabilization energies are gained.[11,12]

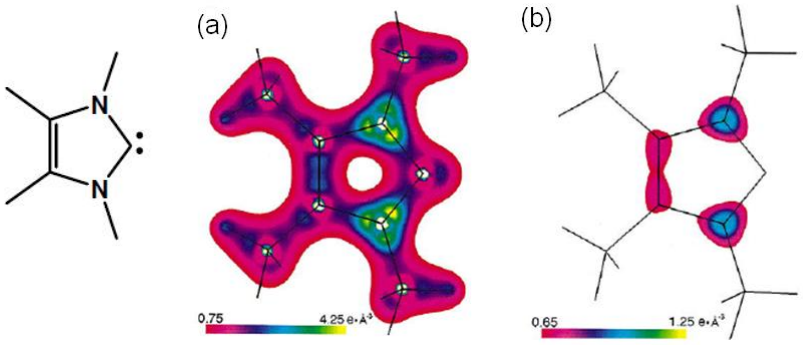

Figure 6. Valence electron density maps of perdeuterio-1,3,4,5-tetramethylimidazol-2-ylidene (a) on the molecular plane and (b) 70 pm above the molecular plane.[13]

The electron distribution and energy diagram determine an NHC's chemical behavior. This means that when NHCs act as ligands to other elements, they can be two-electron donors with weak π-accepting character. The weak π-accepting character is mainly because of non-matching of the high-energy p_π-orbital with the occupied orbital of coordinated element. Therefore, in organometallic chemistry where the ligated atoms are metals with electrons in d orbitals, NHCs are considered as excellent two-electron σ-donor and weak π-acceptor. However, when NHCs connects with conjugated systems containing electrons in 2p-orbitals, the p_π-orbital can still stabilize negative charge. Thus NHCs are often used as organocatalysts.

N-Heterocyclic Carbenes and Their Complexes

There are many examples of NHCs but the most commom are imidazol-2-ylidenes and their derivatives, including 1,2,4-triazoles, thiazoles and related saturated derivatives (Chart 1(a)). There are also many kinds of NHCs with different ring sizes or

different heteroatom distributions in the heterocyclic rings (Chart 1 (b)). These cyclic carbenes can be distinguished as "classical" and "non-classical" NHCs: the classical NHCs are the NHCs stabilized with two adjacent heteroatoms. In contrast, non-classical NHCs have fewer heteroatoms adjacent to the carbene carbons and have smaller σ-p_π energy gaps. Non-classical NHCs are thus often less stable. However, because of less electron-withdrawing inductive substituents adjacent to the carbene carbons, there is higher electron density on the non-classical NHC carbon atoms. As a consequence, the non-classical NHCs are stronger donors. Various terminology systems are also used to classify NHCs: "normal" carbenes are the NHCs that can be represented by a neutral canonical resonance form while "abnormal" carbenes are those NHCs requiring the introduction of formal charges on some nuclei.[14] In non-classical NHCs, a carbene without a heteroatom in the α-position to the carbene is called a "remote" carbene. A remote carbene may be normal (**7** in Chart 1) or abnormal (**13** and **14** in Chart 1). This dissertation only discusses the most commonly used NHCs.

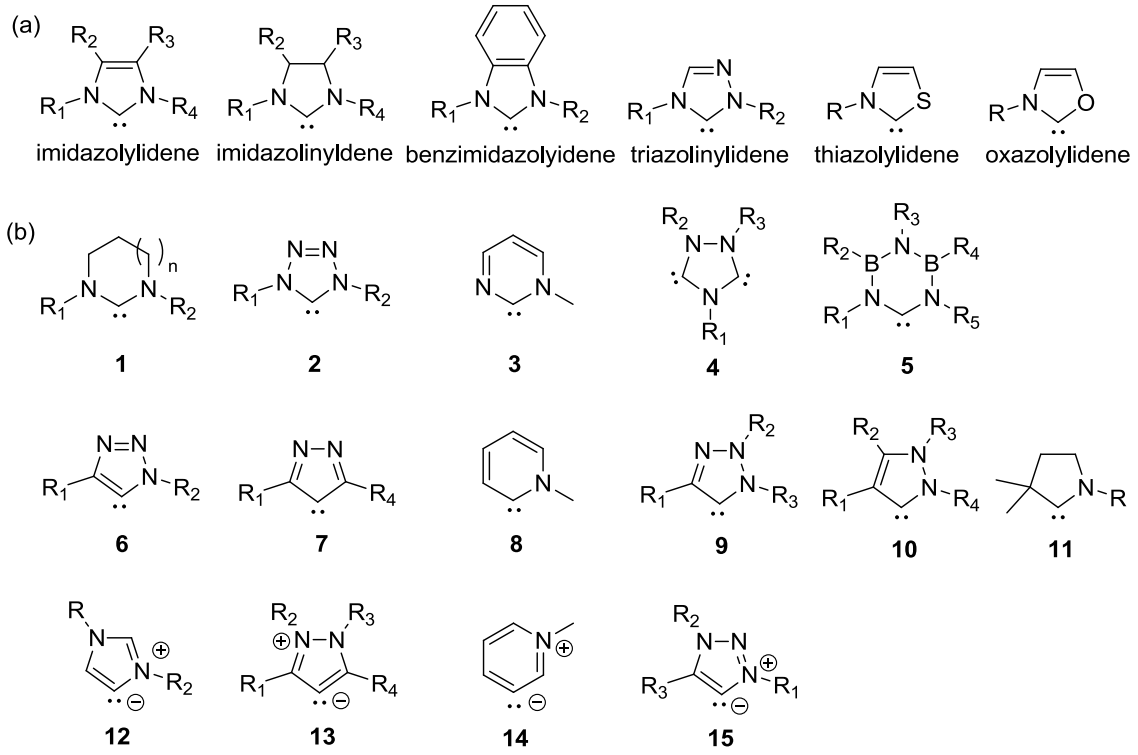

Chart 1. Examples of (a) commonly used NHCs (all are classical and normal NHCs) and their names, (b) less common used NHCs, including classical NHCs (**1-5**), non-classical NHCs (**6-15**), normal NHCs (**1-11**), abnormal NHCs (**12-15**), and remote NHCs (**7**, **13**, **14**).

As a ligand in organometallic chemistry, an NHC is considered as a strong σ-donor and weak π-acceptor. A NHC-metal complex is usually represented as structure **16**, **17** or **18** in Figure 7 (shown for the particular case of imidazolylidene complexes).[15] In structure **16**, the coordination bond of the carbene to metal is emphasized. In general, the structure is simplified as **17** for convenience. However, a more accurate representation is **18** where the structure shows that the NHC has two electrons

coordinating to metal; NHC thus has a formal charge of +1, and the metal has -1 formal charge. In the early literatures, structures like **18d** were often used to represent the NHC-metal complexes. However, this structure over-emphasizes the weak π-interaction between metal and p_π-orbital on the carbon carbon. Indeed, the **18d** is only one of the resonance forms of the NHC-metal complex. In fact, **18b** and **18c** are considered as more important resonance forms than **18a** and **18b**. It is important to notice that the -1 formal charge on metal with low contribution of **18d** resonance form makes the NHC a excellent stabilization ligand for highly oxidized transition metals and late transition metals (late transition metals have higher effective nuclear charge and are generally considered as more electron-deficient metals). To avoid ambiguity about the formal charge, real charge, and oxidation states of the metal ions, a less accurate but more conventional representation **17** will be used to represent a NHC-metal complex in this dissertation.

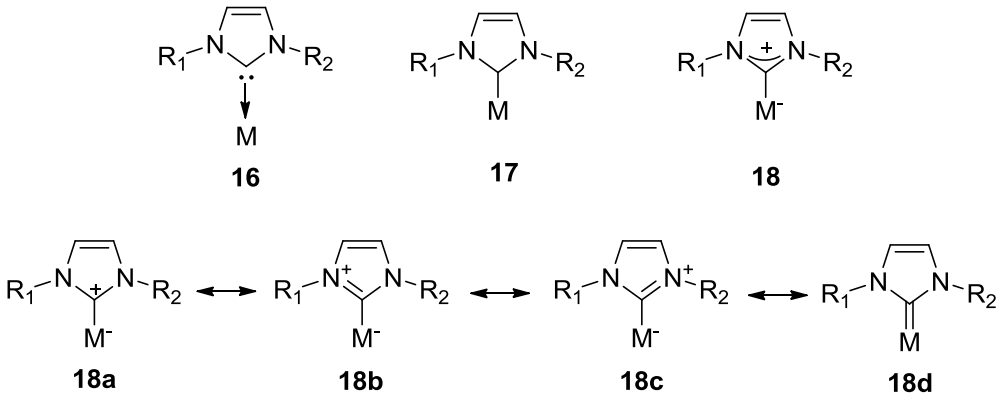

Figure 7. Representation diagrams of NHC-metal complexes and the resonance forms.[15]

In the early 1960s, Wanzlick *et al.* investigated synthesis of the saturated NHC **21** starting from the precursor **19** (Scheme 1).[16] However, they failed to isolate the free carbene **21** but instead obtained the electron-rich olefin **20** (so-called Wanzlick olefin now) as a colorless crystalline compound. The absent of cross-coupling products on mixing of differently substituted "dimers" showed that the dimers were not equilibrium with their monomers. Later Wanzlick, Vorsanger, and Hünig found that the acidic protons on many five- or six- membered heterocyclic cations underwent base-catalyzed H-D exchange. Among these examples, *N*-methylbenzthiazolium cation was most easily deprotonated by triethylamine in a polar solvent like DMF or acetone. While at this point in time, NHCs had not yet been isolated, numerous NHC-metal complexes had been known. Although Wanzlick *et al.* also recognized that aromaticity in unsaturated *N*-heterocyclic five-member rings could contribute to the carbene stability, (cf. Figure 5) they failed to isolate free NHCs in this quest.

Scheme 1. The investigation of the heterocyclic carbenes by Wanzlick *et al.* in 1960s.[16]

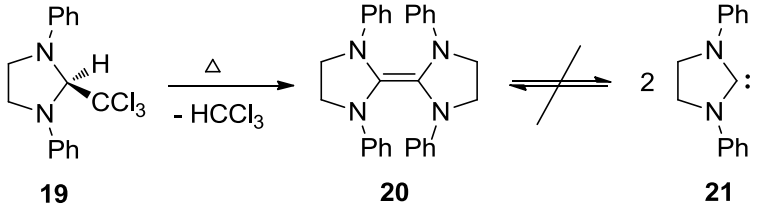

Öfele and Wanzlick *et al.* were the first to prepare NHC ligated metal complexes in 1968 (Scheme 2).[17,18] The subsequent synthesis, characterization, and studies of numerous carbene-metal complexes by Lappert's research group made a significant

contribution to this area of chemistry.[19] However, not much attention was paid to the applications of these complexes until Arduengo *et al.* isolated the first free *N*-heterocyclic carbene in 1991.[20] This work led to an explosion of interest in this area, a level of activity that is still increasing.

In 1992, Herrmann first noted that NHCs as ligands are similar to the known electron-rich phosphines PR_3 in their reactivities so NHCs could be an alternative for the known phosphine ligands in coordination chemistry.[12,21-23] With this beginning, a variety of NHCs with different steric demands and electronic properties were designed and used to prepare coordination compounds with numerous metals for many purposes. At present, it is recognized now that NHCs can serve as ligands to most transition metals and many main group elements (Figure 8).

Scheme 2. NHC-metal complexes synthesized independently by (a) Öfele and (b) Wanzlick *et al.* in 1968.[17,18]

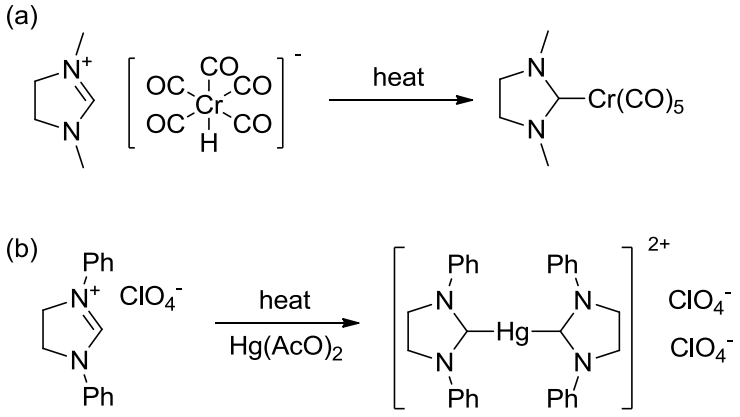

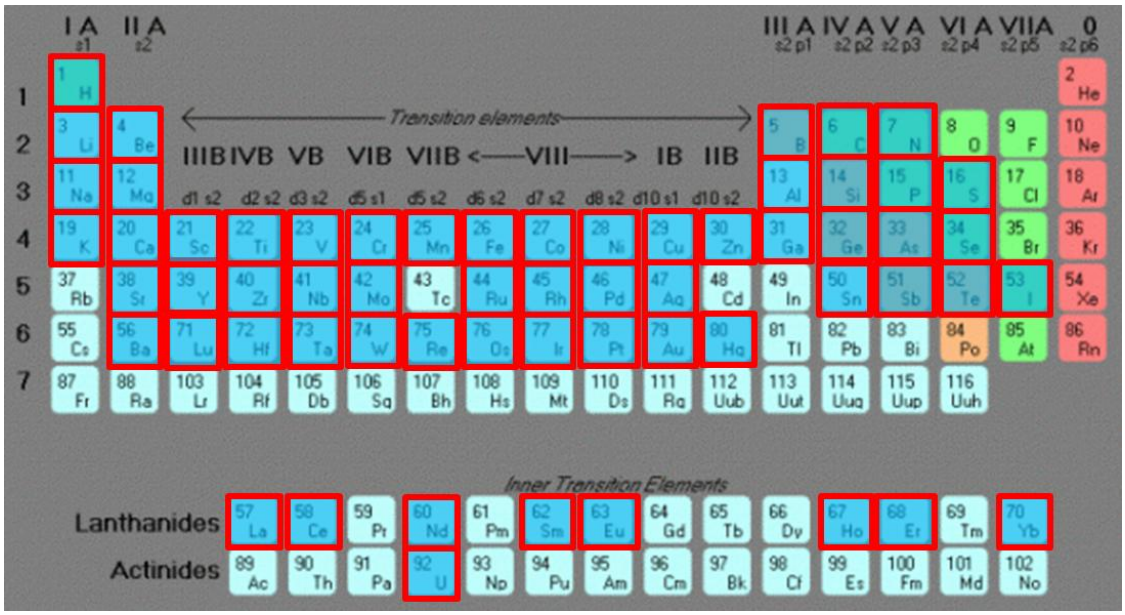

Figure 8. Elements that formed stable complexes with NHCs are highlighted in a periodic table.[12,24]

NHCs have become important in organometallic chemistry because several advantages are gained in using NHCs as ligands in place of their phosphorus analogues: NHCs are less odorous than phosphines and are generally considered as less toxic than phosphines because NHCs, *e.g.* the thiazolylidenes, are found in biological systems. In addition, most NHC ligands are better σ-donors than phosphines.[25] Compared to phosphine-metal complexes, NHC ligands form more stable bonds with metals in general and are kinetically less labile (Scheme 3).[12,26] As a result, NHC–metal complexes are often less sensitive to the air and moisture and have greater thermal stability. These properties make the handling of NHC-metal complexes easier and, as a consequence, NHC-metal complexes can react in wider range of conditions for more

varied purposes. NHC ligands also can be prepared in various ways to tune the steric demands and the electronic properties of NHC ligands. Finally, on many occasions NHC-metal catalysts have been shown to be more effective than phosphine-metal catalysts.

Scheme 3. Dissociation equilibrium of NHC and phosphine-metal complexes.

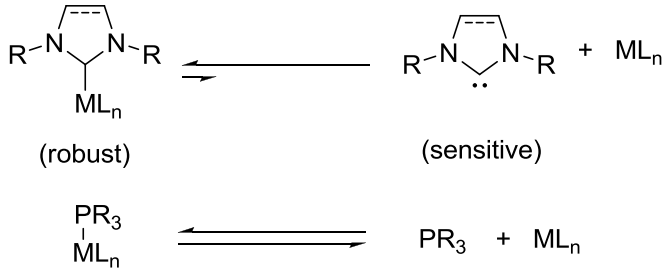

Many methods have been used to prepare NHC-metal complexes. These syntheses can be divided into three general methods: (1) free-carbene generation followed by directly reaction of the carbene with a metal precursor, (2) direct synthesis of an NHC carbene-metal complex from NHC precursors and metal precursors, and (3) initial synthesis of a stable intermediate complex with subsequent transfer of the NHC ligand to another metal via a transmetallation reaction.[15,27] Scheme 4 illustrates these three methods starting with protonated NHCs, *i.e.* imidazol(in)ium, triazolinium, thiazolium, oxazolium salts or their related saturated derivatives. The first method requires preparation and storage of free carbene. Although many NHCs are commercially available, this method requires more careful operations for kinetically less stable free carbenes. This can be problematic when less bulky groups are present on the

N-substituents. A modification of this method is to prepare the carbene *in situ* and to directly react the carbene so-formed with metal precursors in one-pot. This method avoids the requirement of isolation and the storage of free carbenes and is most frequently used to prepare NHC-metal complexes now. The bases most frequently used for deprotonation *in situ* are KO^{t}Bu and KHMDS. These bases are sterically hindered and less likely to coordinate to metals.

Scheme 4. Synthetic strategies of NHC-metal complexes from protonated NHCs.

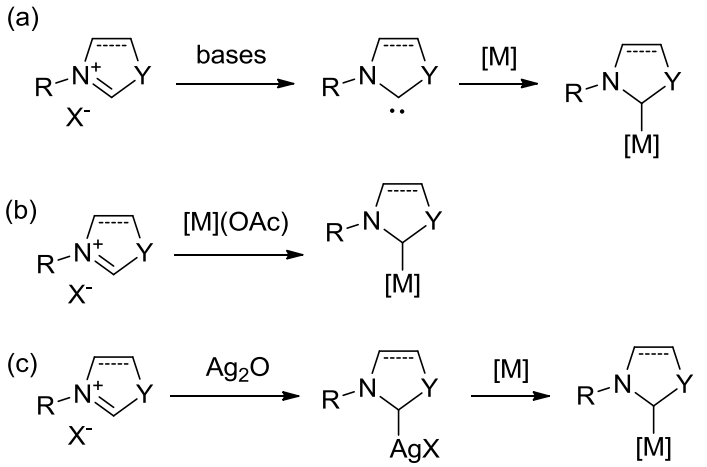

The second general method can be considered as a modification of the first method. In this method, metal salts with basic anions are used to generate the NHC-metal complexes *in situ*. (The basic anions are used as bases and the conjugated acids will be necessary to remove during or after the reaction.) The most commonly used metal salts are acetate. This method usually requires harsher conditions and is less frequently used now. The third general route to carbene corrdination complexes is a

two-step method and is now widely used to generate unsaturated NHC-metal complexes in high yields under mild conditions. This method was first developed by Wang *et al.* in 1998 and most commonly uses NHC-silver complexes as synthetic intermediates.[28] In this method, an NHC precursor is allowed to first react with silver oxide. The NHC precursor is deprotonated by the weakly basic silver oxide and forms NHC-Ag complex *in situ*. The NHC-Ag intermediate can be stored or subsequently mixed with another metal precursor in a transmetallation reaction to afford the desired NHC-metal complexes. These two steps can often be carried out smoothly at room temperature and in many cases, an insert atmosphere condition is not required. While NHC ligand dissociation is, as was noted above, often slow, the NHC transfer from one metal to another occurs smoothly in these cases. This is generally considered to be a thermodynamic driven reaction that leads to formation of more stable species. However, it is the kinetic lability of NHC-Ag complexes that makes this reaction feasible. In addition to NHC-Ag complexes, NHC ligated Cr, Mo, W, Cu, Au, and Mn complexes have also been found to undergo transmetalation. However, NHC-Ag complexes are still most often used as transmetalation precursors to prepare other metal complexes.

In addition to protonated NHCs and NHC-Ag derivatives, many NHC adducts are known to be stable. Such species can be stored and can be easily used to generate free carbenes when needed, too. NHC-HOR, NHC-$HCCl_3$, NHC-HC_6F_5, NHC-CO_2, etc. are adducts that are reported to be useful NHC precursors which can be stored at room temperature or below and can generate free NHCs by heating under reduced pressure to remove the alcohol, chloroform, pentafluorobenzene and carbon dioxide substituents

(Chart 2). Thiourea derivatives that can be prepared from a diamino compound with thiophosgene can also generate NHCs by reduction with potassium (Scheme 5).

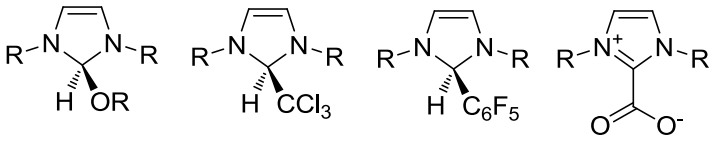

Chart 2. Examples of NHC adducts which can form NHC in vacuum at higher temperature.

Scheme 5. Synthesis of thiourea derivatives as NHC precursors.

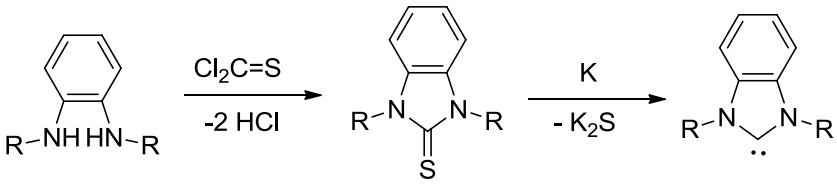

The deprotonation of NHC precursors, like imidazol(in)ium, triazolinium, thiazolium, oxazolium salts or their related saturated derivatives, is key step in most of the synthesis of NHC complexes described above. Thus the preparation of these salts has received attention. Many methods have been reported for the synthesis of these protonated NHC ligand precursors. The simplest way to prepare them is by alkylation of imidazole, thiazole or oxazole. (Scheme 6) If the desired imidazole, thiazole or oxazole is not commercially available or if the desired *N*-substituents are not usual substrates for an S_N2 reaction, a S_NAr reaction or a coupling method, it is necessary to synthesize the protonated NHCs in other ways.

Scheme 6. Preparation of imidazolium, thiazolium and oxazolium salts via direct S_N2 alkylation.

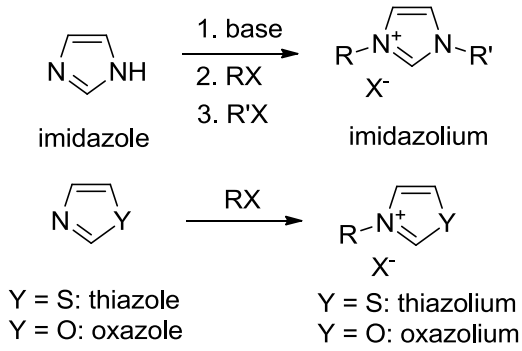

Five general strategies are typically used to prepare the heterocyclic salts that serve as precursors for NHC ligands.[29] The first is a one-pot synthesis of imidazole or imidazolium salts starting from glyoxal, primary amines, and formaldehyde. (Scheme 7) This method is straightforward and can lead to unsymmetrically *N*-substituted derivatives with a subsequent alkylation step. The second method is similar to the first one but involves stepwise formation of a diimine starting with a dialdehyde like glyoxal. The heterocycle is then formed by cyclization with formaldehyde under acidic conditions or with a chloromethyl alkyl ether (Scheme 8). This method can be used to form both unsaturated and saturated NHC precursors. The preparation of saturated imidazolinium salts required an additional reduction of the intermediate diimine to diamine and following by cyclization with a tryalkyl orthoformate. The third and fourth methods are used only for the preparation of imidazolinium salts. Using chemistry like that used in second method, a diamine is first prepared and then cyclized with a tryalkyl orthoformate. In these cases, the desired diamine is prepared either by reduction of a

diamideor by a Pd-catalyzed Buchwald-Hartwig amination coupling (Scheme 9). The fifth method involves the formation of a formamidine which is followed by cyclization with a dihalide compound (Scheme 10).[30] This method has the advantage that it facilitates the synthesis of NHCs with different *N*-substituents and different ring sizes.

Scheme 7. Preparation of imidazolium salts via one-pot synthesis of imidazole or imidazolium salts.

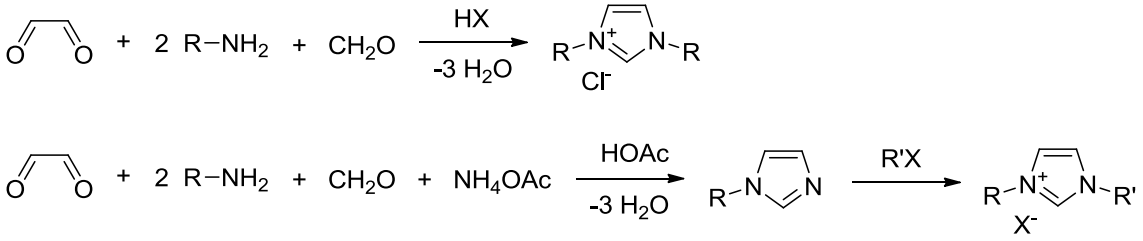

Scheme 8. Stepwise preparation of imidazolium salts and imidazolinium salts.

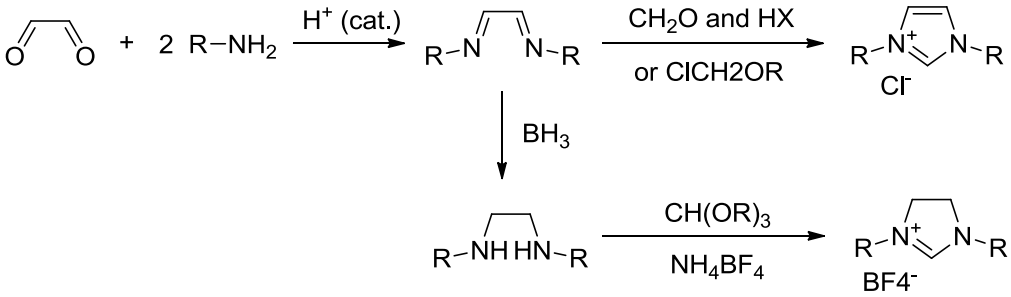

Scheme 9. Synthesis of imidazolinium salts.

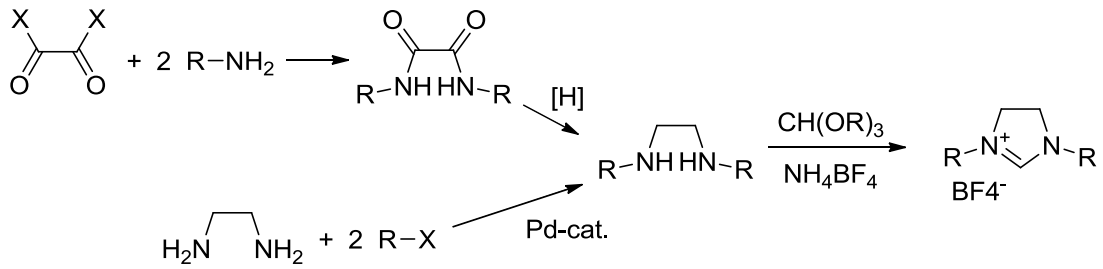

Scheme 10. Synthesis of imidazolinium salts via formamidines.[30]

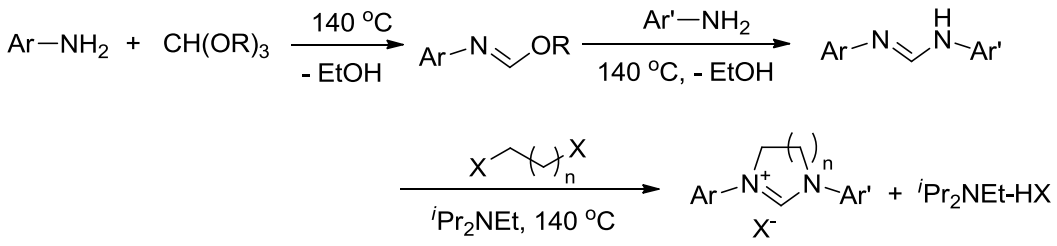

The choice of which synthetic pathways to use depends on many factors. One of the factors is whether the free NHCs is stable enough to isolate. In considering about the isolation of free NHCs, it is important to remember the experimental results from Wanzlick's research group and to realize the factors that affect one's ability to isolate free NHCs. The first problem is the dimerization of NHCs. The dimerization of an unsaturated NHC is estimated to be enthalpically favorable by *ca*. 4 kcal/mol, an enthalpy that does not offset the unfavorable entropy of dimerization (*ca.* -30 cal/mol-K) at room temperature (Scheme 11(a)).[15] While dimerization of an unsaturated NHC will break the aromaticity of the starting NHC and is less enthalpically favored, the saturated NHC gains more stabilization energy from dimerization. Thus the saturated NHCs dimerize rapidly and irreversibly to form Wanzlick olefins unless the carbene carbons are shielded by very bulky substituents (Scheme 11(b)). The benzimidazolylidenes have intermediate behavior relative to the saturated and unsaturated NHCs and exist in the equilibrium between free NHCs and corresponding dimers. The equilibrium favors the dimers by *ca*. 5 kcal/mol (Scheme 11(c)).

Scheme 11. Equlibrium and thermodynamic constants of the dimerization of (a) imidazolylidene, (b) imidazolinylidene and (c) benzimidazolylidenes.[15]

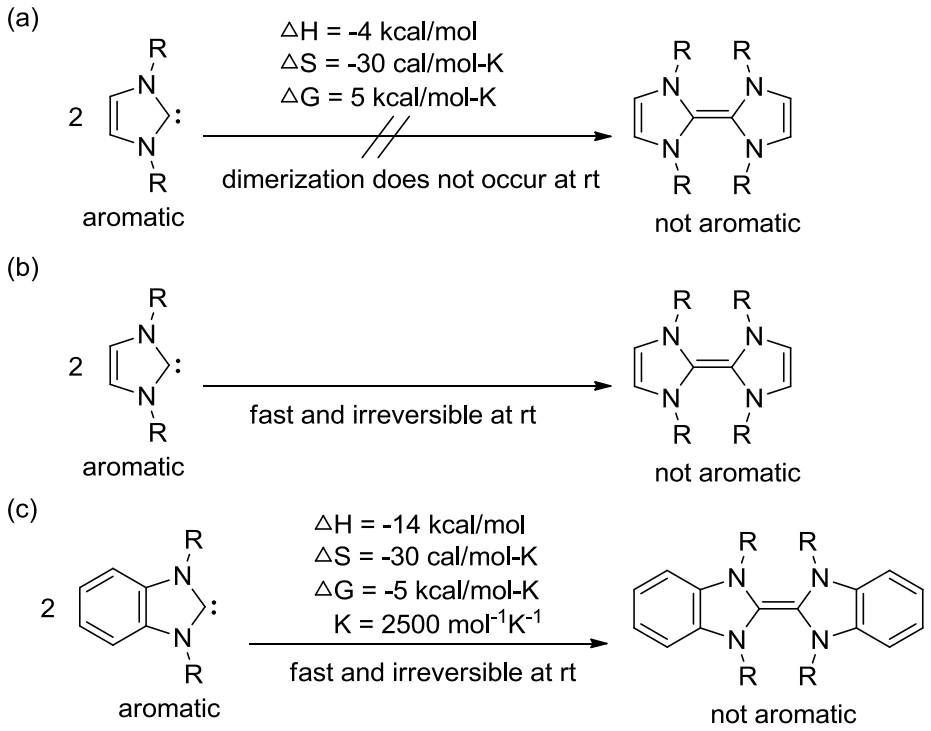

Supported NHC Ligated Complexes

While this dissertation will investigate the synthesis of new NHC precursors and metal complexes as well as will study the chemistry of a variety of NHC-metal complexes in catalysis and in other reactions, the usefulness of NHCs and their metal complexes makes it imperative that better strategies be developed to use NHCs and their complexes in "Greener" way. This can be accomplished by designing NHC ligands and catalysts that can be easily separated, recycled, and reused after reactions. It can also accomplished by designing NHC ligands such that they are effective in various reaction

media other than the normal organic solvents. Either goal can be met by NHC or catalyst modifications that change a catalyst's solubility without affecting its reactivity.

The goal of developing separable, recyclable, and reusable NHC ligated catalysts has in the past been accomplished by preparing modified catalysts using NHC ligands bound to a solid support. In this case, it is easily to separate catalysts by filtration after a catalytic reaction. In this particular case, one has to find a suitable solid support and to design a linkage between the support and the catalyst that does not affect the catalyst reactivity. Similarly, to develop a catalyst suitable for a non-traditional solvent, the goal is to find functional groups which can make the catalyst dissolve in the proposed solvent without influencing the catalyst's reactivity. For instance, to make an NHC-metal catalyst water-soluble, one can design an NHC ligand that cantain a water-soluble polymer or several charged functional groups, or encapsulated the catalyst in a water-soluble cage.

The demand for these NHC modifications to prepare "Greener" catalysts is of considerable current interest for several reasons. First, in the case of NHC-bound metal catalysts, it is desirable to reduce the metal contamination in the catalytic products, especially in medicinal and pharmaceutical chemistry, for the safety and cost reasons. Second, recyclable and reusable catalysts can simplify the operation processes and offer the possibility to high-throughput chemistry and continuous flow reactors. A third reason is that separable catalysts and simpler operation processes help to reduce the chemical wastes generated in a process and thus more environmentally friendly. The desire to make catalysts work in a "Greener" media is based on similar concerns.

Several strategies can be used to design a separable, recyclable catalyst. The most common is to use a modified catalyst attatched to a heterogeneous supports aand to then recover the catalyst separating from products using a simple filtration. The alternative is to design catalysts that be separated from product by solvent selective precipitation, a stimulated phase separation or by simple liquid-liquid extraction.

Although the ideas of supported catalysts can be back to 1960s, there are only modest number of examples of NHC-bound catalysts attached to supports. In 2000, Herrmann *et al*. attached an NHC-palladium catalyst to Wang resin ((4-bromomethyl)phenoxymethyl polystyrene) in the first example of a synthesis of a supported NHC-metal complex.[31] Their results showed that these supported catalysts had similar catalytic abilities for the various coupling reactions but they observed that turnover frequencies were lowered by 1 order, which led to longer reaction times. The supported catalysts were reusable: when coupling 4-bromoacetophenone and styrene with 0.15% of resin-bound NHC-Pd catalyst, the catalyst was reused 15 times without loss of activity. A Heck coupling of 4-bromoacetophenone and *n*-butyl acrylate with 0.02% of resin-bound NHC-Pd catalyst showed a decrease in the cataytic reactivity after 6 cycles. The decrease in activity in Heck coupling was more marked when coupling bromobenzene and *n*-butyl acrylate with 0.02 % of resin-bound NHC-Pd catalyst: the catalytic reactivity dropped after only 4 cycles. Elemental analysis of the catalyst showed that the starting complex may have changed during the reaction as the palladium content was reduced by 0.6% after first cycle. However, the Pd leaching was significantly less in consequent cycle. The successful reuse and low metal leaching of

this supported NHC-Pd catalyst was attributed to the strong bonding of the NHC ligand to Pd catalyst.

Scheme 12. Synthesis of Wang resin-supported NHC-palladium catalyst by Herrmann *et al*. in 2000.[31]

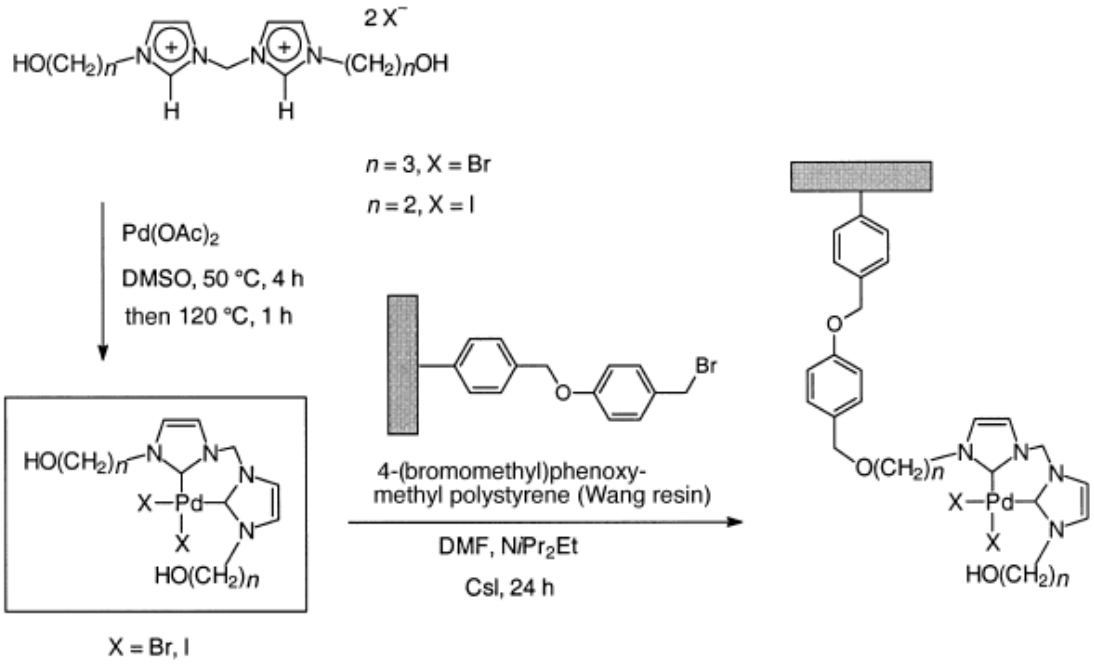

Later, Blechert *et al*. reported a Merrifield-styrene-supported NHC precursor and used it to prepare a modified 2nd generation Grubbs catalyst (Scheme 13).[32] The supported metathesis catalyst worked fine in the first cycle, but more than twice the reaction time was required to complete the ring-crossing metathesis in the second run. This suggested the catalytic propety losing from cycle to cycle.

Scheme 13. Synthesis of Merrifield resin-supported NHC-ruthenium catalyst by Blechert *et al*. in 2000.[32]

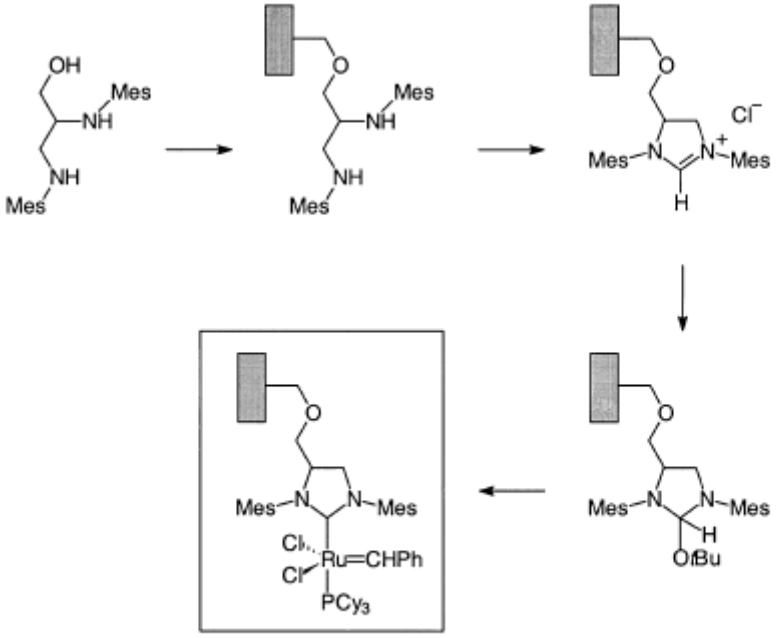

As discussed above, the prior examples of reusable NHC-metal catalysts have mainly focused on insoluble supports or always biphasic systems. Studies using soluble polymers have largely been restricted to the use of polar polymers like poly(ethylene glycol) where the supported catalysts are separated with solvent selective precipitation or by aqueous extraction. Of interest in this dissertation is an alternative approach developed in the Bergbreiter's group.[33-39] This strategy emphasized the use of organic phase soluble polymers as catalyst supports. Polyisobutylene (PIB) is of particular interest since ligands and transition metal complexes formed with this polymer as a phase handle can partition into nonpolar solutions with products remaining in a more polar phase after catalyst recovery in a post-reaction separation step. Thus, catalysts and

products can be separated by a simple biphasic liquid/liquid separation after a monophasic reaction.

PIB oligomers are readily available commercial materials that are mainly used in the applications as oil or fuel additives. These PIB derivatives have the advantage that they have a structurally simple and chemically inert alkane backbone. Functional groups attached to such polymers can be readily analyzed by solution state spectroscopy. For example, ^{1}H NMR spectroscopic analyses of PIB is simplified because there are only two major types of protons present on the polymer and because these protons appear in the 1 - 2 ppm region of the ^{1}H NMR spectrum, a region that does not obscure signals from most functional groups. The result of these properties is that terminal groups on PIB can be easily analyzed by ^{1}H NMR spectroscopy as shown by the example in Figure 9. The commercially available PIB derivatives used in this work have a vinyl terminus that can be modified by simple chemistry to prepare many sorts of soluble polymeric reagents and ligands including PIB-bound phosphine ligands,[40] olefin metathesis catalysts,[41,42] salen catalysts, organocatalysts, Cu(I) catalysts for atom transfer radical polymerizations, azide-alkyne cyclizations, Rh(II) and Cu(I) cyclopropanation catalysts.[33] Because PIB is a noncrystalline polymer, it is soluble even at low temperatures in nonpolar and weakly polar solvents like alkanes, chlorinated alkanes, arenes, and ethers. However, it is generally not soluble in polar solvents like acetonitrile, DMF, ethanol, and water though it does dissolve in many solvent mixtures containing these solvents at elevated temperature. This phase selective solubility makes PIB and its derivatives attractive because the polymer and species attached to it can be

easily separated from reaction mixtures by extraction or by a gravity-based separation of an immiscible mixture of polar and nonpolar liquid phases of different density.

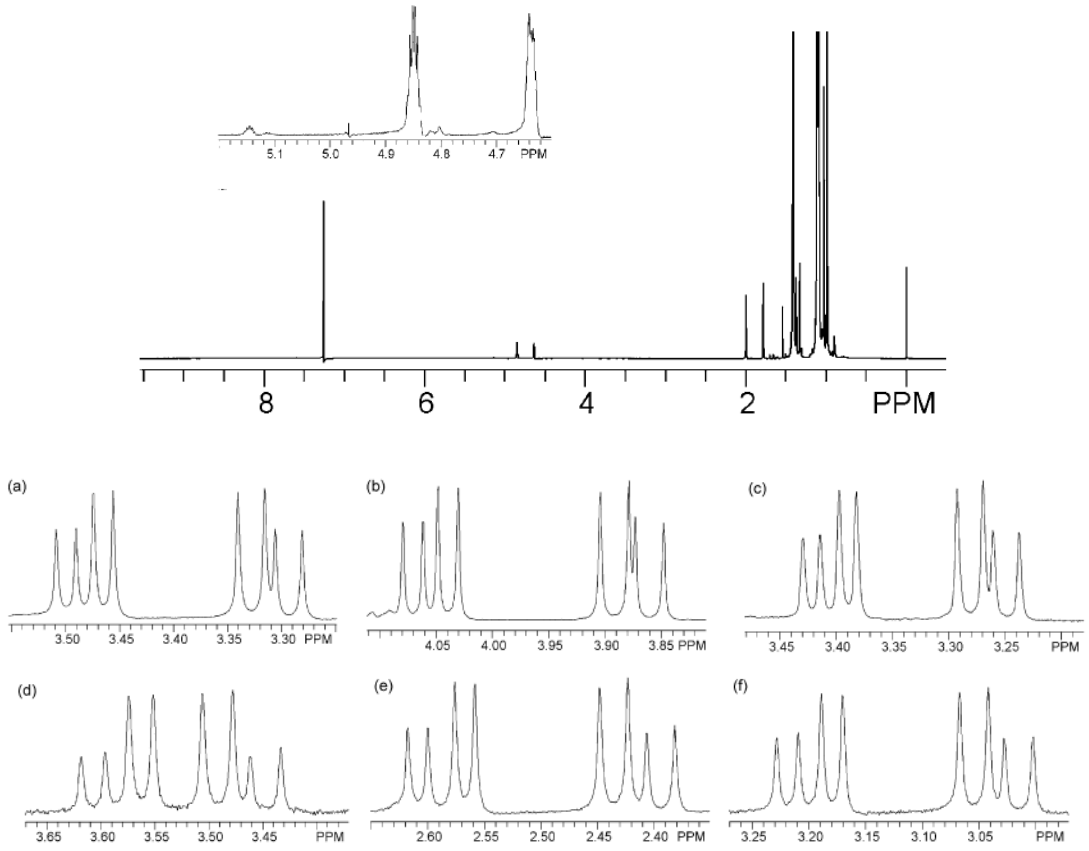

Figure 9. ^{1}H NMR spectra of PIB (top) and CH_2 splitting next to the functional group of some PIB derivatives (bottom: (a) PIB-OH; (b) PIB-OMs; (c) PIB-Br; (d) PIB-phthalimide; (e) PIB-NH_2; (f) PIB-N_3) showing that the peaks from the PIB main chain is located in a relatively less important region and does not obscure signals from most functional groups.[34]

Previous work from Bergbreiter's research group has shown that PIB is a useful support for ligands. The ligands attached to PIB behave like their low molecular weight counterparts in metal coordination and will be useful in catalysis. In this dissertation, several types of imidazol(in)ium salts are connected to PIB polymers. The metal complexes of the heptane-soluble NHC ligands so-formed are discussed in more detail in the following chapters.

CHAPTER II

PIB-SUPPORTED NHC-PALLADIUM(II) CATALYSTS*

Introduction

Studies of NHC-Pd catalysts started with work by Herrmann *et al.* in 1995.[21] Since then many NHC-ligated palladium catalysts have been designed and studied. Because of the similarity of the properties of the NHC ligands and phosphines, the designs of these NHC-Pd catalysts were often based on known phosphine-Pd catalysis chemistry and the results of catalytic studies were compared with the chemistry of their phosphine-Pd analogs. Thus, in order to put the NHC-Pd chemistry in context, this chapter begins with a review of the history of Pd-mediated reactions and phosphine-Pd chemistry.

Palladium was discovered as a steel-white metal by William Hyde Wollaston in 1803 and named in 1804. In 1866, Thomas Graham first noted that palladium can absorb hydrogen. It is now known that palladium can absorb up to 900 times its own volume of hydrogen at room temperatures and atmospheric pressure and that is a reversible process. The palladium's uncommon affinity for hydrogen led to the use of palladium in related catalysis, *i.e.* in hydrogenation and other reactions involving hydrogen transformations.

Modern Pd chemistry started in late 1950s with the discovery of an industrial

---

* Part of the data reported in this chapter is reprinted with permission from "Polyisobutylene-supported N-heterocyclic carbene palladium catalysts" by D. E. Bergbreiter, H.-L. Su, H. Koizumi and J. Tian, *J. Organomet. Chem.* **2011**, *696*, 1272, Copyright 2010 by Elsevier B. V.

process for the production of acetaldehyde by the air oxidation of ethylene with catalyst mixture of $PdCl_2$ and $CuCl_2$. This process is now known as the Wacker process. The mechanism of this process is illustrated in Scheme 14.

Scheme 14. Wacker process.[43-45]

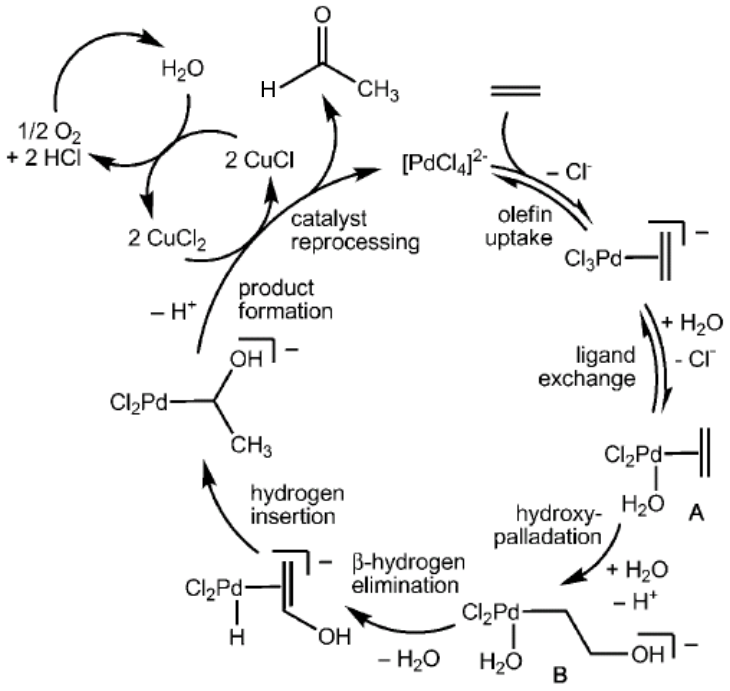

In 1969, Richard F. Heck and Shiichiro Teranishi *et al*. reported that stoichiometric palladium catalyzed the coupling of arylmercuric halides with alkenes respectively (Scheme 15). In 1971, Tsutomu Mizoroki described an extension of this work in which iodobenzene and styrene coupled to form stilbene in methanol at 120 °C in the presence of potassium acetate as a base and using palladium chloride as a catalyst. A 1972 Heck's publication acknowledged the Mizoroki's work and detailed

independently discovered work of different reaction conditions with a hindered amine as a base and palladium acetate as a catalyst. This paper also suggested that the actual catalyst in the reaction is a Pd(0)-alkene species. In 1974, Heck described that the addition of phosphine significantly accelerated the coupling reaction.

Scheme 15. (a) Heck's and (b) Teranishi's initial works of stoichiometric palladium-catalyzed coupling of in 1969.

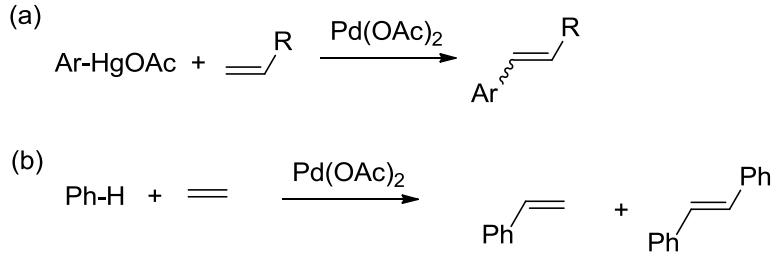

This discovery of phosphine-Pd catalysis has subsequently led to many other Pd-catalyzed reactions with varied substrates. These reactions have been well studied, are widely used in organic synthesis and are now in many cases name reactions. These reactions are summarized in Scheme 16. Because of the importance of these reactions in organic synthesis, Richard F. Heck, Ei-ichi Negishi, and Akira Suzuki shared the 2010 Nobel Prize in Chemistry.

Scheme 16. Named Pd-catalyzed reactions: (a) Heck reaction, (b) Hiyama coupling, (c) Kumada coupling, (d) Negishi coupling, (e) Stille reaction, (f) Sonogashira coupling, (g)

Suzuki coupling and (h) Buchwald-Hartwig aryl amination. X in this scheme is halides or pseudohalides, such as OTf, N_2^+, etc.

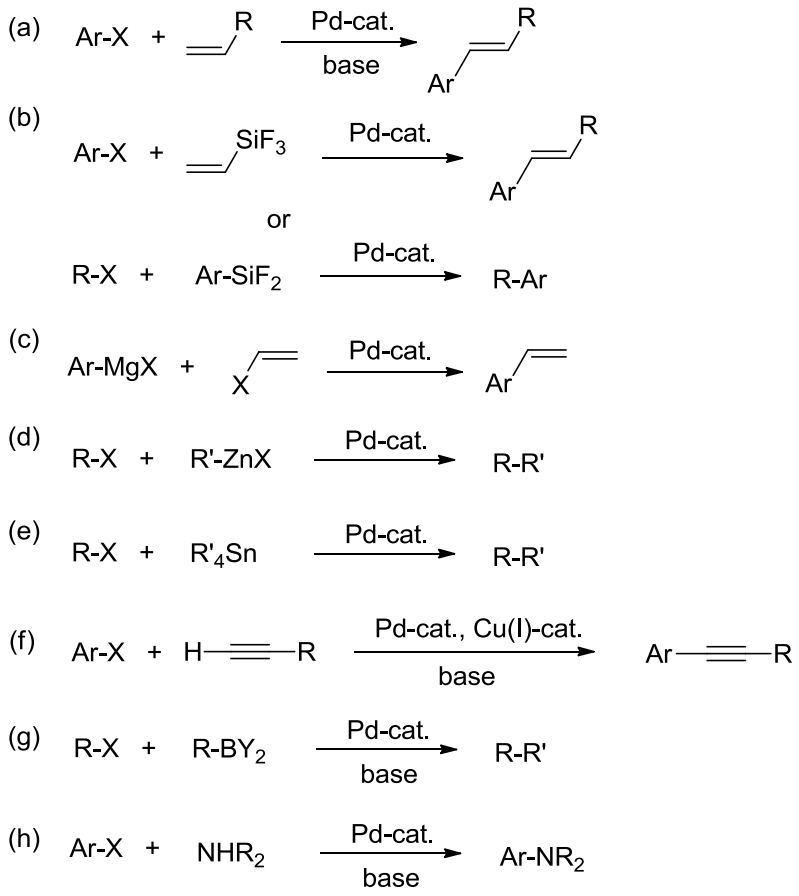

Although a wide variety of phosphine-Pd catalysts promote these reactions, most of these catalysts are sensitive to air and moisture. The phosphines used in this chemistry have also been shown to undergo significant P-C degradation at elevated temperature. Therefore, the successful use of phosphine-Pd catalysts generally required air-free handling to minimize ligand oxidation and/or catalyst degradation. Thus, Herrmann's discovery that NHC ligands can be effective analogs of phosphine in Pd-

chemistry in 1995 led to many studies of NHC-Pd catalysis.[21] In general, these studies have shown that NHC-Pd complexes are found to be more stable than their phosphine analogs yet are also highly active. Chart 3 illustrates a variety of NHC-Pd complexes that have been found to be useful in catalytic coupling reactions as catalysts or precatalysts.

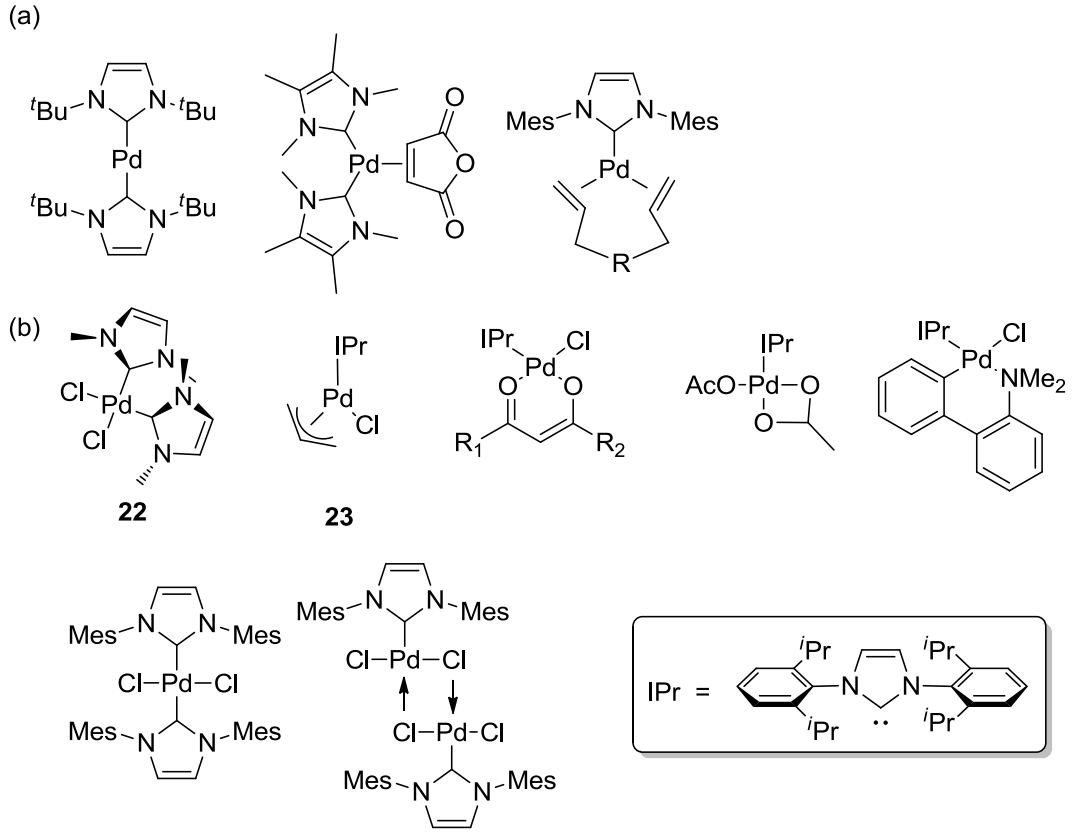

Chart 3. Examples of active (a) NHC-Pd(0) and (b) NHC-Pd(II) catalysts.

In general, these Pd-catalyzed coupling reactions proceed via a three-step mechanism with palladium undergoing Pd(0)/Pd(II) oxidation state changes (Scheme 17). The initial palladium source may be either a Pd(0) or Pd(II) complex. However, it

is believed Pd(0) species are the actual active catalysts in catalytic cycles. When a Pd(II) complex was used in a catalytic reaction, a reduction agent is required to form the active Pd(0) catalyst. The reduction agents are often phosphines or amines. The initial step in the three-step catalytic cycle goes through an oxidative addition of an aryl halide with the Pd(0) species leading to Pd(II) intermediates. A transmetallation reaction then yields a Pd(II) species containing the two groups that are coupled in the last reductive elimination step, in which the Pd(0) regenerates. In this mechanism, the nature of aryl halides and the Pd(0) complexes determine the rate-determining step. For example, a less reactive substrate like an aryl chloride or an unactivated aryl bromide makes the oxidative addition more difficult. As a consequence, coupling reactions with aryl chlorides or unactivated aryl bromides usually proceed more slowly or require more active catalysts. Such catalysts can be formed with suitable ligands. Moreover, ligands can also affect the stabilities of the intermediates and lead to changes in the rate-determining step.

In 2004, a PIB-supported SCS-Pd catalyst and a PIB-supported phosphine-Pd catalyst were prepared and found to be competent catalysts for these reactions. These catalysts were successfully recycled for four reaction cycles without loss of catalyst activity. The success of these PIB-supported catalysts and the stability and highly reactivity of NHC-Pd catalysts suggested that an investigation of PIB-supported NHC-Pd catalysts would warranted as such PIB-bound NHC-Pd catalysts might be good candidates as recyclable and reusable cross-coupling catalysts.

Scheme 17. General mechanism of Pd-catalyzed reactions.

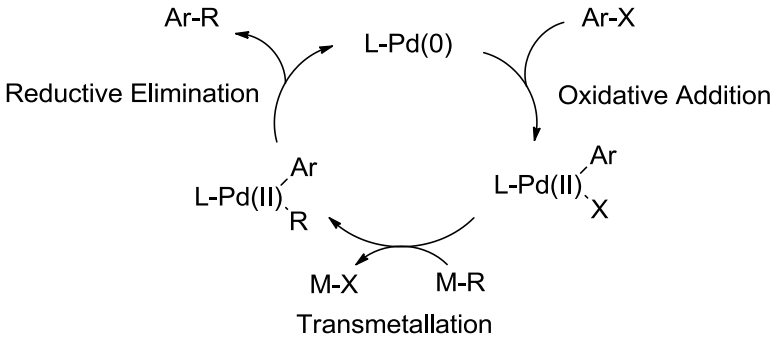

In planning this approach, many NHC-Pd cross-coupling catalysts were considered. These included Pd complexes with both simple *N*,*N*'-dialkyl NHC ligands or more elaborate Pd complexes prepared from sterically encumbered *N*,*N*'-diaryl NHC ligands. For example, the complex **22** in Chart 3 is a NHC-Pd complex with two *N*-alkyl substituents on an NHC ligand. This complex is analogous to one described in 1995 by Herrmann.[21] (IPr)PdCl(allyl), the complex **23** in Chart 3, is an example of an NHC-Pd complex with sterically hindered *N*-aryl substituents.[46] This catalyst is analogous to low molecular weight species designed and studied by Nolan's group. The complex **22** had been shown to be active for Heck catalysis while the complex **23** had been shown to catalyze aryl animation, Suzuki-Miyaura crosscouplings, and α-arylation of ketones (Scheme 18). The balance of this chapter describes the synthesis of **24** and **25** as PIB versions of these NHC-complexed Pd catalysts and the attempted recycling of these catalysts in cross-coupling chemistry using the general scheme shown in Figure 10.

Scheme 18. Reactions catalyzed by NHC-Pd complexes (a) **22** and (b) **23**.

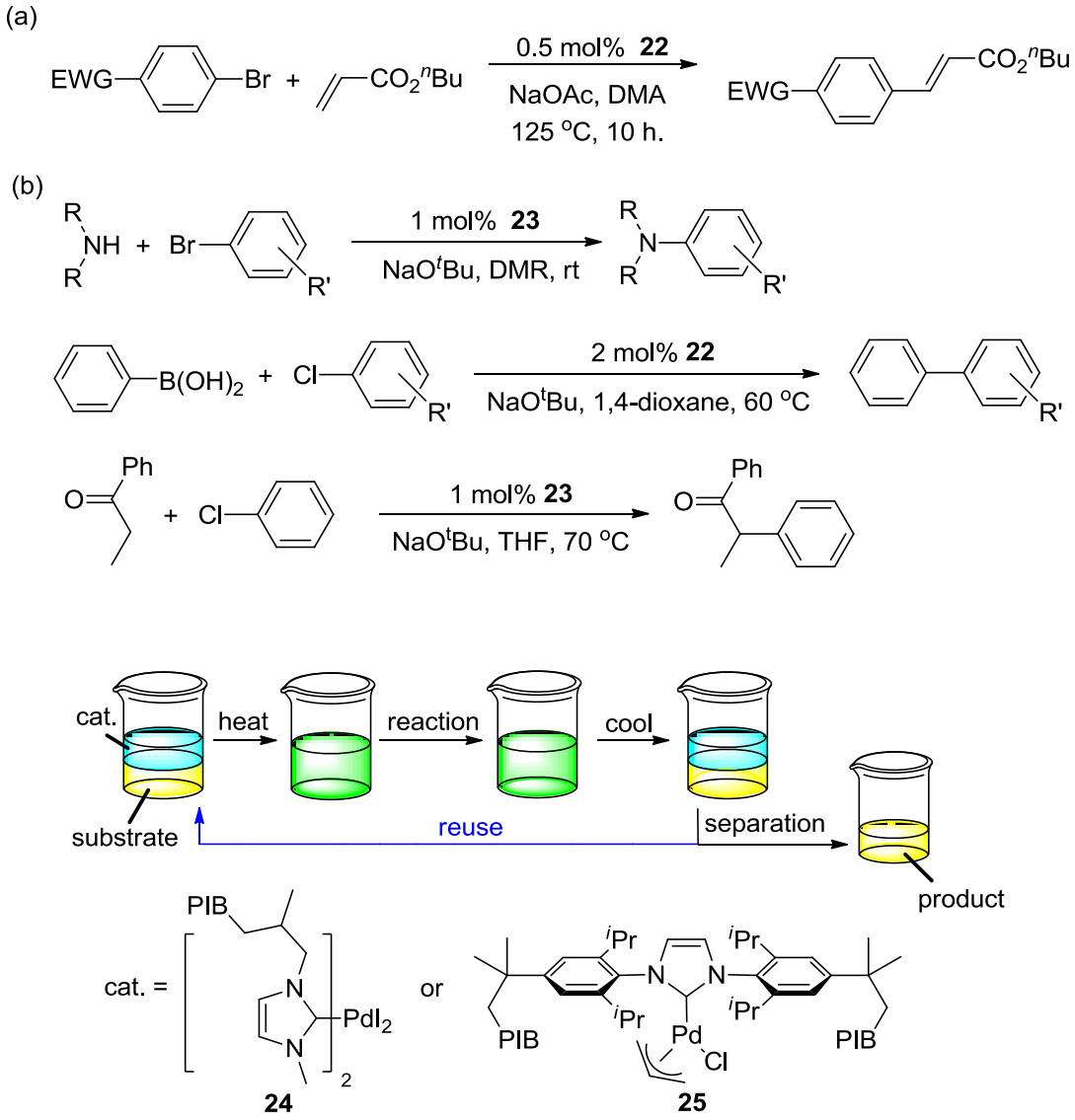

Figure 10. Proposed PIB versions of NHC-Pd complexes and the utilities of them for recyclable catalysts.

Synthesis of PIB-bound Imidazolium Salts

Synthesis of the PIB supported imidazolium salt **28**, a precursor of the desired PIB-bound NHC-Pd complexes, is relatively straightforward and proceeds via a S_N2 reaction of an *N*-methylimidazole on an appropriately substituted PIB derivative

(Scheme 19). While the ligands herein were prepared with PIB whose average molecular weight was 1300 Da, the same chemistry works with other molecular weight PIB derivatives. In this case, the necessary PIB substrate was obtained by a hydroboration-oxidation reaction of an alkene-terminated polyisobutylene. The product hydroxy-terminated polyisobutylene **26** was then converted into the PIB-mesylate **27**. This PIB mesylate was then allowed to react with *N*-methylimidazole in the presence of sodium iodide to form the desired imidazolium salt **28**. This product was characterized by ^{1}H and ^{13}C NMR spectroscopy. The ^{1}H NMR spectrum was diagnostic in that it contained a peak at 10.59 ppm which was assigned as the acidic proton at the 2-position of the imidazolium ring.

The synthesis of the imidazolium salt **31** followed a prior synthetic procedure (see Chapter I and Scheme 19) used to prepare an *N*,*N*'-bisarylimidazolium salt from the PIB-bound aniline **29**. The desired starting material **29** was prepared from the reaction of polyisobutylene with 2,6-diisopropylaniline at 200 ^{o}C in the presence of aluminum chloride. Under these conditions, the Friedel-Crafts reaction of the alkene-terminated PIB and the 2,6-disubstituted aniline was successful leading to a 65% yield of the desired 4-polyisobutyl-2,6-diisopropylaniline **29**. The PIB-bound aniline **29** was treated with glyoxal to generate a diimime **30** and following cyclized with chloromethyl ethyl ether to afford the desired imidazoliumsalt **31** on a two-gram scale.

Scheme 19. Synthesis of the PIB-bound imidazolium salts **28** and **31**.

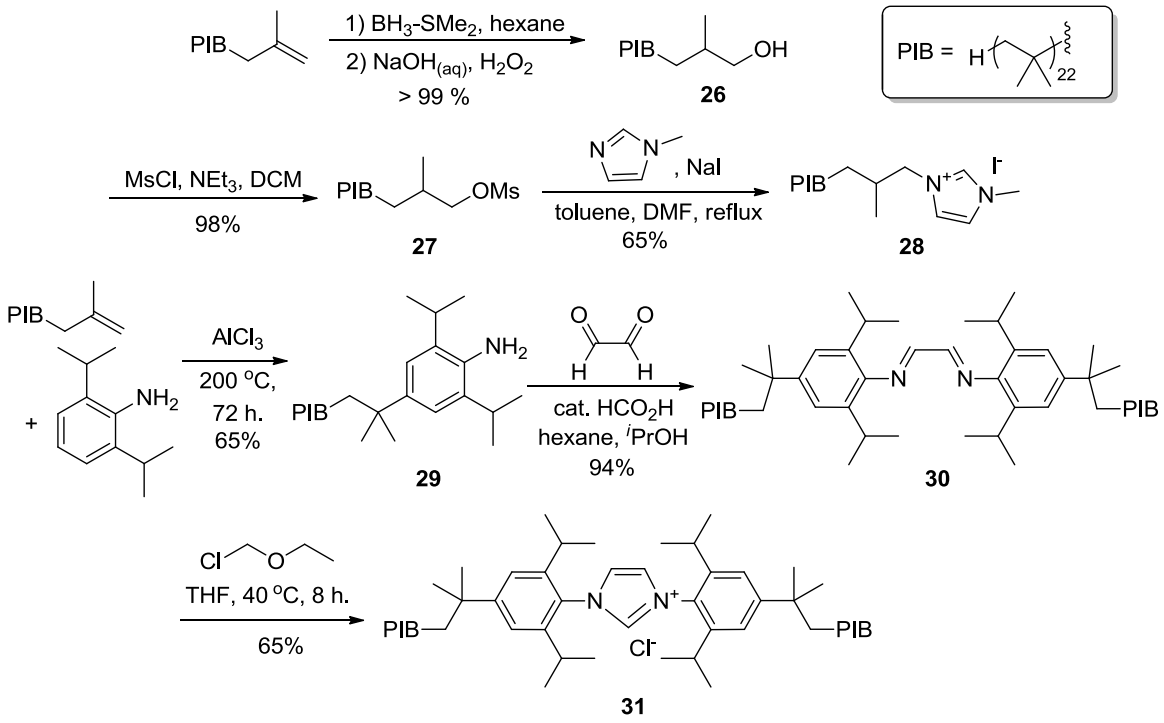

Synthesis of PIB-bound NHC-Pd Catalysts

The desired PIB-bound (IPr)PdCl(allyl) catalyst **25** was prepared via a PIB-bound NHC-Ag intermediate **32**, (Scheme 20) which was prepared in quantitative yield from **31** using silver oxide following procedures reported by others. The silver complex was then used in a transmetallation reaction with the allylpalladium chloride dimer to form the PIB-bound (IPr)PdCl(allyl) catalyst **25**.

Scheme 20. Synthesis of the PIB-bound (IPr)PdCl(allyl) catalyst **25**.

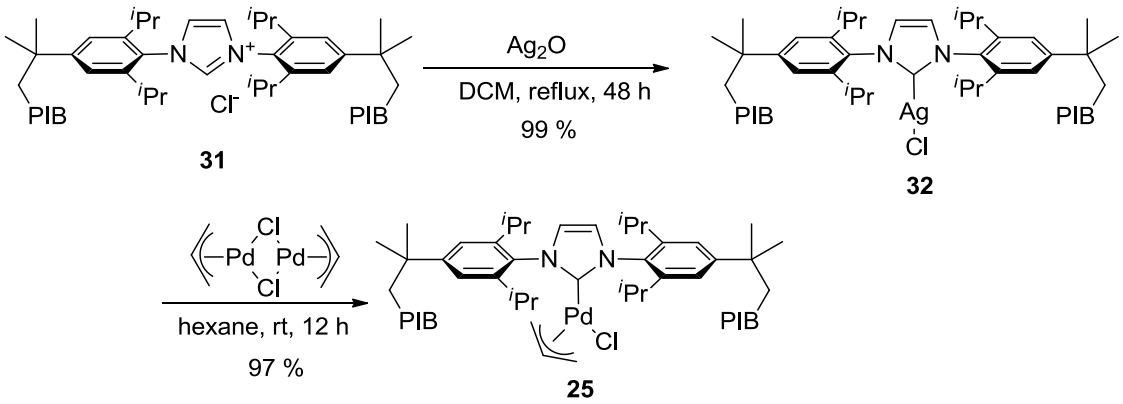

A second PIB-bound NHC-Pd complex was prepared by treating imidazolium salt **28** first with potassium *t*-butoxide and then with bis(benzonitrile)dichloro-palladium(II) (Scheme 21). This deprotonation-metalation reaction was carried out in the presence of NaI and led to a 58% yield of the product **24**. This reaction was monitored by ^{1}H NMR spectroscopy. The disappearance of the peak at 10.59 ppm (which was assigned to the proton at the 2-position of the imidazolium ring) was followed to determine when this reactionwas complete. Complex **24** was then isolated and characterized spectroscopically.

Scheme 21. Synthesis of the PIB-bound palladium catalyst **24**.

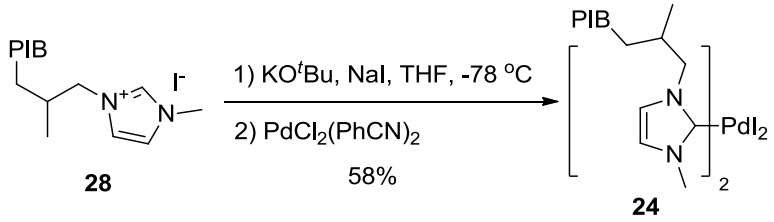

Reactivity and Recyclability of PIB-bound NHC-Pd Complexes in Pd-catalyzed Cross-coupling Reactions

The PIB-bound NHC complexes **24** and **25** were found to be stable for up to two years when stored on a bench top and were visually phase selectively soluble in heptane versus polar solvents. This phase selective solubility is illustrated in Figure 11. This figure shows that both **24** and **25** are phase selectively soluble in heptane versus acetonitrile or DMF.

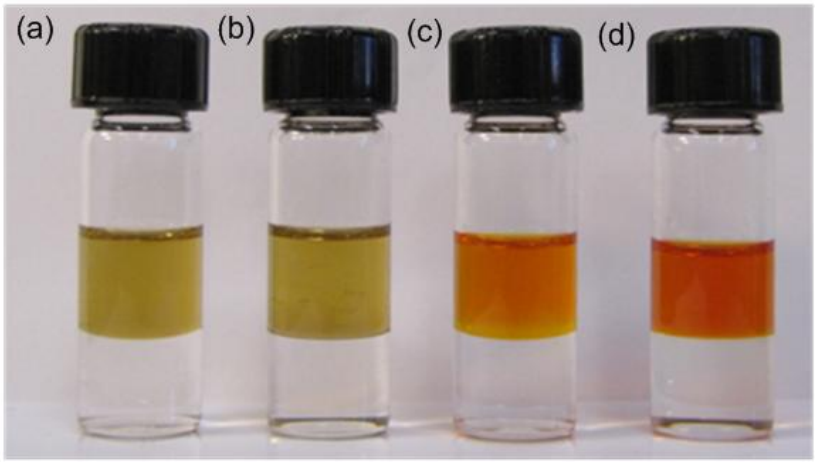

Figure 11. The phase selective solubility of **25** and **24** in heptane vs. polar solvents at room temperature: (a) **25** in heptane vs. acetonitrile; (b) **25** in heptane vs. DMF; (c) **24** in heptane vs. acetonitrile; and (d) **24** in heptane vs. DMF.

The PIB-bound catalyst **25** was first examined in a Buchwald-Hartwig aryl amination reaction (Scheme 22). With 1 mol% catalyst, 4-bromotoluene underwent complete conversion to *N*-(4-methylphenyl)morpholine within 20 min at 80 ^{o}C in

heptane or 1,2-dimethoxyethane. However, it was also observed that the solution discolored during the reaction forming a dark brown solution. In the case of the heptane reaction, the active catalyst was separated by using acetonitrile to extract the reaction product from this dark brown solution. This led to a biphasic mixture of an acetonitrile solution of the *N*-(4-methylphenyl)morpholine product and a heptane phase that was presumed containing the PIB-bound NHC-Pd catalyst. This heptane solution was successfully used in a second reaction cycle. However, complete conversion of 4-bromotoluene to the product required extended reaction time to 8 h. Attempts to separate product from the catalyst phase and reuse the catalyst in a third cycle were even less successful with the reaction not proceeding to completion after 16 h at 80 ^{o}C.

Scheme 22. The use of the PIB-bound palladium complex **25** as a catalyst for Buchwald-Hartwig reaction.

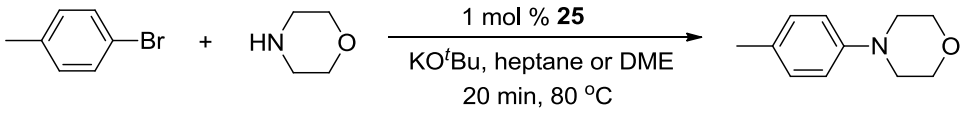

The catalyst **25** was also examined for a Heck coupling reaction (Scheme 23). Recycling of **25** in this Heck reaction led to similar results as seen above for recycling **25** in amination chemistry. The coupling between 4-iodoacetophenone and *n*-butyl acrylate in the presence of Et_3N in the mixture of decane and DMF at 65 ^{o}C required 10 h in the first cycle. However, the catalyst reactivity decreased in a second and third

cycle with complete formation of a Heck product only occurring after 36 h at 100 ^{o}C in the third cycle.

Scheme 23. The use of the PIB-bound palladium complex **25** as a catalyst for a Heck reaction.

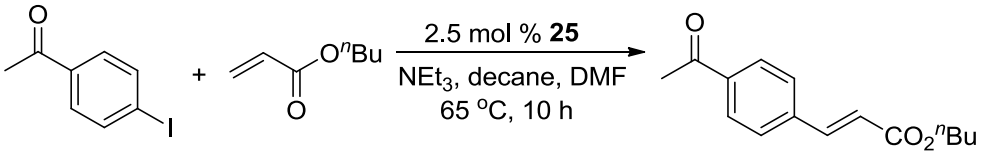

To understand why recycling of **25** was ineffective, the following tests were done to examine the stability of **25** under the reaction conditions. First, complex **25** was dissolved in benzene-d6 and its ^{1}H NMR spectrum was measured. Then 50 equivalents of potassium *t*-butoxide were added. After 3 h at 60 ^{o}C, the solution became brown. ^{1}H NMR spectroscopic analysis of this solution showed that the peaks in the region of 4.90-2.50 ppm (which were assigned to the allylic protons of **25**) became broad. This suggested some decomposition of **25** had occurred. If an acrylate ester and an aryl iodide were added at this point, no conversion to a Heck product was seen in 10 h at 60 ^{o}C. Darkening of Pd catalyst solutions is often associated with formation of Pd colloids. To determine if this was the case, **25** was dissolved in decane and the solution was placed in capillary tubes that were examined under a microscope. In the absence of base, no discoloration and no precipitation was apparent after heating at 100 ^{o}C for 60 h. However, when another solution of **25** was prepared containing 10 equivalents of Et_3N, the solution formed some black precipitate after several days at room temperature or

after heating at 60 ^{o}C for 1 h. Figure 12 shows an example of the observed black precipitate. The precipitate is presumed as the Pd colloids. The decomposition of **25** is believed as the reasons why solutions of **25** darken and become increasingly inactive in both the Buchwald-Hartwig and Heck reactions.

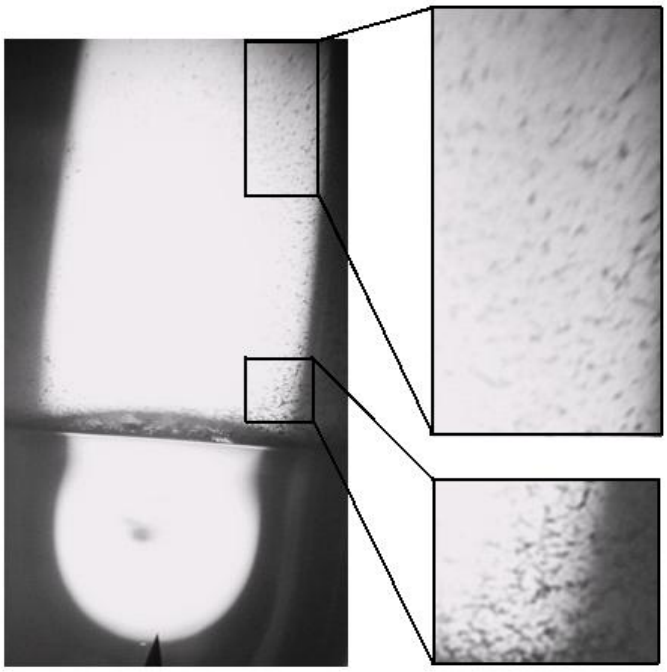

Figure 12. Complex **25** was dissolved in decane in a capillary tube and examined microscopically after the addition of Et_3N and heating at 60 ^{o}C for 1 h. The black precipitate observed is believed to be palladium colloid formed in decomposition of **25**.

Given the problems in recycling **25**, the simpler *N*,*N*'-dialkyl NHC-Pd complex **24** was also studied. This premise was tested by examining the use of **24** in the Heck coupling of 4-iodoacetophenone and *n*-butyl acrylate in the presence of Et_3N in a

thermomorphic mixture of heptane and DMF at 75 ^{o}C. Recycling was examined with various catalyst loading levels. While the reactivity of the catalyst is unexceptional, the results in Scheme 24 show that recycling was successful. These recycling experiments used a thermomorphic mixture of heptane and DMF that is miscible hot but immiscible at room temperature. In this case, a biphasic mixture forms when the monphasic reaction mixture was cooled to room temperature. In this mixture, the upper heptane-rich phase contained the PIB-bound catalyst, some DMF, and some product. No starting material was present. The lower DMF phase contained most of the product. The absence of starting material in this phase and in the upper phase allowed us to estimate that the conversion was >97%. As is true in other themomorphic systems, some extractable product remains in the catalyst-containing upper phase. While as the prior work shown, the product concentration in the upper phase rapidly becomes constant because the heptane-rich phase becomes saturated in product. Thus, high yields of product can be isolated from the polar phase after several cycles of such separations. Just as was done previously, we separated the lower polar product-containing phase by a gravity separation. Recycling simply involved the addition of fresh substrates, base and DMF to the heptane-rich phase. This procedure was used for 10 cycles without any change in measured conversion of substrate to product. In this study, ^{1}H NMR spectroscopy was used to determine the extent of conversion of 4-iodoacetophenone to product.

Scheme 24. Synthesis of the PIB-bound palladium catalyst **1** and the use of catalyst **24** as a reusable catalyst for Heck reaction.

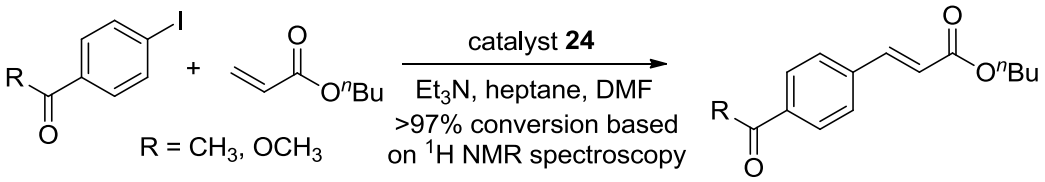

catalyst loading	Temperature	reaction time	cycle tested
5 mol %	75 ^{o}C	14 h	10
1 mol %	75 ^{o}C	46 h	10
1 mol %	130 ^{o}C (MW)	0.5 h	6

This catalyst was also used with a different aryl iodide substrate, methyl 4-iodobenzoate. In this experiment, methyl 4-iodobenzoate was substituted as a substrate after four cycles of a Heck coupling of *n*-butyl acrylate and 4-iodoacetophenone. The subsequent catalytic reaction led to 100% conversion of methyl 4-iodobenzoate to the expected Heck product based on ^{1}H NMR spectroscopy. The experiments were also briefly examined using microwave conditions. At 130 ^{o}C in a microwave reactor, the reaction time was considerably shortened but catalyst recycling was still equally effective. These results are summarized in Scheme 24.

While I did not look for the Pd colloid formation with microscope in this reaction, an ICP-MS (inductively coupled mass spectroscopy) analysis was carried out to determine the metal leaching in the DMF phase from a Heck coupling of 4-iodoacetophenone and *n*-butyl acrylate with 1 mol% of **24**. That analysis showed that a modest amount of metal leaching occurred with ca. 1% of the charged Pd metal loading being lost in cycle 2 and 3 and 0.2% in cycle 10.

Conclusion

Two imidazolium salts bound to a nonpolar solvent-soluble polymer, polyisobutylene, were prepared. On deprotonation, either can bind to palladium(II) to form NHC-Pd(II) complexes that can be phase isolated in the heptane phase of a mixture of heptane and an immiscible polar solvent. These complexes' catalytic properties and the abilities for recycling and reusing are examined. Using a PIB-bound NHC-allylPd catalyst **25**, aryl amination, even with a relatively unreactive aryl bromide, showed that **25** had activity in a heptane solution like that of its low molecular weight counterpart. However, the instability of this complex in the reaction mixture made recycling this catalyst more than two cycles problematic in aryl amination or even in reactions with very reactive Heck substrates. Catalyst recyclability was more successful with simpler PIB-bound NHC-complexed Pd catalyst **24**.

The decomposition mechanism of **25** (and its low molecular weight counterpart **23**) is still not clear now. However, as has been observed in other cases, this incompletely understood Pd-catalyst decomposition mechanism and the deactivation of the Pd-catalysts is evidenced by Pd colloid formation. In my case, microscopic analysis and visual examination of the reaction solution provided a simple, easy and quick way to judge the catalyst stabilities and provided evidence for a decomposition pathway that led to the formation of Pd colloids.

The stability of **25** on a bench top and in heating conditions but quick decomposition in the present of large amounts of potassium *t*-butoxide and Et_3N suggested the decomposition may due to these bases/nucleophiles, which can attack the

allyl groups and generate Pd(0) species quickly. While the Pd(0) complex is expected to be the actual active species for a coupling reaction, it may also be labile without substrates present in the solution, *i.e*. the coupling reaction and the Pd(0) aggregation may be two competition reactions. Nolan has noted that "in contrast to the plethora of Pd(II) complexes stabilized by NHC ligands, examples of NHC-Pd(0) are relatively scarce,"[3] suggesting that although NHC-Pd(II) complexes are stable, the NHC ligands may be less effective in stabilizing Pd(0). This makes the recycling of the catalysts problematic. The reasons why **24** or some other catalysts can be recycled and reused for many times could be explained by slow activation rate of those precatalysts. The successful development of recyclable and reusable catalysts in these cases may require the development of Pd(0) stabilization ligands or of a catalytic process in which the more stable Pd(II) catalysts can be regenerated after each catalytic reaction.

CHAPTER III

PIB AS A PHASE ANCHOR FOR NHC-RUTHENIUM(II) BASED OLEFIN METATHESIS CATALYSTS*

Introduction

The word "metathesis" is derived from two Greek words "μετά" and "θεσις" meaning "change" and "position," respectively. In chemistry, metathesis refers to a category of chemical reactions involving the position exchange of two atoms or two functional groups. The concept of metathesis reactions is demonstrated in Scheme 25 with several examples of metathesis reactions. In this dissertation, only olefin metathesis will be discussed.

Scheme 25. General equations and examples of different types of metathesis reactions.

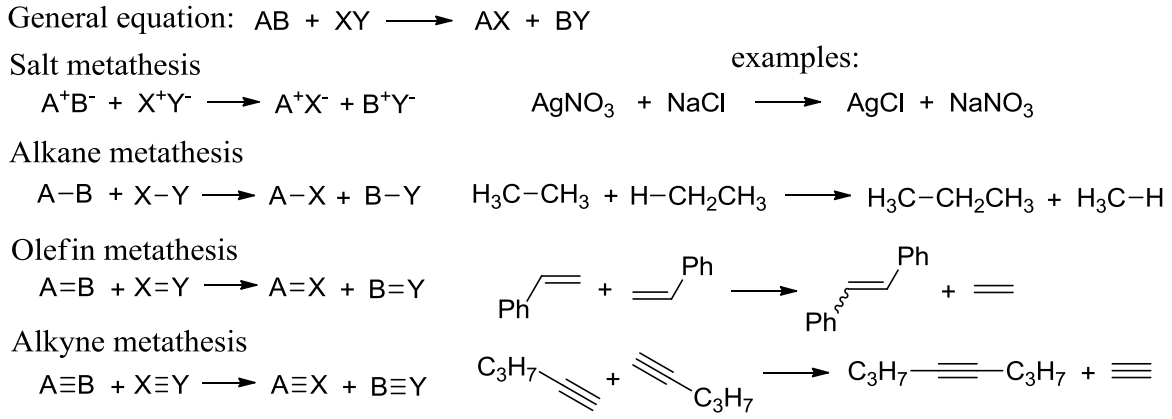

* Part of the data reported in this chapter is reprinted with permission from "Polyisobutylene Phase-Anchored Ruthenium Complexes" by H.-L. Su, C. Hongfa, H. S. Bazzi, and D. E. Bergbreiter, *Macromol. Symp.* **2010**, *297*, 25-32, Copyright 2010 by WILEY-VCH Verlag GmbH & Co.KGaA, Weinheim.

Olefin metathesis was first observed by industrial researchers as a side reaction in the study of polymerization when developing Ziegler-Natta catalysts in 1950s.[47] Later, more examples involving olefin metathesis were discovered when using nickel, molybdenum, tungsten, and titanium-based catalysts. However, this chemistry could not be explained at the time. In 1967, Calderon *et al.* at Goodyear Tire & Rubber Co. proposed the first exchange mechanism and named the reaction "olefin metathesis."[48] From then on, numerous mechanisms involving various intermediates were proposed. Many experiments were carried out to support the proposed intermediates or to rule out incorrect mechanisms. A mechanism involving metal alkylidenes and 4-membered metallacycle intermediates was first proposed by Par Jean-Louis Hérisson and Yves Chauvin in 1971 to explain the statistical distribution of olefin metathesis products.[49] This mechanism, as shown in Scheme 25, is accepted as the actual olefin metathesis mechanism today.

Scheme 26. Proposed olefin metathesis mechanism by Hérisson and Chauvin in 1971.[49]

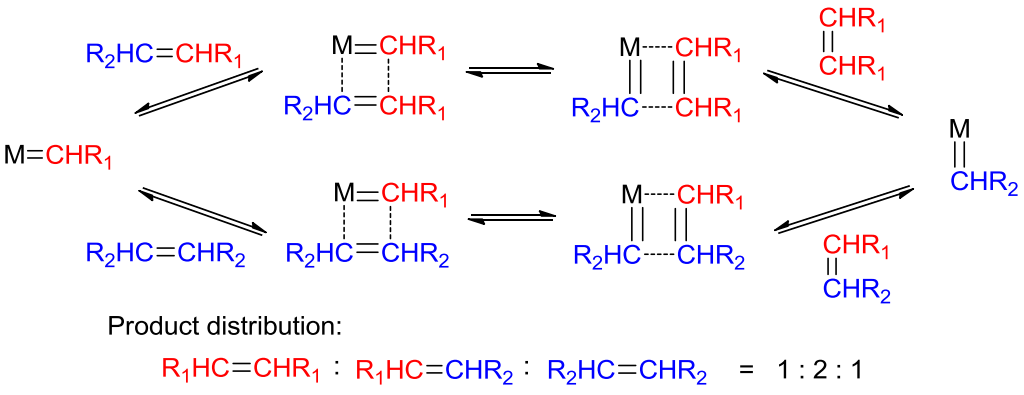

For a long period of time (1950s-1980s), the development of olefin metathesis catalysts was focused on the early transition metal-based catalysts. Late transition metal candidates were initially ignored.[50] During this period of time, many well-defined catalysts were developed, such as the Tebbe reagent and molybdenum-based catalysts created by Schrock (Chart 4). However, although these catalysts are active in olefin metathesis reactions, they are sensitive to moisture and are difficult to prepare and handle. [50] Thus, conducting olefin metathesis usually required strict reaction conditions, such as dry degassed solvents and inert atmosphere. These limitations restricted the application of olefin metathesis.

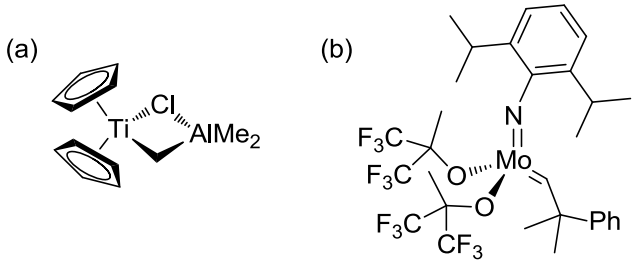

Chart 4. (a) The Tebbe reagent and (b) molybdenum-based olefin metathesis catalyst developed by Schrock.[50]

In 1992, the first well-defined ruthenium alkylidene-based metathesis catalyst was announced by the Grubbs' group (Chart 5).[51] The reactivity of the Grubbs' earliest generation of a ruthenium alkylidene-based metathesis catalyst was low and it could only polymerize highly-strained olefins. In order to find appropriate ligands to improve the catalyst reactivity, Grubbs and coworkers spent a year testing a variety of ligands.[50]

Finally, a more active catalyst was developed by substituting the triphenylphosphine ligand with a highly electron-donating and sterically crowded trycyclohexylphosphine ligand.[52] This new catalyst was active in ring-closing metathesis (RCM), ring-opening metathesis polymerization (ROMP), acyclic diene metathesis (ADMET) polymerization, etc. These phosphine-ligated ruthenium catalysts came to be known as the 1st generation Grubbs catalyst.

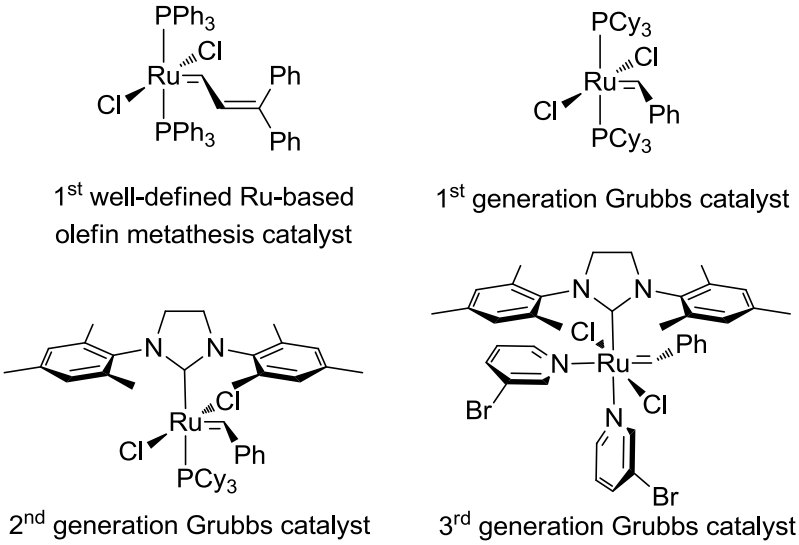

Chart 5. Some ruthenium-based olefin metathesis catalysts developed in Grubbs' group.

Because NHCs had been earlier shown to be effective analogs of phosphine (or even better ligand with stronger σ-donation) in organometallic chemistry, they were potential effective ligands for Grubbs catalyst. In 1998, Herrmann's group pioneered using NHCs to substitute the two phosphine ligands in the 1st generation Grubbs

catalyst.[53] However, the new bis(NHC)-based catalysts provided only slight improvement in activity. In the following year, a series of complexes with mixed NHC and phosphine ligands were prepared and studied in Herrmann's,[54] Nolan's,[55] and Grubbs'[56] groups. Many of these catalysts showed superior reactivity to the bis(NHC) and bis(phosphine) complexes with notable tolerance to air and various functional groups. These catalysts are now called the 2nd generation Grubbs catalysts.

Since the discovery of more active ruthenium-based olefin metathesis catalysts, many groups studied the details of the catalytic mechanism in order to modify the catalysts to improve their activity, stability, regioselectivity, stereoselectivity and recyclability. These studies are focused on the effects of using different ligands, anions, and alkylidenes in Grubbs catalyst. Four factors are generally considered when comparing these Grubbs-type ruthenium catalysts' reactivity. One is the rate at which the active species for the catalytic cycle is generated. Generally, this factor is represented as the ligand dissociation constant k_1 in Scheme 27. The second factor relates to how the active species acts. Because the active species may bind with an olefin to proceed the reaction or bind to the dissociated ligand L' and regenerate the catalyst, the activity of the active species is usually represented as k_2/k_{-1}. When an olefin is bound to the ruthenium, the complex will undergo the metathesis via a 4-membered metallacycle intermediate. This step is normally faster than other steps and ignored though this is not the case in comparing the 1st and 2nd generation Grubbs catalyst where 1st generation catalysts activity is much lower (1:10000).[50] However, this step is still important in considering regioselectivity and stereoselectivity because the details of this

rearrangement step determine the product geometry. The last consideration is the lifetime of the catalysts. For the Grubbs-type ruthenium catalysts, the effects of ligand substitutions have been systematically studied with regard to these factors. The conclusions of these studies are summarized in Figure 13. The conclusion of importance to the work below is that the NHC-based 2nd generation Grubbs catalyst shows better tolerance of functional groups and is more stable at high temperature. It also has a higher catalytic reaction rate and a longer lifetime.

Scheme 27. The reaction mechanism of Grubbs-type olefin metathesis catalysts.[50]

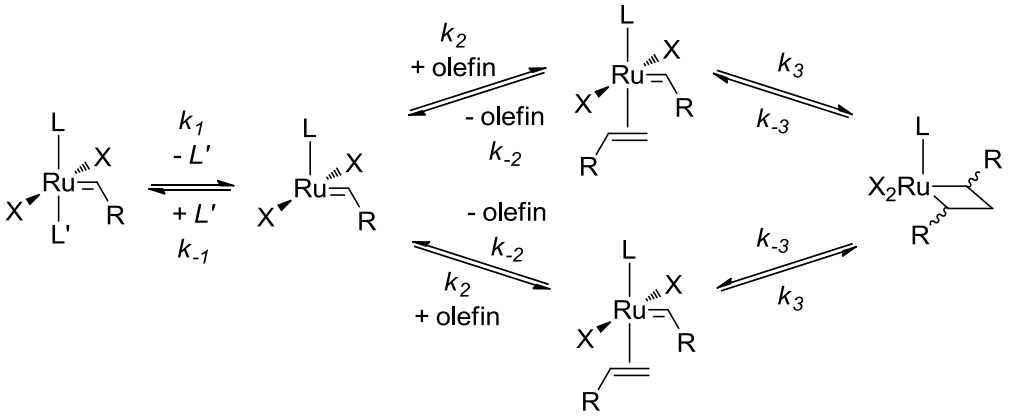

In early 2000s, Grubbs and coworkers found that excess amount of pyridine can replace the phosphine ligand in the 2nd generation Grubbs catalyst and created a new type of catalysts.[57] The labile pyridine ligands dissociated easily so the catalyst demonstrated a very high initiation rate in olefin metathesis. Among various pyridine-ligated catalysts, the catalyst with *m*-bromopyridine provided the highest initiation rate and is now called the 3rd generation Grubbs catalyst.[58] Theoretically, the 2nd and 3rd

generation catalysts share the same active species and should have similar reaction speed and catalyst lifetime. However, with pyridines as "throw-away" ligands, the 3rd generation Grubbs catalyst has a shorter induction period.

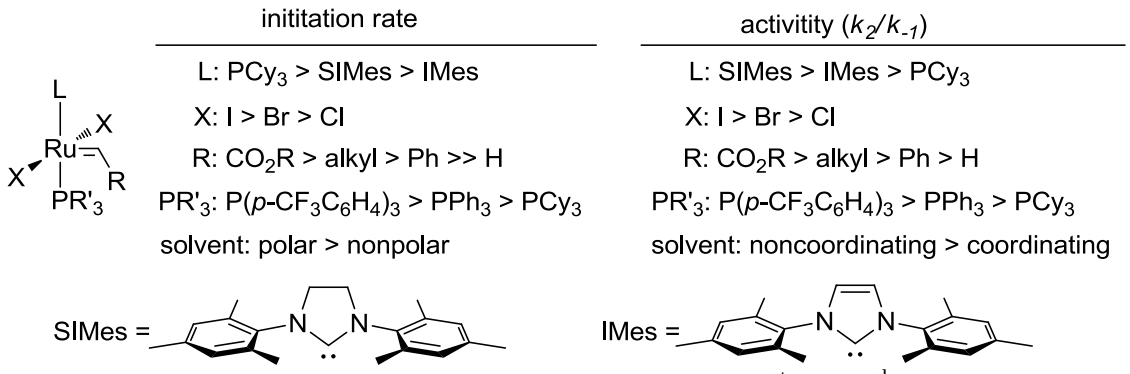

Figure 13. A brief summary of the substitution effects in 1st and 2nd generation Grubbs-type ruthenium-based olefin metathesis catalysts in terms of initiation rate and activity.[50,59]

At little earlier, the Hoveyda group also successfully developed a new category of catalysts based on 1st and 2nd generation Grubbs catalysts.[60,61] In their work, a phosphine ligand was replaced with an isopropyloxy group attached to benzylidene ligand (Chart 6). In these complexes, the benzylidene isopropyl ether serves as a chelating ligand. In addition, both species in Chart 6 are more stable than the Grubbs catalysts and can be purified with column chromatography. These catalysts are termed the Hoveyda-Grubbs catalysts.

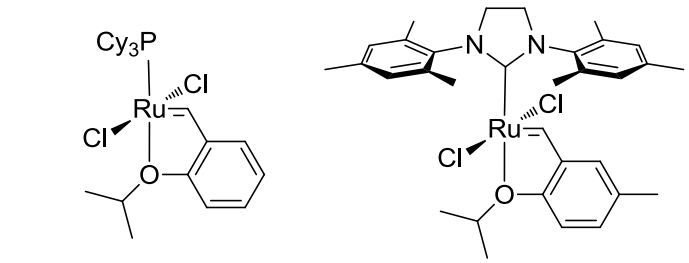

1st generation Hoveyda-Grubbs catalyst

2nd generation Hoveyda-Grubbs catalyst

Chart 6. Hoveyda-Grubbs catalysts.[60,61]

The successful development of highly active and stable catalysts for olefin metathesis has had a significant impact in synthetic chemistry. Many medical chemicals can be prepared more efficiently when olefin metathesis is involved in the synthetic strategies, especially in the macrocyclic compounds' synthesis. These catalysts have also led to new materials developed via olefin metathesis polymerization. The overall impact is further evident by the fact that Yves Chauvin, Robert H. Grubbs, and Richard R. Schrock shared the 2005 Nobel Prize in Chemistry for their contributions to olefin metathesis chemistry.

The widespread use and the many applications of the ruthenium-based olefin metathesis catalysts in synthetic and industrial chemistry have in turn led to interest in developing a simple method to purify the reaction products. This is in part because ruthenium residues typically contaminate the products and have to be removed. In addition, since ruthenium is an expensive metal, the recyclability of the catalysts after reactions has become increasing important.

Figure 14 summarizes the various ways recyclable 2nd generation Grubbs or Hoveyda-Grubbs catalysts have been approached. These approaches can be classified into four types: connecting supports to NHC ligands, to anions, to alkylidenes, or to dissociating ligands. In these designs, the recyclability of the catalysts with supports attached onto alkylidene or dissociated ligands, *i.e.* phosphines or benzylidene ethers, relied on the release-return (or so-called "boomerang") mechanism. Modifications on anions are relatively rare but can be successful in the reaction environments that do not contain other anions. Supports that focus on the NHC ligands, which often serve as non-dissociated ligands, are considered to be the best designs for a recyclable Ru metathesis catalyst.

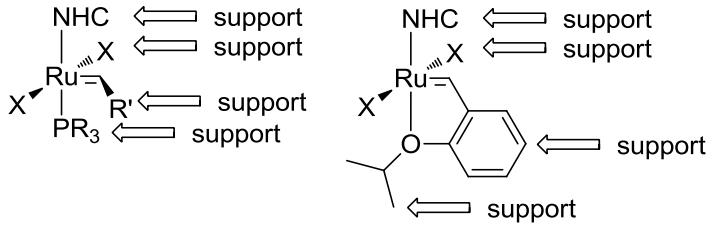

Figure 14. General designs of connecting positions of supported materials onto Grubbs or Hoveyda-Grubbs catalysts.

The Bergbreiter research group started developing recyclable Hoveyda-Grubbs catalysts in 2006. The first example was a catalyst with PIB attached to benzylidene isopropyl ether (**33** in Figure 15). Although *ca.* 96% of the Ru catalyst was recovered after reaction, a photograph of the RCM products (Figure 15) makes it is visually obvious that the product was contaminated by highly colored ruthenium residues.[41] A

better approach to the synthesis of supported Hoveyda-Grubbs catalysts was published in 2009 that involved attaching PIB onto a NHC ligand (**34** in Figure 15).[42] This catalyst could be recycled 11 times without losing catalytic reactivity. With elongation of the reaction time, the catalyst can work for 20 cycles.

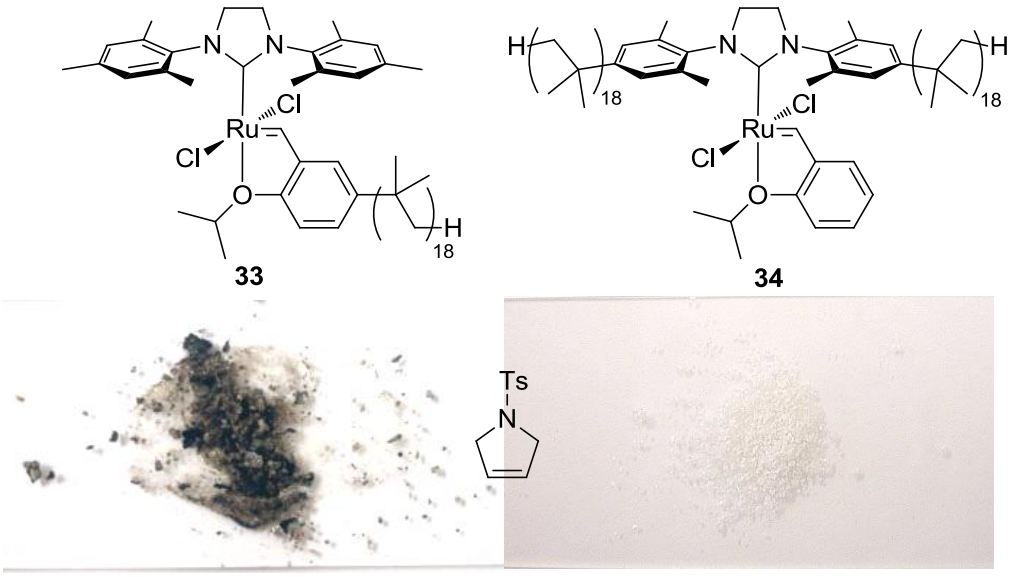

Figure 15. Recyclable Hoveyda-Grubbs catalysts in Bergbreiter's group and their RCM products.[41,42]

New NHC Ligand Designs and the Synthesis of Their Ruthenium Complexes

Many efforts have been made on tuning the stability and reactivity of ruthenium-based olefin metathesis catalysts through changing the substituent groups on NHC ligands and the labile ligands. For instance, when a bulkier 2,6-diisopropylphenyl group was used in place of the mesityl group in a 2nd generation Grubbs catalyst, higher activity in the cross metathesis (CM) of terminal olefins was found.

Another approach to design a better Ru metathesis catalyst is to design a catalyst with a hemilabile ligand. Initial designs of hemilabile ligands attached to ruthenium-based olefin metathesis catalysts were focused on improving the catalyst stability. Hemilabile ligands are a class of chelating ligands with very different coordination properties to the metal atom: one is tightly bound and the other is labile (Scheme 28). The Grubbs-type ruthenium catalysts require both a non-dissociated ligand and a labile ligand which makes hemilabile ligands potential candidates for Ru catalysts. Chart 7 lists some chelating NHC ligands which have been used to date in organometallic chemistry. However, only a few examples of these ligands have been tried for ruthenium-based olefin metathesis catalysts. In many cases, the chelating NHC ligands used to bind to ruthenium contained anion substituents and were not hemilabile ligands. An NHC ligand with a triazole functional group is a good candidate as a hemilabile ligand (Scheme 28) because the triazole group is an easily dissociation ligand. Moreover, triazoles can be easily synthesized from an alkene or alkyne and an azide. An additional advantage of this type of ligand is that it could also be easily attached to a polymer support for recycling. Some organometallic compounds containing this type of ligands were studied at the same time as this work in other groups.

Scheme 28. The concept of using hemilabile ligands in organometallics and the proposed ligands with NHC and triazole functional groups.

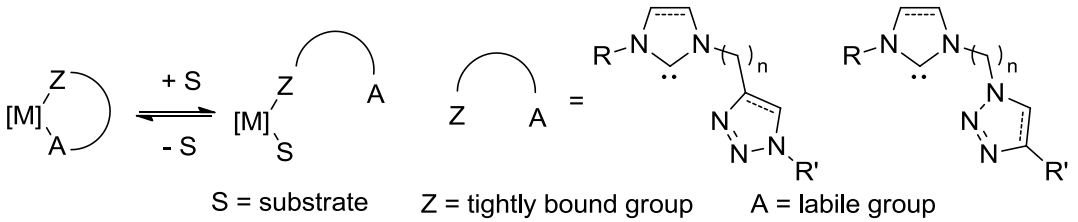

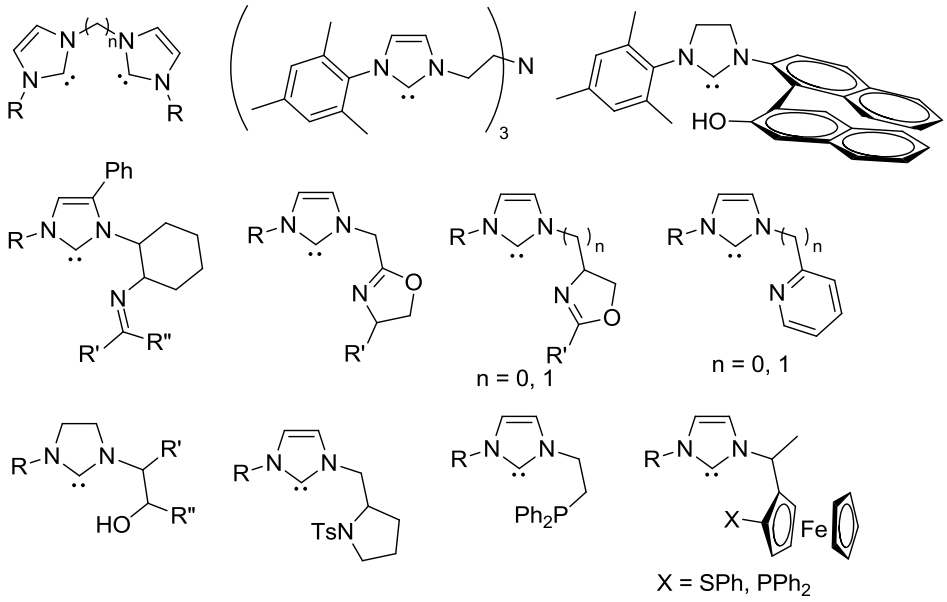

Chart 7. Some examples of chelating NHC ligands.

A retrosynthesis analysis for the imidazolinium salt **35** is shown in Scheme 29. In this analysis, formimidate **36** would be the first synthesized by heating an equimolar mixture of 2,4,6-trimethylaniline and triethyl orthoformate. However, in the actual experiment, both formimidate **36** and the formimidamide **37** were found in the product. To minimize the formation of the formimidamide, an excess amount of triethyl

orthoformate was used. Distillation of the ethanol by-product forced the reaction to completion affording 97 % of formimidate **36** (Scheme 30). The reaction went faster when catalytic amount of acid was added but also produced more formimidamide product. Formimidate **36** is a yellowish oil while formimidamide **37** is a white solid. Formimidate **36** is unstable in the present of catalytic amount of acid and water. It was also noted that storing keeping purified formimidate **36** under air for several days led to formation of a white solid in the bottom of the flask. This solid was characterized by NMR spectroscopy and found to be identical to formimidamide **37**. This degradation process can be explained by the proposed mechanism shown in Scheme 31.

Scheme 29. The retrosynthesis analysis of triazole functional group attached imidazolinium salts.

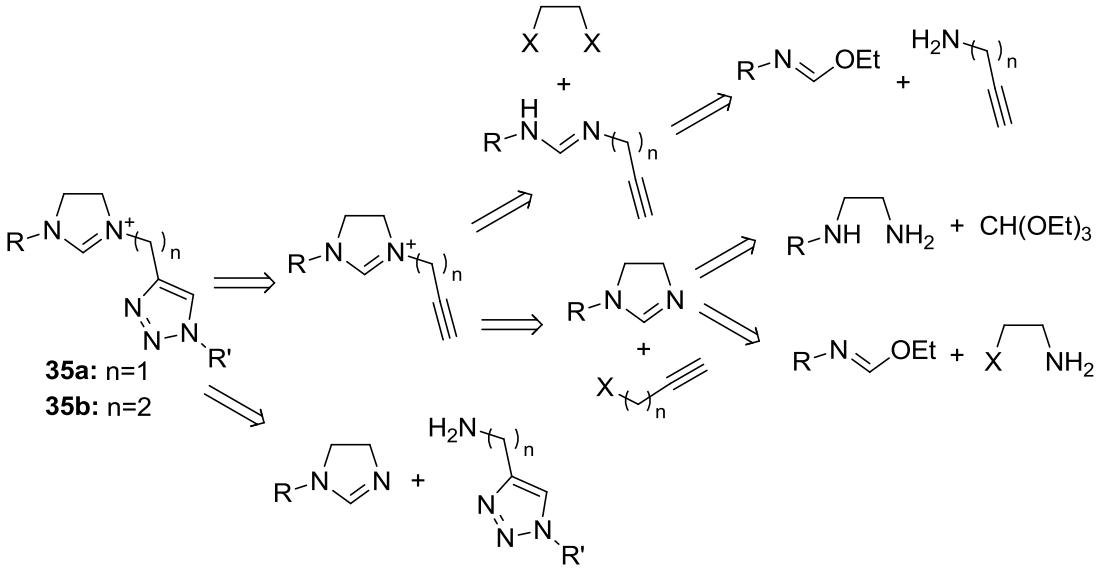

Scheme 30. The preparation of formimidate **36**.

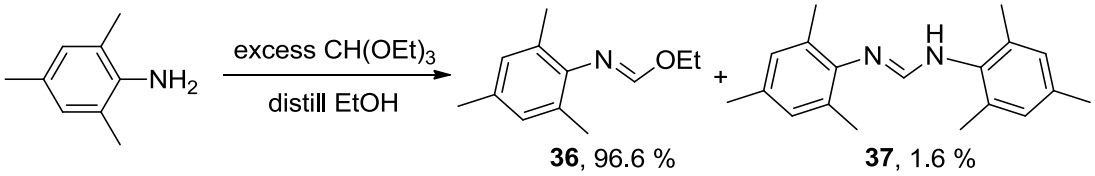

Scheme 31. The proposed mechanism of formimidate **37** decomposition.

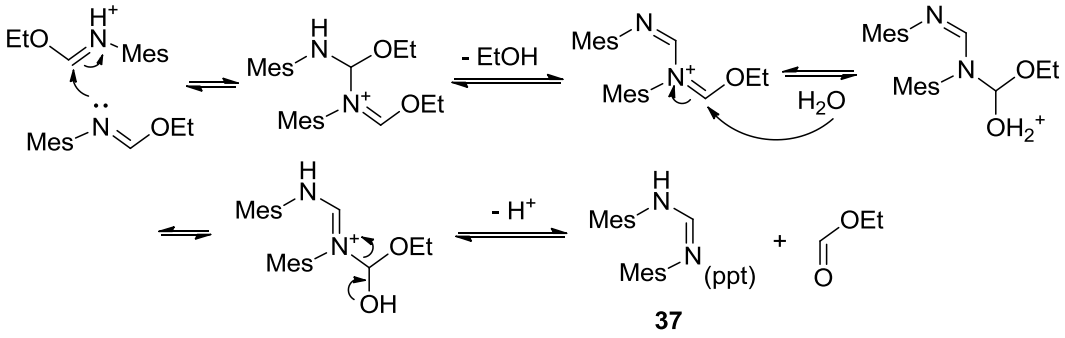

The desired unsymmetrical formimidamide **38** need for synthesis of **35a** was successfully synthesized from freshly prepared formimidate **36** and propargyl amine (Scheme 32). With heating, a complicated product mixture was observed using ^{1}H NMR spectroscopy. However, stirring a mixture of **36** and propargyl amine at room temperature for 2 days produced a precipitate that was characterized as the desired product by using ^{1}H and ^{13}C NMR spectroscopy. Unfortunately, the cyclization of unsymmetrical formimidamide **6** with dichloroethane or dibromoethane in the present of Hünig's base yielded a complicated product mixture.

The mesitylimidazoline **39** was successfully prepared when formimidate **36** was treated with 2-bromoethylamine hydrobromide and a base. In this chemistry, the starting

2-bromoethylammonium salt was deprotonated *in situ* to avoid the formation of aziridine or polyethyleneimine. The reaction was carried out with either diisopropylethylamine or sodium carbonate. **39** can also be generated from *N*-mesitylethylenediamine **40** in a better yield (Scheme 32). Alkylation of mesitylimidazoline **7** with 4-bromo-1-butyne in the present of base afforded complicate product again. However, when the cyclization and alkylation reactions were carried out in one pot, the desired product was isolated in 55% yield. The reasons why many reactions failed in the synthesis will be discussed later.

Scheme 32. The synthesis of *N*-mesityl-*N'*-(but-3-yn-1-yl)-imidazolinium bromide **41**.

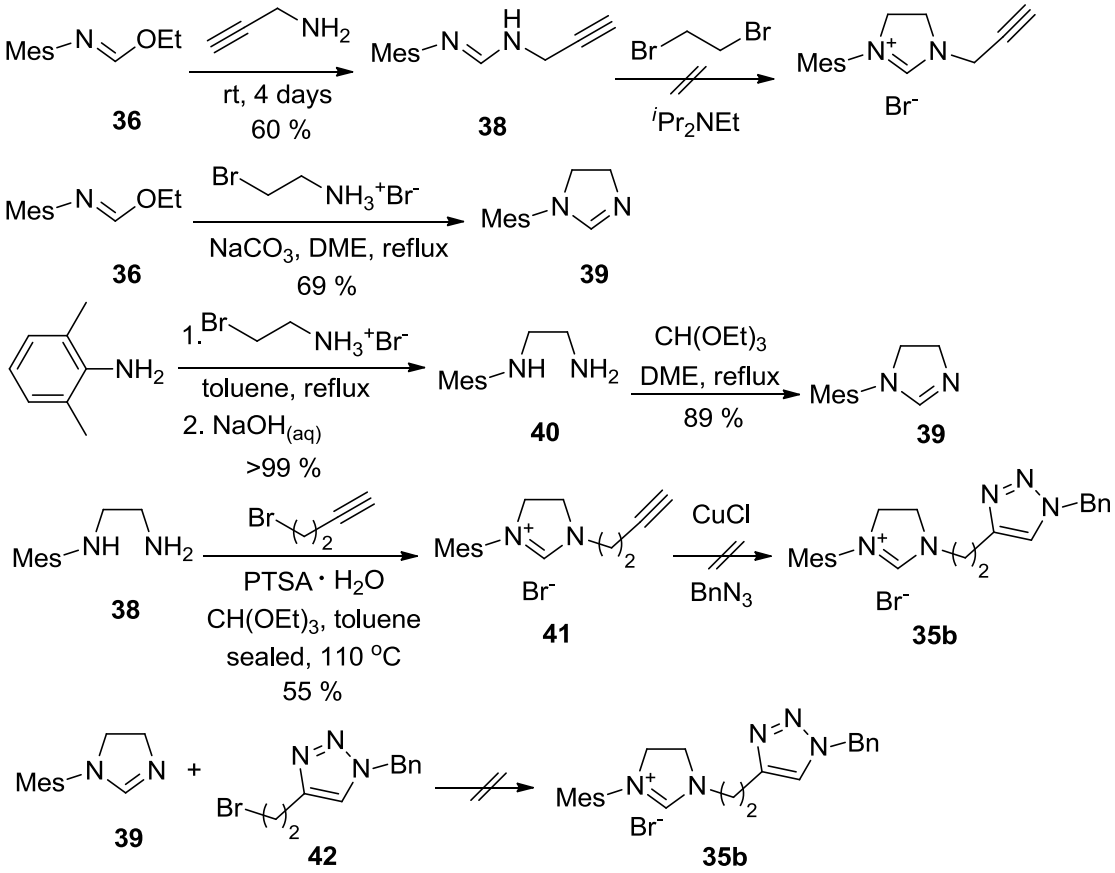

In order to prepare the proposed imidazolinium salts **35b**, the unsymmetric imidazolinium salt **41** was treated with benzyl azide and using CuCl as catalyst in a Cu(I)-catalyzed [3+2] azide-alkyne cycloaddition (CuAAC). However, this reaction provided a complicated product mixture. An alternative synthetic route to prepare the desired imidazolinium salts **35** via an alkylation reaction from mesitylimidazoline **39** and the triazole **42** was equally unsuccessful (Scheme 32).

The problem in the syntheses above eventually recognized in an entirely different project. This other project involved the reaction of an *N*-mesityl-*N'*-alkyl-imidazolinium bromide with Ag_2O. The goal was to prepare the corresponding silver complex **43**. This reaction failed but the actual product could be characterized by NMR spectroscopy as the hydrolysis product (Scheme 33). This hydrolysis was thought to be due to the water generated *in situ* so 4 Å molecular sieve was added to the reaction to avoid the problem. The desired silver complex did form in the reaction but significant amount of the hydrolysis product was still formed. These experimental results suggested that *N*-mesityl-*N'*-octadecylimidazolinium is sensitive to trace amount of water and base. Similar results have been observed by others and a recent paper discussed the hydrolysis of imidazole(in)ium salts and provided the computational calculation explanations.

Scheme 33. Reactions of *N*-mesityl-*N'*-alkylimidazolinium bromide and Ag_2O.

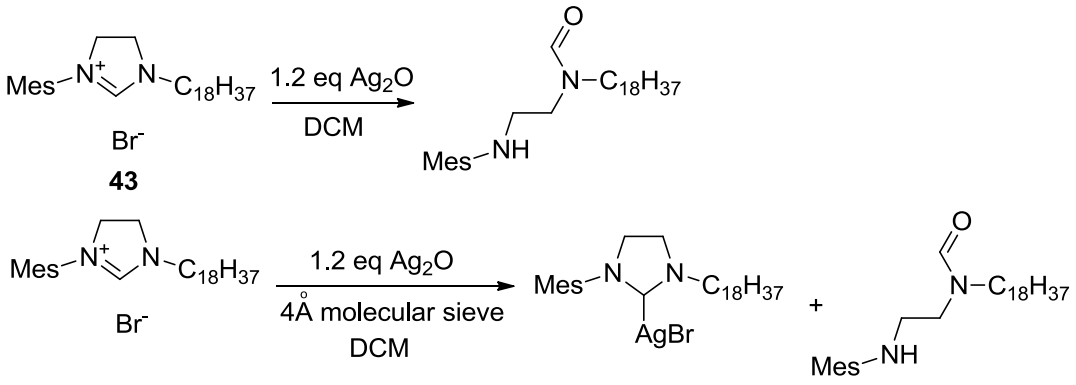

While the preparation of **3** failed, analogs like **44** and **45** that have an imidazolium ring were prepared smoothly (Scheme 34). In these syntheses, the *N*-mesitylimidazole was first prepared using Arduengo's method.[62] This *N*-mesitylimidazole was alkylated with a bromoalkyne. A CuAAC then afforded the desired *N*-mesityl-*N'*-(2-(1-benzyl-1,2,3-triazol-4-yl)ethyl)imidazolium bromide **44**. *N*-mesitylimidazole can also react with other triazoles containing primary alkyl bromides to produce imidazolium salts like **44** and **45** directly.

The imidazolium salts **44** prepared above could be treated with Ag_2O to form the NHC-silver complex **46**. The NHC-silver complex was then allowed to react with 1st generation Hoveyda-Grubbs catalyst in toluene at 60 ^{o}C. Transmetallation occurred but occurred more smoothly at room temperature when 0.6 equiv. of triphenylphosphine was added in the reaction mixture. When the reaction was monitored by ^{31}P NMR spectroscopy, it was found that the tricyclohexylphosphine of the Hoveyda-Grubbs

catalyst was first replaced by triphenylphosphine. Then the triphenylphosphine was substituted by the NHC ligand (Scheme 35).

Scheme 34. Synthesis of triazole connected imidazolium salts.

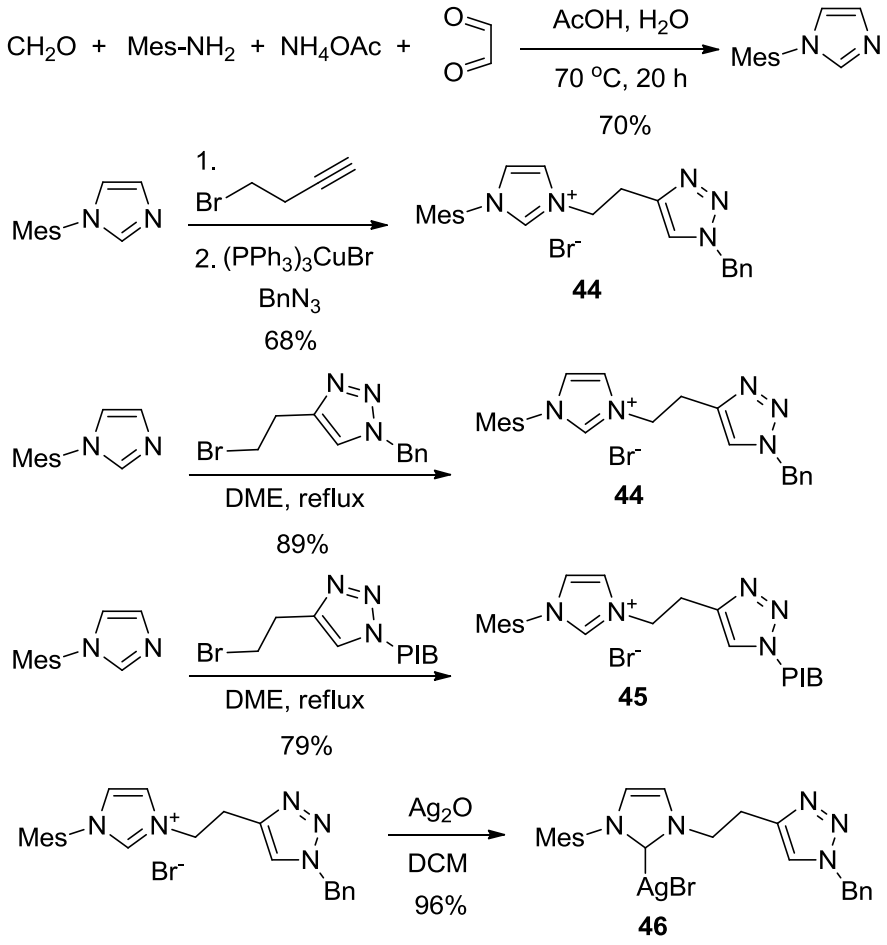

Scheme 35. Transmetallation reaction to prepare the desired NHC-Ru complex with or without the presence of the additional triphenylphosphine.

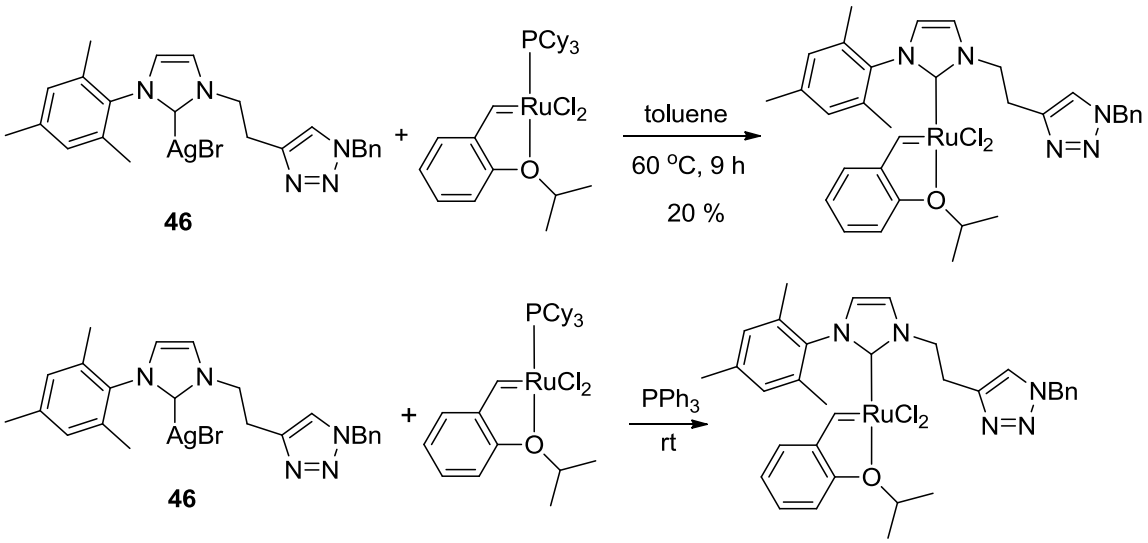

Although the appearance of a new peak at 16.5 ppm on ^{1}H NMR spectrum indicated the formation of a new ruthenium-alkylidene species, the product decomposed during purification process. The reason why the new species decomposed is still unknown and the instability of the Ru-complex led us to discontinue this part of my work.

Polymer-supported Vinyl Ethers as Sequestrants for Metathesis Catalysts

Although using polymer-supported ligands for catalysts is a successful strategy for the removal of ruthenium species from a reaction mixture, the preparation of such catalysts requires several steps. An alternative and simpler approach would be to use a polymer-attached sequestration agent. After reactions, the sequestration agent could react with the catalyst and thus remove the Ru from products. Similar purification

approaches have found to be generally useful in high-throughput syntheses and often involve using polymer-bound sequestrants to trap excess reagents, products, or by-products.[63] This same strategy is usually based on commercially available cross-linked polymer-supported scavengers for other homogeneous catalysts.[64]

The idea of using polymer-supported scavengers could be to the design of soluble polymeric reagents to capture Ru-containing products after olefin metathesis chemistry. This idea is illustrated in Figure 16(a). The particular approach of interest here was focused on using a soluble functional polymer to react with the Ru alkylidene intermediates to form a Fischer carbene. Ethyl vinyl ether is a sequestrant commonly used in quenching Ru-catalyzed polymerization processes. However, the use of polymer-bound vinyl ethers is limited. Indeed, there are only two reports describing the use of polymer-supported scavengers for ruthenium species. In one report, Breinbauer used an insoluble resin-bound bisphosphine to capture Ru species[65] and in a second report, Kilbinger used poly(ethylene oxide)-poly(propylene oxide) diblock copolymers and an insoluble resin supported vinyl ether to sequester ruthenium species[66] (Figure 16(b)).

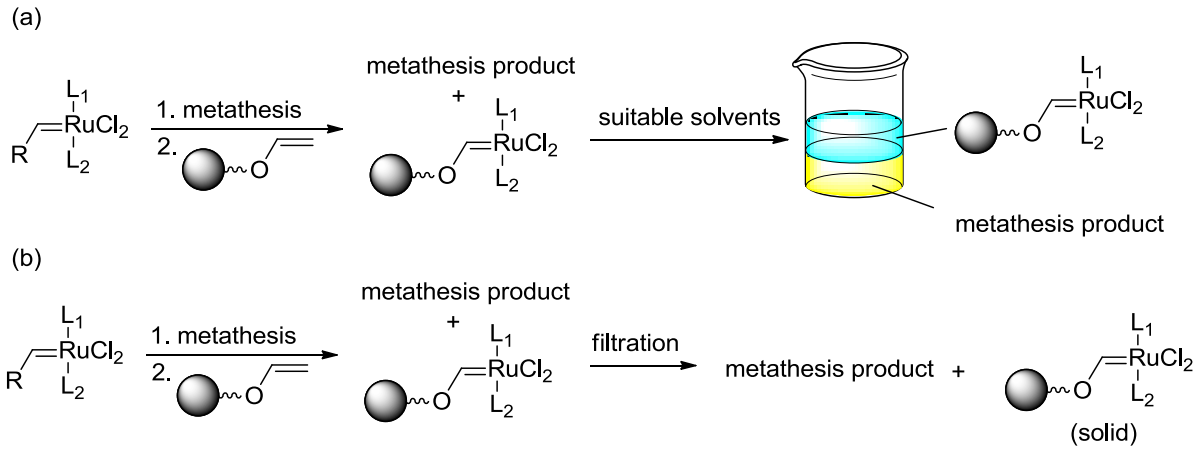

Figure 16. Illustration of using (a) a soluble polymer-supported scavenger and (b) an insoluble resin to support scavenger.

My approach was to prepare PIB-supported vinyl ether as a scavenger for ruthenium. To prepare this PIB-bound vinyl ether, an alkene-terminated PIB was first converted to PIB alcohol. This alcohol was then used in a vinyl ether exchange in the presence of a palladium catalyst, (phen)Pd(OAc)$_2$, to afford the PIB vinyl ether **47** in good yield (Scheme 36). This vinyl ether was fully characterized by ^{1}H and ^{13}C NMR spectroscopy.

Scheme 36. Synthesis of PIB vinyl ether.

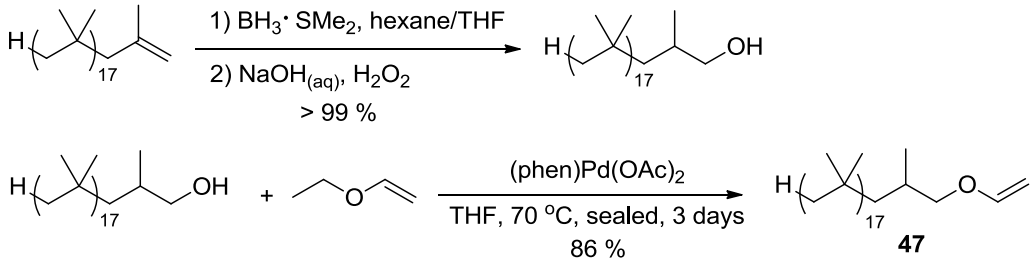

To test the utility of the PIB vinyl ether **47** as a sequestrant for ruthenium, the PIB vinyl ether **47** was tested as a sequestrant for the 2nd generation Hoveyda-Grubbs catalyst **48**. ^{1}H NMR spectroscopy was used to monitor this reaction. It was found that a new peak at δ 13.9 ppm formed but diminished over time. This result suggested that the Fischer carbene **49** was formed but also decomposed quickly in the solution. It was speculated that the Fischer carbene **49** formed but that decomposition of this Fischer carbene occurred due to the instability of this 14-electron species (Scheme 37). If our hypothesis was correct, the Fischer carbene **51** would be more stable if there were a phosphine ligand present. Therefore, a similar experiment was carried out using the 2nd generation Grubbs catalyst **50** and **47**.

Scheme 37. Reactions of PIB vinyl ether with (a) 2nd generation Hoveyda-Grubbs catalyst and (b) 2nd generation Grubbs catalyst.

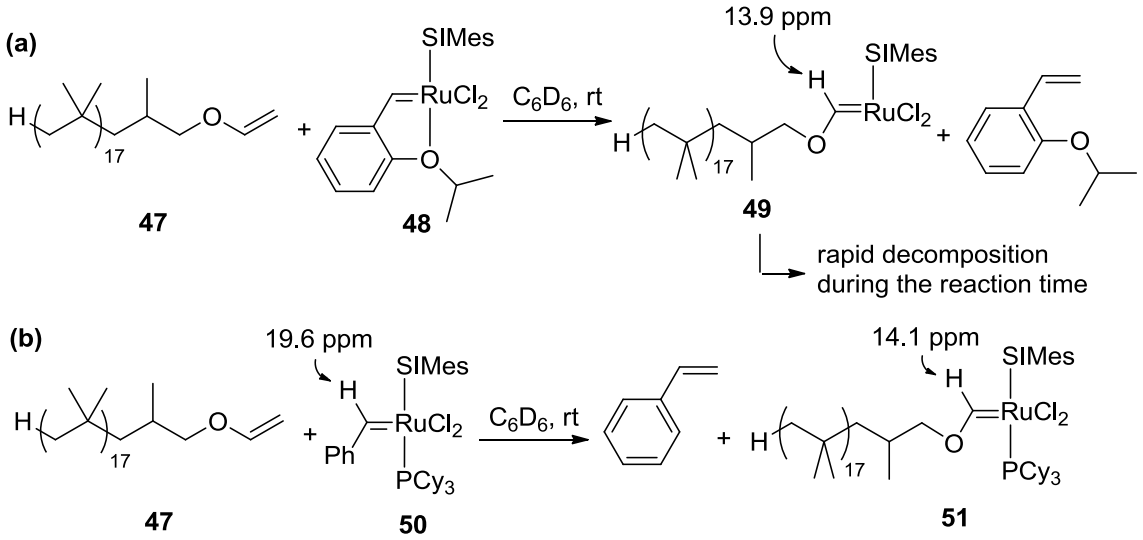

The results of this second study showed that this hypothesis was proved correct. ^{1}H NMR spectroscopy studies of the reaction of **47** and **50** showed that a new peak at δ 14.1 ppm formed while the benzylidene proton of **42** at δ 19.6 ppm diminished. The new peak at δ 14.1 ppm was assigned to the alkylidene proton of the Fischer carbene **51**. When monitoring this reaction under an inert atmosphere in a sealed NMR tube, it was found that the spectrum of the reaction mixture did not change when sitting for 2.5 days after the reaction completed. This suggested that Fischer carbene **51** was stable under an inert atmosphere (Figure 17).

A plot of conversion *vs.* reaction time was drawn based on the integration ratio of the peaks at δ 19.6 ppm and at δ 14.1 ppm (Figure 18). To compare the efficiency of PIB vinyl ether **47** as a sequestratant for the 2nd generation Grubbs catalyst with its low molecular weight counterpart, ethyl vinyl ether were added to a solution with the same concentration of 2nd generation Grubbs catalyst in benzene-d_6. This reaction was also monitored using ^{1}H NMR spectroscopy. The plots for these reactions in Figure 18 are superimposed and show that the reaction rates of 2nd generation Grubbs catalyst with PIB vinyl ether **47** and ethyl vinyl ether are virtually identical**.**

In order to examine the phase selective solubility of the product PIB-bound Fischer carbene **51**, acetonitrile and hexanes were added to the reaction mixture after the reaction between **50** and **47** was complete. As shown in Figure 19, the PIB Fischer carbene **51** was selectively soluble in the nonpolar phase of a hexanes-acetonitrile biphasic mixture.

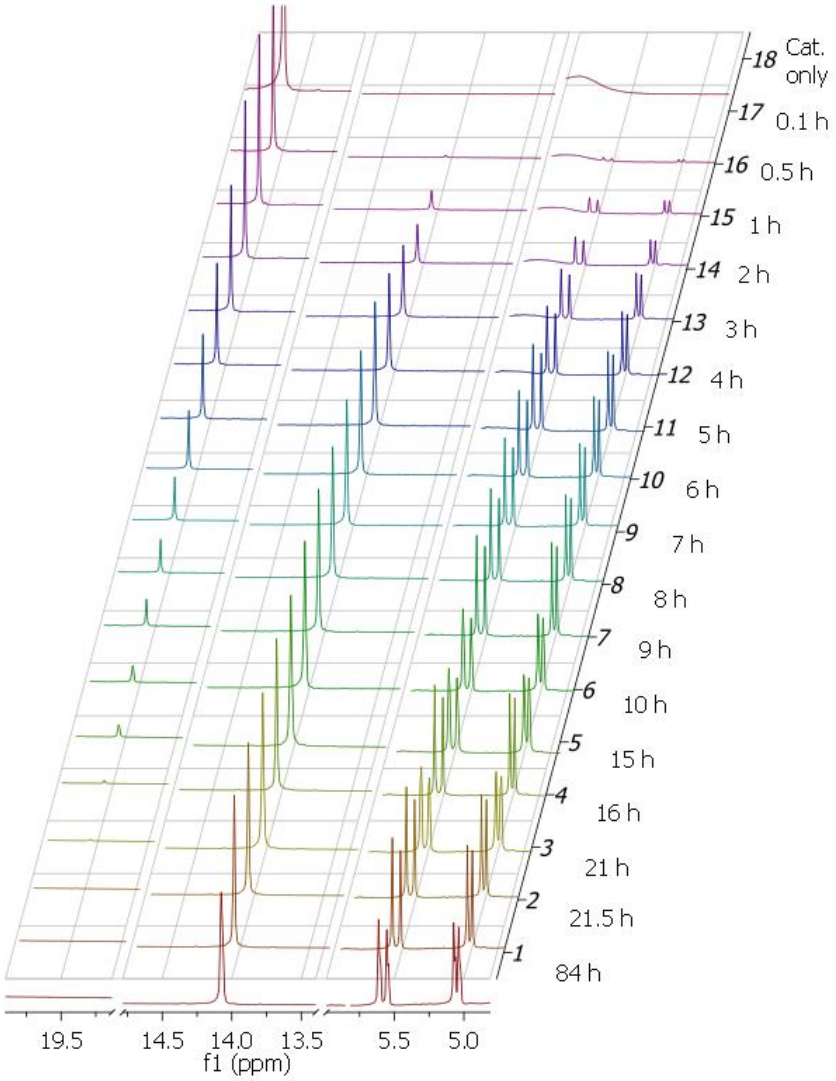

Figure 17. The reaction between PIB vinyl ether **47** and 2nd generation Grubbs catalyst **18** was monitored with ^{1}H NMR spectroscopy. The diminishing peak at δ 19.6 ppm is the benzylidene proton in 2nd generation Grubbs catalyst **50**. The growing signal at δ 14.1 ppm is assigned to the alkylidene proton of the PIB-bound Fischer carbene **51**. Two doublets at δ 5.6 and 5.1 ppm result from the formation of styrene.

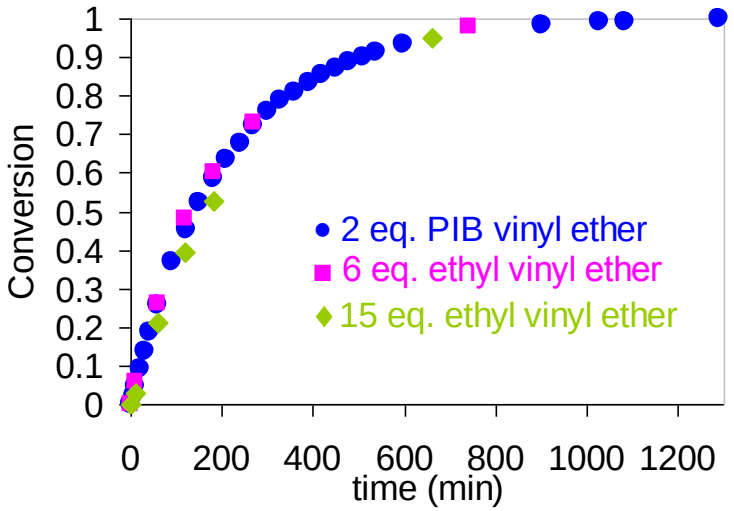

Figure 18. Kinetic studies of the reactions among PIB vinyl ether **47** and different amounts of ethyl vinyl ether with 2nd generation Grubbs catalyst **50**. The conversion was based on the signal integration ratio of the residual benzylidene at δ 19.6 ppm and the formed alkylidene peak at δ 14.1 ppm.

Figure 19. PIB-bound Fischer carbene **51** was phase selectively soluble in nonpolar phase (top) in a hexanes-acetonitrile biphasic mixture.

Since PIB vinyl ether was found to be a successful scavenger for the Grubbs catalyst **50**, it was subsequently tested in quenching both ring-closing metathesis (RCM)

and ring-opening metathesis polymerization (ROMP) chemistry (Scheme 38). Unfortunately, while **47** reacts rapidly with **50**, it was found that the formation of the Fischer carbene at room temperature was much slower with the Ru species present at the end of a RCM reaction ($t_{1/2}$ ~ 40 h by monitoring the reaction mixture on ^{1}H NMR spectroscopy for 2 d). This rate decrease was believed due to the formation of a less reactive ruthenium species during the course of the metathesis reaction. Indeed, when monitoring a RCM chemistry by ^{1}H NMR spectroscopy, a new peak was observed at δ 18.4 ppm during the reaction. This peak was assigned to the methylidene protons of compound **52** (Scheme 39). The Ru-complex **52** has actually been isolated previously by Grubbs *et al.* in 2001[67] and the benzylidene proton of compound **52** was reported to have a chemical shift at δ 18.41 ppm in benzene-d_6. Compound **52** was also reported having a very low phosphine dissociation rate constant (10^{-3} s^{-1} at 85 ^oC). Since phosphine dissociation is presumably required for formation of a Fischer carbene, **47** is not very effective in quenching the Ru intermediate in this RCM chemistry to form a species like **51**.

Scheme 38. PIB vinyl ether as a scavenger for ruthenium residue after RCM and ROMP

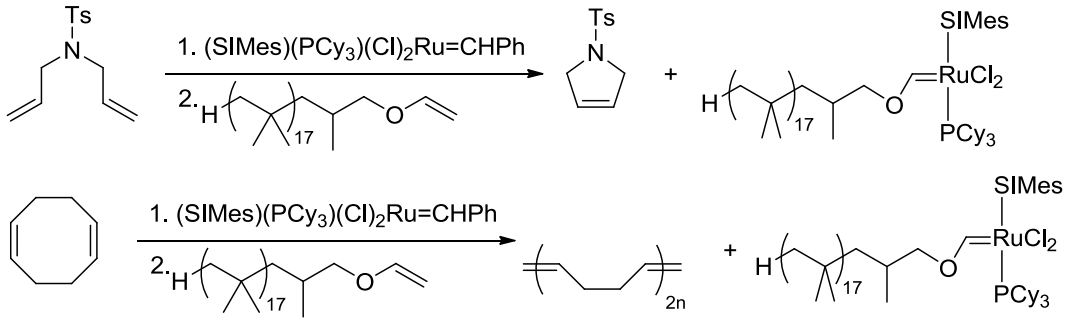

Scheme 39. After RCM reaction, PIB vinyl ether was added as a scavenger. Because of the compound **20**'s slow dissociation rate, the quenching process was very slow.

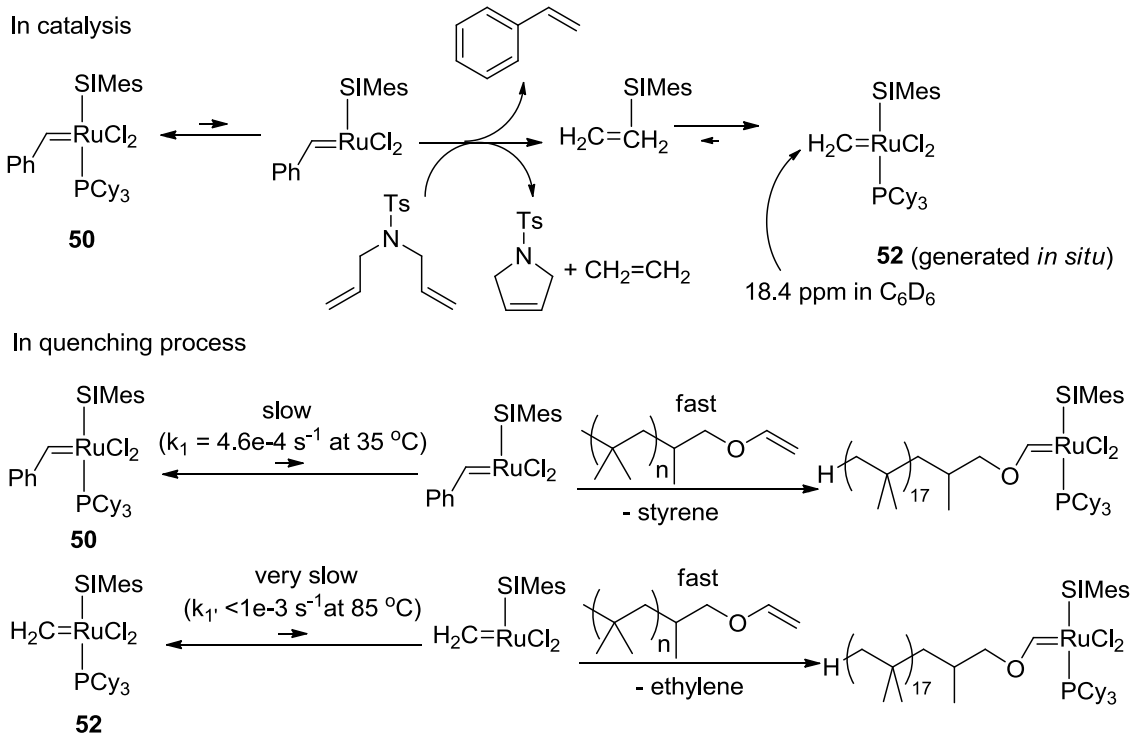

Given the low phosphine dissociation rate of compound **52** at ambient temperature, a quenching process at 60 ^{o}C was tested. It was found that at 60 ^{o}C, the quenching reaction proceeded to completion in 10 h. After the quenching reaction completed, hexanes and acetonitrile were added to separate the PIB-bound Fischer carbene species in the reaction mixture. Both phases were analyzed with ^{1}H NMR spectroscopy. It was found that no remaining RCM product in the nonpolar phase and all of the PIB-bound Fischer carbene was present in the nonpolar phase. None of the PIB-bound Fischer carbene was present in the polar phase based on ^{1}H NMR spectra.

Given the success in using PIB vinyl ether as a quenching agent, I have also

carried out preliminary studies with polyethylene oligomer in place of PIB. Unlike PIB, which is soluble in nonpolar or weak polar solvents at room temperature, polyethylene is insoluble in any solvent at room temperature. However, at elevated temperatures, polyethylene with low molecular weight is soluble in toluene. In my study, a polyethylene oligomer with molecular weight of 550, which can dissolve in toluene at 65 ^{o}C, was used.

The synthesis of polyethylene vinyl ether was carried out with a vinyl ether exchange in the presence of catalyst (phen)Pd$(OAc)_2$ using the same procedure used to prepare PIB. This reaction was successful. The polyethylene vinyl ether so formed was then tested as a sequestrant for the 2nd generation Grubbs catalyst. In this test, an equal equiv. of polyethylene vinyl ether and 2nd generation Grubbs catalyst in toluene-d_8 was mixed in an NMR tube. No quenching reaction was observed when the mixture was kept at room temperature for 2 h. However, when the temperature was elevated, the polyethylene vinyl ether reacted with 2nd generation Grubbs catalyst quickly. The reaction was complete in 10 min. at 65 ^{o}C. This test suggested that at room temperature, the polyethylene vinyl ether could be added to a reaction mixture without affecting the catalysis. The metal removing process with polyethylene-bound sequestrant could be done after catalysis with simply increasing temperature to 65 ^{o}C for a period of time. After back to room temperature, the polyethylene-bound Fischer carbene will precipitate and removing the Ru species from the solution.

Conclusion

A new class of hemilabile ligands including NHC liands and labile triazole ligands was prepared. Although the target compound, hemilabile ligand ligated ruthenium complex, was not as stable as designed, some new chemistry was found in this research. This included the effects of the additional phosphine on transmetallation, a result that led to systematic study of NHC ligand exchange process on NHC-silver halides. These research results are described in the next chapter.

The work on Ru catalysts and olefin metathesis chemistry also led to the development of polymer-supported sequestrants for ruthenium-based metathesis catalysts. The synthesis of this PIB vinyl ether was successful and my studies showed that it was useful as predicted. The PIB vinyl ether was found to be an efficient sequestrant for the 2nd generation Grubbs catalyst. Kinetic analyses showed that the activity of the PIB vinyl ether is identical to ethyl vinyl ether. Like other PIB derivatives, the sequestrated product, the PIB-bound Ru-Fischer carbene was selectively soluble in a nonpolar phase of a hexane-acetonitrile biphasic mixture enabling me to separate Ru efficiently from metathesis products. Using PIB as a sequestrant support with a liquid/liquid phase separation provides a simple method to separate deeply colored, metal-containing by-products from metathesis reaction mixtures.

CHAPTER IV

KINETIC STUDIES OF NHC-SILVER(I) COMPLEXES

Introduction

Silver is a soft, white, lustrous transition metal with symbol Ag (Latin: *argentum*), atomic number 47, and atomic weight 107.8682(2) g/mol. In nature, silver is composed of two stable isotopes, ^{107}Ag and ^{109}Ag. ^{107}Ag has the most natural abundance of *ca.* 51.8% while ^{109}Ag has 48.2%. Both ^{107}Ag and ^{109}Ag has 1/2 nuclear spin and gyromagnetic ratio -1.0828 and -1.2448, respectively.

Like many other NHC-metal complexes, NHC-ligated Ag(I) complexes can be useful catalysts.[68] However, NHC-Ag(I) complexes have received more attention as intermediates for the synthesis of other transition metal NHC complexes (cf. Chapter I). While the transmetalation of NHC ligands is an important synthetic process and while NHC-ligated transition metal catalyst use is increasing, relatively little attention has been paid to the dynamic behavior of NHC ligands on metals. This is even true for NHC-Ag(I) complexes though the literature includes many examples of NHC-Ag complexes whose carbene carbons were reported variously as either as doublets of doublets, as broad doublets, as broad singlets, or as singlets in ^{13}C NMR spectroscopy.[69-71] Indeed, one report noted that the carbene carbon peak was a broad singlet at room temperature and a doublet of doublets at -50 ºC which is consistent with NHC ligand exchange on Ag.[72] Since Ag has two almost equally abundant spin 1/2 isotopes, the carbene carbon of a NHC-Ag(I) complex should be a doublet of doublets if the NHC ligand does not exchange rapidly on the NMR timescale. However, if NHC ligand exchange is fast on

the NMR time scale, this doublet of doublets should change to a pair of doublet and eventually become a singlet. This exchange process should also be temperature dependent. Such a phenomenon is known for other silver complexes and has been used previously to study exchange of both silver containing phosphorous and carbon ligands.[73-76] For example, there are many reports that discuss variable temperature (VT) ^{31}P NMR spectra of phosphine-silver complexes where the ^{31}P NMR spectrum of a P-containing Ag complex is a doublet of doublets at low temperature and where this ^{31}P NMR signal coalesces to a broad doublet, then a broad singlet, and finally a sharp singlet when the temperature is increased.

In this chapter, several NHC-silver complexes were prepared and characterized. Among these complexes, the carbene carbon signal of (*N*-mesityl-*N*′-alkylimidazolylidene)silver halides appeared as singlets at room temperature and as a doublet of doublets at -80 ºC on ^{13}C NMR spectroscopy. Therefore, they were chosen to study this temperature-dependent behavior. The results showed that the ligand exchange goes through an associative process and that both counterions and additives significantly affect the multiplicity of the carbene carbons for these NHC ligands on Ag(I).

Synthesis of NHC-Ag Complexes

Several types of NHC-Ag(I) complexes were prepared to test if the multiplicity of the carbene carbons in NHC-Ag(I) complexes changed with temperature. At room temperature, the carbene carbons of these complexes appeared either as singlets or as doublet of doublets in ^{13}C NMR spectra (Figure 20). When measuring VT ^{13}C NMR for

these compounds, the doublet of doublets for the carbene carbon of **55** in DMSO-d_6 at 20 ºC became a broad doublet at 100 ºC while the carbene carbon signals of (*N*-mesityl-*N′*-methylimidazolylidene)silver iodides **63** that were broadened singlet at 20 ºC became a doublet of doublets on cooling to -80 ºC. This suggested that this NHC silver halide complexes could be an ideal candidate to study the dynamics of NHC exchange processes in NHC-Ag(I) complexes if these complexes' VT NMR ^{13}C NMR spectra could be studied.

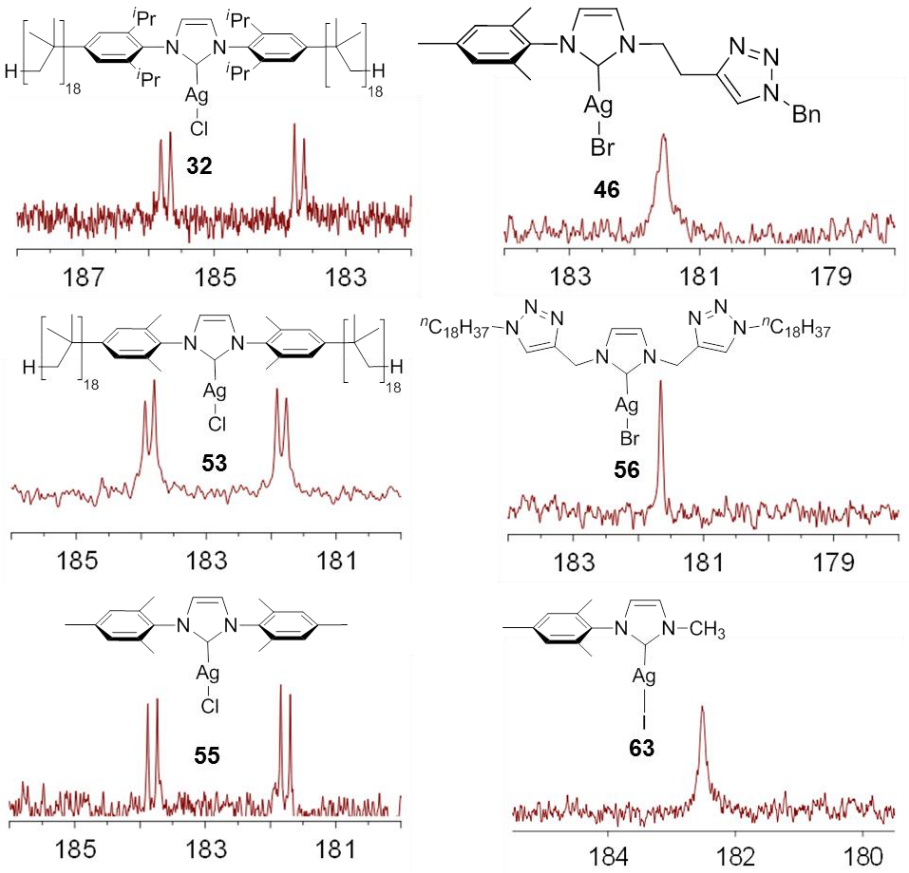

Figure 20. Some examples of NHC-Ag(I) complexes and their ^{13}C NMR spectra in the carbene carbon region at room temperature.

The initial problem I faced in studying NHC-Ag(I) exchange processes was that the ^{13}C signal for the carbene carbon in these complexes has a very low intensity. For example, in Figure 20, the spectra of the carbene carbon of **63** at 0.2 N $CDCl_3$ solution was obtained after 4 h of data accumulation but still had two S/N ratio. For VT studies at the same concentration, the accumulation would require more than 40 h of spectrometer time. This effectively precluded a thorough study of NHC silver halide dynamic NMR spectroscopy. To address this issue, I prepared *N*-mesityl-*N*′-methylimidazolium salts that was enriched with ^{13}C labels on the 2-position of the imidazolium ring. These species could in turn be used to prepare NHC Ag(I) halide complexes that contained ^{13}C labels at the carbene carbon and allowed me to study line-broadening in the VT NMR spectra of these Ag complexes even when the NHC-Ag(I) complexes were present at concentrations as low as 1×10^{-2} N concentration. This strategy of using a label to facilitate spectroscopic characterization of the carbene carbon signal that is of relatively low intensity has precedent in the prior work that used ^{13}C-labeled NHC ligands in solution and solid state NMR spectroscopic of a (*N*,*N*'-dimesitylimidazolylidene)silver chloride.[77]

I prepared ^{13}C-labeled imidazole and NHC-Ag halide complexes using Arduengo's method (Scheme 40).[62] Integration of the doublet in the ^{1}H NMR spectrum of the labeled imidazole due to ^{13}C-^{1}H coupling versus the ^{1}H singlet for the ^{12}C-containing impurity was used to determine that the ^{13}C-enriched imidazole contained 92% of ^{13}C. The ^{13}C-labeled imidazole was then *N*-methylated with different methyl halides to form imidazolium salts. While the reaction with methyl iodide went

smoothly, methylations with methyl bromide or methyl chloride required forcing conditions and required reactions in a sealed tube. The most difficulty of these reactions was methylation with methyl chloride which had to be carried out at 120 ºC in CH_3CN in a sealed tube with excess amount of methyl chloride. The ^{13}C-enriched (*N*-mesityl-*N*′-methylimidazolylidene)silver halide complexes were then prepared from these ^{13}C labeled imidazolium halide salts using Ag_2O (Scheme 40).

Scheme 40. Synthesis of (*N*-mesityl-*N*′-methylimidazolylidene)silver halides.

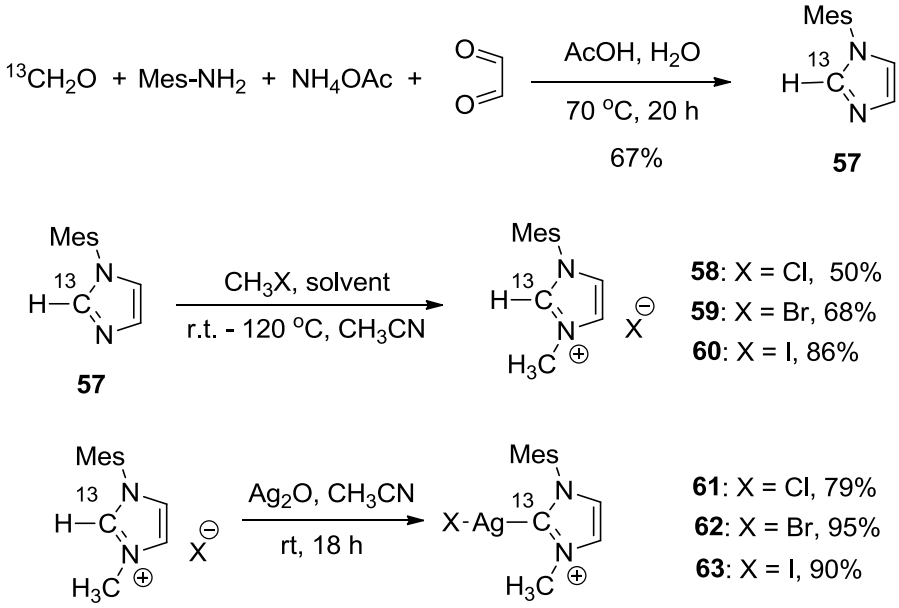

The neutral NHC silver halide complexes **61**, **62**, and **63** were characterized by ^1H and ^{13}C NMR spectroscopy and by elemental analysis. (*N*-mesityl-*N*′-methylimidazolylidene)silver chloride **61** and bromide **62** products were also successfully recrystallized from CH_3CN/ether and were characterized

crystallographically. Their crystal structures are shown in Figure 21 and selected bond distances and bond angles are given in Table 1.

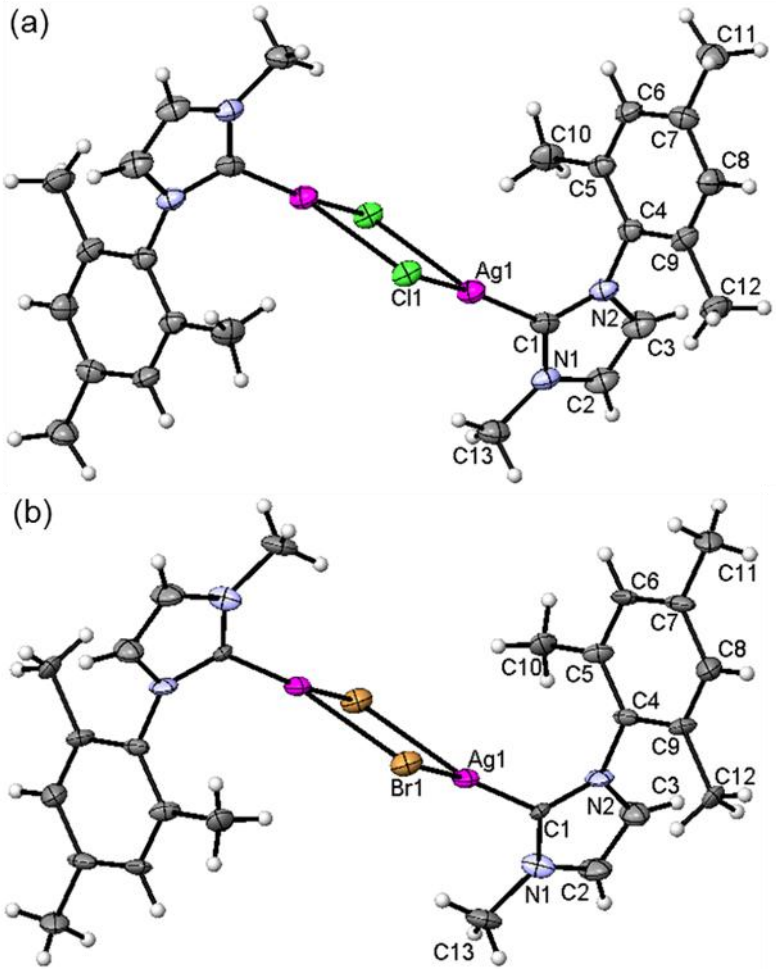

Figure 21. ORTEP view of X-ray crystal structures of (a) (*N*-mesityl-*N*′-methylimidazolidylene)silver chloride **61** and (b) (*N*-mesityl-*N*′-methylimidazolylidene) silver bromide **62** with thermal ellipsoids at 50% probability.

Table 1. Selected bond distances [Å] and bond angles [°] of compound **61** and **62**.

	Compound **61** [$C_{26}H_{32}Ag_2N_4Cl_2$] (X = Cl)	Compound **62** [$C_{26}H_{32}Ag_2N_4Br_2$] (X = Br)
Bond lengths		
Ag(1)-C(1)	2.074(6)	2.081(10)
Ag(1)-X(1)	2.3844(14)	2.495(3)
Ag(1)-X(1A)	2.9017(13)	2.928(3)
C(1)-N(1)	1.346(6)	1.350(12)
C(1)-N(2)	1.374(7)	1.363(14)
Bond angles		
C(1)-Ag(1)-X(1)	163.18(14)	158.42(30)
C(1)-Ag(1)-X(1A)	108.38(14)	110.82(31)
X(1)-Ag(1)-X(1A)	88.43(4)	90.76(7)
Ag(1)-Cl(1)-Ag(1A)	91.57(4)	89.27(7)
N(1)-C(1)-N(2)	103.2(5)	102.3(9)
N(1)-C(1)-Ag(1)	129.4(4)	128.9(7)
N(2)-C(1)-Ag(1)	127.4(4)	128.4(7)

Attempts to grow crystals of (*N*-mesityl-*N*′-methylimidazolylidene)silver iodide were however less successful. After repeated attempts, two structures were obtained but neither corresponded to the structure of the neutral (*N*-mesityl-*N*′-methylimidazolylidene)silver iodide **63**. Both structures that were characterized crystallographically contained silver cations complexed by two NHC ligands. In one case, the anion was disordered and could not be identified. However, this compound was also characterized by EDX which showed that the crystals had an Ag/I ratio of 1/1 based on energy dispersive X-ray analysis. The crystal structure for this material is shown in Figure 22 and the selected bond distances and bond angles are given in Table 2. We also obtained a small amount of an additional product **64** that may have been formed as a result of light exposure during the crystallization process (eq. 1). This latter product, bis(*N*-mesityl-*N*′-methylimidazolylidene)silver iodide **64** has the crystal

structure shown in Figure 23 and the selected bond distances and bond angles are given in Table 3.

Figure 22. Ball and stick representation of X-ray crystal structures of (*N*-mesityl-*N*′-methylimidazolylidene)silver cation of complex **63.** Hydrogen atoms were omitted for clarity.

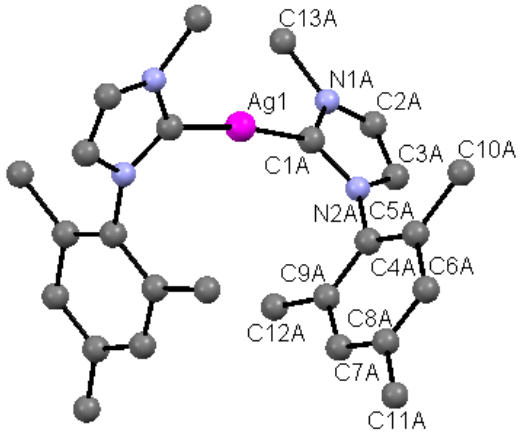

Table 2. Selected bond distances [Å] and bond angles [°] of compound **63**.

Bond lengths			
Ag(1)-C(1)	2.12(1)	C(1)-N(1)	1.412(3)
Ag(1)-C(1A)	2.12(1)	C(1)-N(2)	1.344(3)
Bond angles			
C(1)-Ag(1)-C(1A)	172.7(7)	N(1)-C(1)-Ag(1)	132.8(3)
N(1)-C(1)-N(2)	98.42	N(2)-C(1)-Ag(1)	128.6(3)

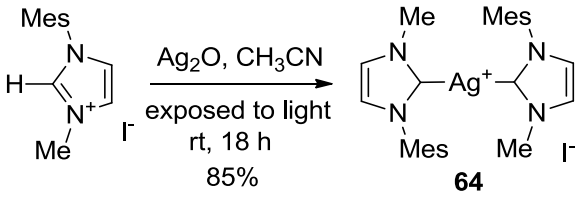

(1)

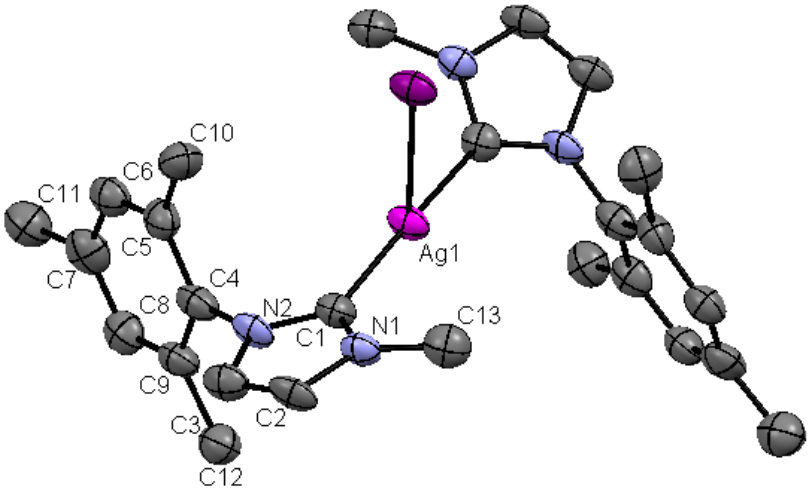

Figure 23. ORTEP view of X-ray crystal structure of bis(*N*-mesityl-*N*′-methylimidazolylidene)silver iodide **64** with thermal ellipsoids at 50% probability. Hydrogen atoms were omitted for clarity.

Table 3. Selected bond distances [Å] and bond angles [°] of compound **64**.

Bond lengths			
Ag(1)-C(1)	2.097(16)	C(1)-N(1)	1.355(21)
Ag(1)-C(1A)	2.097(15)	C(1)-N(2)	1.365(21)
Ag(1)-I(1)	3.289		
Bond angles			
C(1)-Ag(1)-C(1A)	175.09(91)	N(1)-C(1)-N(2)	104.6(14)
C(1)-Ag(1)-I(1A)	92.46	N(1)-C(1)-Ag(1)	129.1(11)
I(1)-Ag(1)-C(1A)	92.45	N(2)-C(1)-Ag(1)	125.3(12)

Variable Temperature NMR Studies of NHC-Ag Complexes

A 0.06 N solution of ^{13}C labeled NHC-silver iodide **63** dissolved in CD_2Cl_2 had a carbene carbon signal appeared as a broad singlet at 20 ºC in ^{13}C NMR spectroscopy. On cooling to -85 ºC, this singlet changed into a doublet of doublets (Figure 24). At 20 °C, the ^{13}C NMR spectra with higher concentrations of **63** were similar to the spectrum of the 0.06 N solution of **63** with slight differences that the singlet became sharper as the concentration of **63** was changed from 0.06 to 0.12 to 0.24 N. ^{13}C NMR spectra of higher concentrations of **63** at -85 ºC slightly varied as the concentration of **63** increased. This is most apparent in the -85 ºC spectrum of the 0.24 N solution where two sets of doublets of doublets are seen indicating that two kinds of NHC silver species are present. The major component had $^1J(^{13}C\text{-}^{107}Ag)$ and $^1J(^{13}C\text{-}^{109}Ag)$ coupling constants of 241 and 274 Hz while the minor component had smaller coupling constants of 179 and 207 Hz . The minor component was also present in the 0.06 and 0.12 N solutions but at a lower relative intensity. In a solution that was 0.24 N in **7**, the ratio of the two components was *ca*. 5:1 but the ratio was *ca*. 20:1 in a 0.06 N solution. This minor component had not been observed in our initial studies that did not use ^{13}C-enriched compound **63** because of the low intensity of the carbene carbon for unlabeled **63**. The changes in the concentration of the minor product with changes in the concentration of **63** suggested that the minor component might be in equilibrium with the major component. As discussed below, we believe that the two species in these spectra are an equilibrium mixture of the neutral **(***N*-mesityl-*N*'-methylimidazolylidene)silver iodide complex as the

major component and the bis(*N*-mesityl-*N*'-methylimidazolylidene)silver(I) diiodoargentate ion pair ($(NHC)_2Ag^+$ AgI_2^-) as the minor component (eq. 2).

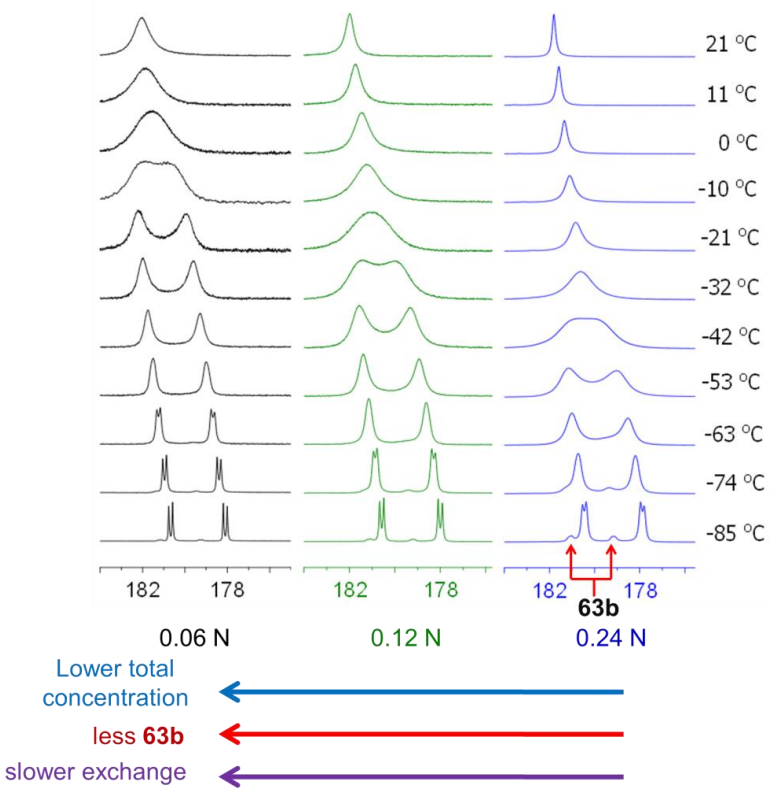

Figure 24. Variable temperature ^{13}C NMR spectra over a -85 ºC to 21 ºC temperature range for 0.06 - 0.24 N CD_2Cl_2 solutions of ^{13}C-enriched (*N*-mesityl-*N*′-methyl-imidazolylidene)silver iodide **63**. At -85 ºC, a minor component is clearly visible. Coalescence is seen in all the spectra as the temperature increases and the coalescence temperature increased as the concentration of **63** decreased.

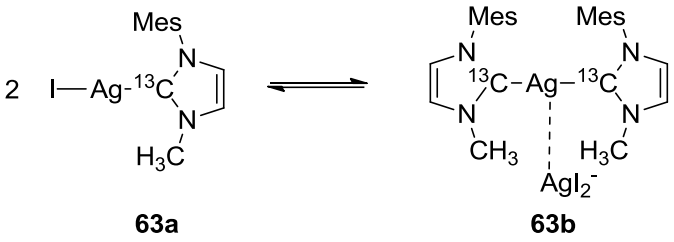

(2)

When studying the CD_2Cl_2 solition of silver chloride complex **61** at various concentrations, the results from VT ^{13}C NMR spectroscopy are shown in Figure 25. The dynamic behavior of **61** is qualitatively similar to the behavior of **63** seen in Figure 24. In this case, coalescence of the doublet of doublets at low temperature to form a broad singlet was only seen for a 0.12 N solution of **61**. In more dilute solutions and in particular in the 0.02 and 0.01 N solutions, the 22 ºC spectra only show broadened doublet. The spectra of **61**, like the spectra of **63**, show small amounts of an impurity whose relative concentration increases with concentration. As discussed below, these two species are presumed to be the neutral **(***N*-mesityl-*N*'-methylimidazolylidene)silver chloride complex (NHCAgCl) as the major component and the bis(*N*-mesityl-*N*'-methylimidazolylidene)silver(I) cation dichloroargentate ion pair ($(NHC)_2Ag^+$ $AgCl_2^-$) as the minor component.

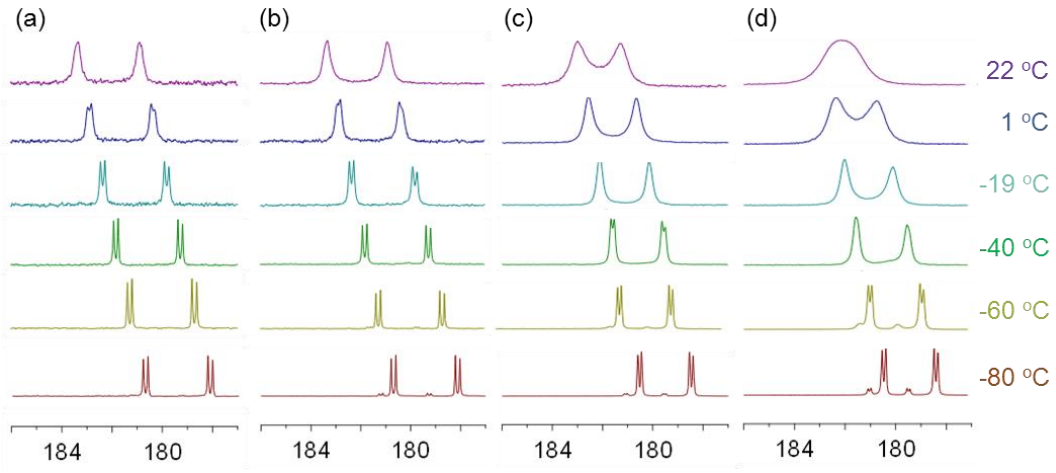

Figure 25. VT ^{13}C NMR spectra of **61** in the concentration of (a) 0.01 N, (b) 0.02 N, (c) 0.06 N, and (d) 0.12 N.

Several prior reports have suggested that a NHC-ligated silver bromide and chloride complexes can form mixtures of neutral and ionic species and that these species can be in equilibrium with one another.[28,71,78-80] These reports did not examine the concentration dependence of these species, but one report did observe that the concentration of the two carbene complexes formed in the synthesis of IMesAgCl (IMes = *N*,*N*′-dimesitylimidazolylidene) varied with solvent polarity.[78] Higher solvent polarity contained larger amount of the ion pair. In this work, Nolan assigned the structure IMesAgCl to the major component and the structure $(IMes)_2Ag^+$ $AgCl_2^-$ to the minor component. He also described other ion pairs including $[(IMes)_2Ag^+]_2$ $[Ag_4I_6]^{2-}$ suggesting that NHC-silver halide complexes can form a variety of neutral and ion pair structures. Another report discussed NHC ligated Ag(I) with various anions noted that $(NHC)_2Ag^+$ complexes have Ag-C coupling constants ($J(^{107}Ag\text{-}^{13}C)$ are in the range of

173 - 188 Hz) that are consistently smaller than the Ag-C coupling constant of a neutral complex ($J(^{107}Ag\text{-}^{13}C)$ are in the range of 222 - 228 Hz).[70,81] The major species in the 0.24 N solution in Figure 24 has a $^{107}Ag\text{-}^{13}C$ and $^{109}Ag\text{-}^{13}C$ coupling constants of 241 and 274 Hz, respectively, and the minor species has $^{107}Ag\text{-}^{13}C$ and $^{109}Ag\text{-}^{13}C$ coupling constants of 179 and 207 Hz, respectively. These coupling constant values suggest that the minor species are the ion pair.

Following Nolan's procedure, I also prepared the mixture of (IMes)AgCl and $(IMes)_2Ag^+$ $AgCl_2^-$ species.[78] This mixture of a neutral form and ion pair of an NHC-AgCl complex had $^{107}Ag\text{-}^{13}C$ and $^{109}Ag\text{-}^{13}C$ coupling constants of 238 and 273 Hz for the neutral form and $^{107}Ag\text{-}^{13}C$ and $^{109}Ag\text{-}^{13}C$ coupling constants of 180 and 209 Hz for the ion pair at - 80 °C. As was true in prior work, the coupling constant of the bis-NHC Ag cation species was lower than that of the neutral form. The $^{107}Ag\text{-}^{13}C$ and $^{109}Ag\text{-}^{13}C$ coupling constants for the neutral NHCAgCl species containing a single NHC ligand on Ag are also comparable to coupling constants of other NHC-Ag(I) halides containing a single NHC ligand. Finally, as was true in Nolan's work, the concentration of the neutral and ionic forms changed with changes in solvent polarity. In CD_2Cl_2 at 23 ºC, the ratio of $(IMes)AgCl/(IMes)_2Ag^+AgCl_2^-$ was 3/1 on ^1H NMR spectrum. In DMSO-d_6, the ratio of $(IMes)AgCl/(IMes)_2Ag^+AgCl_2^-$ was *ca*. 1/1 on 23 ºC ^1H NMR spectrum. Nolan reported that the ratio of $(IMes)AgCl/(IMes)_2Ag^+AgCl_2^-$ was 4/1 in acetonitrile-d_3 and 2/1 in DMSO-d_6.

The coalescence seen in Figure 24 is clear evidence that NHC ligands exchange between different silver species just like phosphine or alkyl groups exchange in prior

studies of ligand exchange in Ag complexes. It is also noteworthy that the solution state ^{13}C NMR peaks of **63** with different concentrations coalesce at different temperatures, *i.e.* the coalescence temperatures increased when the concentration of **63** decreased after performed several serial dilutions. For example, the coalescence temperature for **63** was *ca*. -42 C for a 0.24 N solution of **63**, *ca*. -25 ºC for a 0.12 N solution of **63** and *ca*. -5 ºC for a 0.06 N solution of **7**. The same trend was also seen in the VT NMR spectroscopic studies of solutions of NHCAgCl **61** and NHCAgBr **62**. For example, the coalescence temperature was *ca*. 20 ºC for a 0.12 N solution of NHCAgCl **61**, and was greater than room temperature for a solution of **61** with concentration smaller than 0.06 N (Figure 25). Likewise, VT NMR spectroscopic studies of **62** showed coalescence temperature at *ca*. 20 ºC for a 0.02 N solution and above 20 ºC for a 0.01 N solution (Figure 26). This concentration-dependant behavior suggested that the NHC ligand exchange occurs through an associative process.

Effects of Bridging Anions on NHC Ligand Exchange Rates in NHC-silver Halide Complexes

In the Lin's study of NHC-Ag complexes,[28] it was postulated that halides were bridging anions connecting two silvers and facilitated NHC transfer (cf. Scheme 41). This postulate is supported by the VT NMR spectra of **61**, **62**, and **63** solutions at the same concentration which show that halide identity has a significant effect on the coalescence temperature with the exchange rate varying as I, Br > Cl.

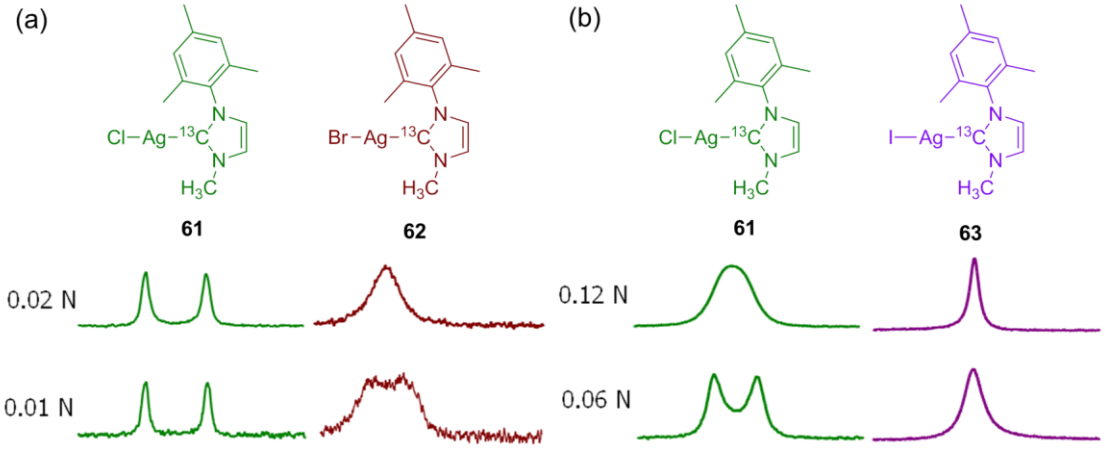

Figure 26. 20 ºC ^{13}C NMR spectra of (a) 0.01 N and 0.02 N solutions of **61** and **62** in CD_2Cl_2 and (b) 0.12 N and 0.06 N solutions of **61** and **63** in CD_2Cl_2. It is visually noticeable that the coalescence temperatures were different with different anions and different concentrations.

Scheme 41. Proposed mechanism of NHC ligand exchange of NHC-Ag complexes by Lin *et al.*[28]

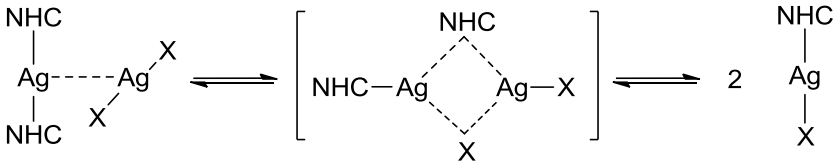

Addition of tetrabutylammonium halides to 0.06 N solutions of **61** provides further evidence of the effects of halide on the exchange process. Figure 27 shows that when additional halides were present in the solution, the coalescence temperatures decreased and the exchange went faster. Also, the effect of additional halides followed

the same trend noted above with bromide anion having a larger effect than chloride. Figure 28 shows that coalescence temperature decreases with addition amount of $Bu_4N^+Br^-$. Also, the addition of tetrabutylammonium halides affects the distribution between the neutral NHCAgX form and ion pair NHC_2Ag^+ AgX_2^-. This result is consistent with Nolan's work:[78] an increase in the amount of tetrabutylammonium bromide would form a more polar solution and therefore, the partition of the ion pair would increase as the amount of tetrabutylammonium bromide increased.

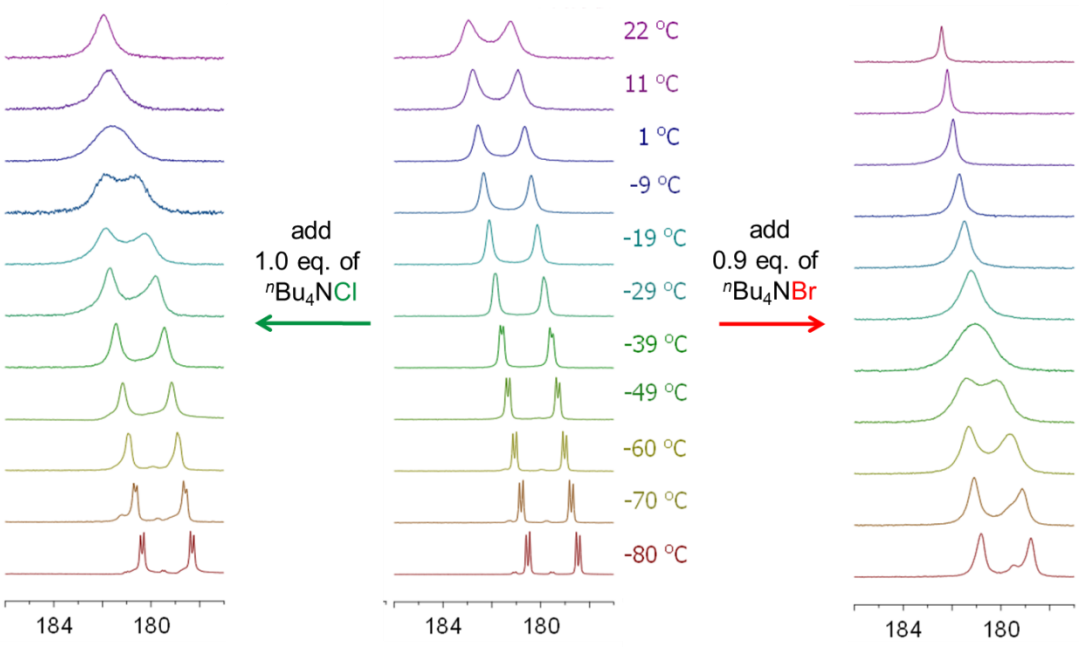

Figure 27. VT NMR spectra of 0.06 N solution of **61** (center) and 0.06 N solution of **61** with addition of 1 equiv. of tetrabutylammonium chlorides (left) or 0.9 equiv. of tetrabutylammonium bromides (right).

The coalescence temperature changes with adding tetrabutylammonium bromide do not follow a linear relationship. When a large amount of bromide anion was added, the change of the coalescence temperatures decreased. The relationship between the coalescence temperatures and the amounts of additional bromide anion followed an exponential decay as shown as Figure 29. However, at present, I do not have enough information to mechanistically explain this trend.

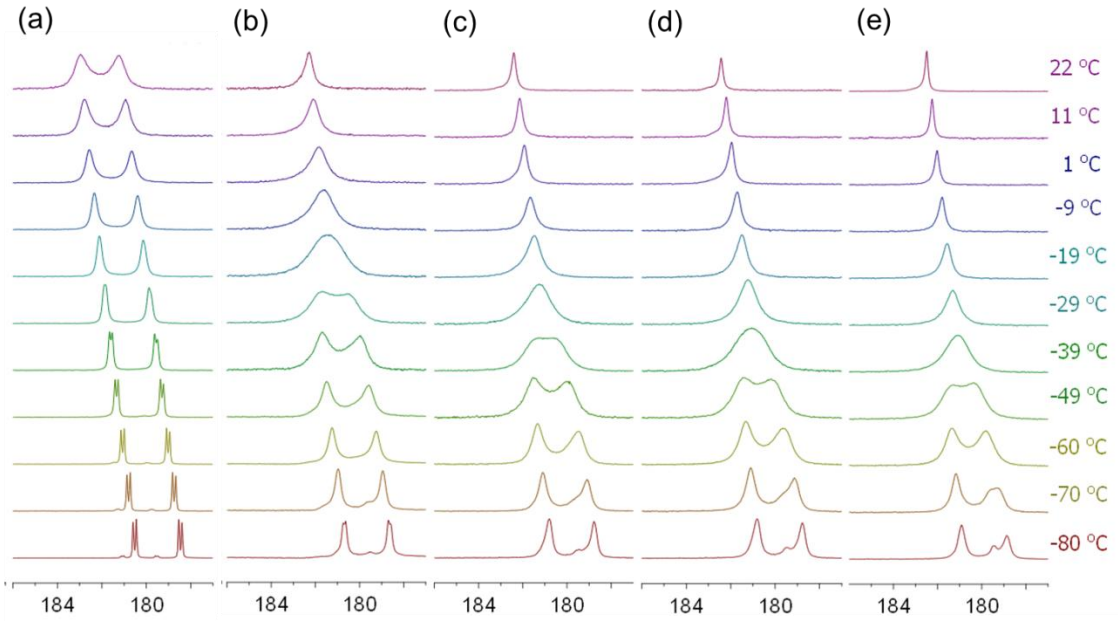

Figure 28. VT ^{13}C NMR spectra of (a) a 0.06 N solution of **61** with addition of (b) 0.3, (c) 0.6, (d) 0.9 and (e) 1.69 equiv. of tetrabutylammonium bromide.

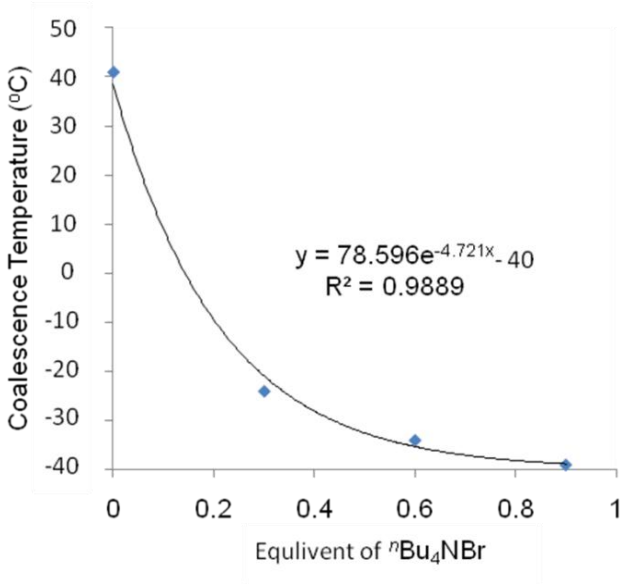

Figure 29. The plot of the coalescence temperatures 0.06 N solution of **5** in CD_2Cl_2 *vs*. the amount of the added tetrabutylammonium bromide.

As noted above, I was unable to obtain a crystal structure of **63** but I did obtain a crystal structure of bis(*N*-mesityl-*N*′-methylimidazolylidene)silver iodide **64** when a sample had been exposed to light. We therefore briefly examined the dynamic behavior of the NHC groups in **64**. In this case, exchange of the NHC ligands did not occur on the NMR time scale. A doublet of doublets was observed at all temperatures from 20 ºC to -80 ºC. Also, the ^{107}Ag-^{13}C and ^{109}Ag-^{13}C coupling constants of 178 and 206 Hz seen for **64** were more like the ^{107}Ag-^{13}C and ^{109}Ag-^{13}C coupling constants seen for the minor component present in a 0.24 N solution of **63** (*i.e.* the presumed bis(*N*-mesityl-*N*'-methylimidazolylidene)silver(I) dichloroargentate ion pair species). However, we were able to use this solution of **64** to show that NHC ligand exchange between the NHC groups of bis(*N*-mesityl-*N*'-methylimidazolylidene)silver(I) cation and the NHC groups

of a neutral ((*N*-mesityl-*N*'-methylimidazolylidene)silver(I) iodide was fast. When 0.01 equiv. of **63** was added to a 0.04 N solution of **64**, the carbene signal in ^{13}C NMR spectrum became a broad doublet at room temperature. When 0.03 equiv. of **63** added, the carbene signal became a broad singlet at room temperature. This provides further evidence that NHC ligand exchange between ion pairs and neutral species is facile.

Lineshape Analysis and Kinetic Parameter Estimation for the Dynamic NMR

Multiple methods for the lineshape analysis were performed to estimate the kinetic parameters ($\Delta H^{\ddagger}$, $\Delta S^{\ddagger}$, and $\Delta G^{\ddagger}$) for this exchanging system. The characteristic NMR lineshape phenomena due to dynamic processes in spin systems have been known for a long time.[82-85] Dynamic NMR spectroscopy has been a common technique applied to study processes of chemical exchanges and conformational equilibrium. For the simplest case of a two-site exchange process as an example, the signals for the two magnetic environments are separated when there is no exchange. As the exchange rate increases, the lines broaden. When the exchange rate nears the frequency difference between the sites, the broaden lines coalesce. In the limit of fast exchange, the signal sharpens eventually becoming a single sharp line. The lineshape in this case can be described using a modified set of Bloch equations. For a more complicated system like that in this study, a full density matrix description is needed, since the coherence associated with a single transition in one site may be spread among several transitions in another site.[86,87] Fortunately, now this calculation is relatively straightforward to do with modern computer tools because many reliable computer programs for simulating

exchange lineshapes are available.[88] Knowing the rates and the spin parameters, I was able to simulate the spectrum without dealing with large amounts of complicated calculations. The analysis with these computer programs is achieved by fitting the simulated spectrum to the observed spectrum visually and reporting the rate constants.

It is important to state here that the rate constants provided by the computer programs are pseudo-first-order rate constants because the nature of dynamic behavior observed by the VT NMR technique. Therefore, if a coalescence temperature is concentration-dependent, like my case, the pseudo-first-order rate constant generated by these computer programs is concentration-dependent. The real rate constant should be generated by removing the concentration-dependence. For example, if the exchange is a second-order kinetics, the real rate constant is the pseudo-first-order rate constant divided by concentration. This rate constant should be the one used in the Eyring equation for kinetic parameter calculations.

A preliminary estimation of the kinetic parameters ($\Delta H^{\ddagger}$, $\Delta S^{\ddagger}$, and $\Delta G^{\ddagger}$) for my exchange system was performed following the procedure used in Lang's group to study the VT ^{31}P NMR spectra for phosphine-silver complexes.[89] In this analysis, the NHC ligand exchange behavior was considered to be analogous to the phosphine ligand exchange. Therefore, the analysis method used to study the VT ^{31}P NMR spectra for phosphine-silver complexes could be applied to my analysis of ^{13}C NMR spectra. Instead of dealing with the complicated lineshape analysis at each temperature, this analysis focused on the rate constant estimations at two coalescence temperatures: at one of the coalescence temperatures, the doublet of doublets coalesced to a broad doublet; at

the other coalescence temperature, a broad singlet coalesced from a broad doublet was observed. The analytical procedure described by Lang was followed and the rate constants of ligand exchange at the coalescence temperatures (k_c) were determined using eq. 3. The corresponding activation free energy at the coalescence temperature ($\Delta G^{\ddagger}_c$) was then determined using the Eyring equation (eq. 4). These two coalescence temperatures (T_{c1} and T_{c2}) provided two values for $\Delta G^{\ddagger}_c$ ($\Delta G^{\ddagger}_{c1}$ and $\Delta G^{\ddagger}_{c2}$) while $\Delta H^{\ddagger}$ and $\Delta S^{\ddagger}$ could be calculated from Gibbs–Helmholtz equation (eq. (5)–(7)). The activation free energies estimated with this method were *ca.* 12.0, 11.3, and 11.3 kcal/mol at 20 ºC for **61**, **62** and **63**, respectively.

$$k_c = \pi\Delta\nu/\sqrt{2} \tag{3}$$

$$k = (k_bT/h)\exp[-\Delta G^{\ddagger}/RT] \approx (2.08 \times 10^{10}T)\exp[-\Delta G^{\ddagger}/RT] \tag{4}$$

$$\Delta G^{\ddagger}_c = RT_c[23.76 + \ln(T_c/k_c)] \text{ kcal/mol} \tag{4a}$$

$$\ln(k/T) = -(\Delta H^{\ddagger}/R)(1/T) + [\Delta S^{\ddagger}/R + \ln(k_b/h)] \tag{4b}$$

$$\Delta G^{\ddagger} = \Delta H^{\ddagger} - T\Delta S^{\ddagger} \tag{5}$$

$$\Delta S^{\ddagger} = (\Delta G^{\ddagger}_{c1} - \Delta G^{\ddagger}_{c2})/(T_{c1} - T_{c2}) \tag{6}$$

$$\Delta H = \Delta G^{\ddagger}_{c1} + T_{c1}\Delta S^{\ddagger} = \Delta G^{\ddagger}_{c2} + T_{c2}\Delta S^{\ddagger} \tag{7}$$

The second method for the kinetic parameter estimation used the WinDNMR-Pro program.[90] WinDNMR-Pro is a user-friendly program and has been used to estimate kinetic parameters of many dynamic behaviors.[91,92] Examples of the simulated spectra are shown in Figure 30.

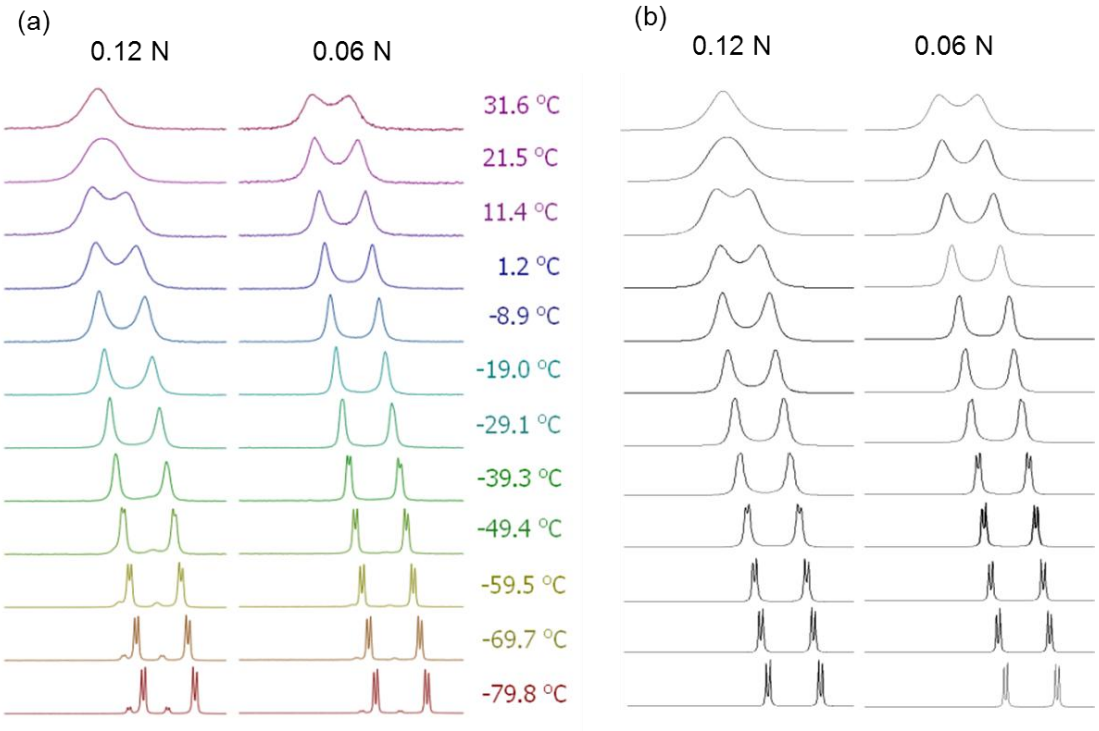

Figure 30. (a) VT ^{13}C NMR of 0.06 N and 0.12 N solutions of **61** in CD_2Cl_2: the solution with lower concentration has higher coalescence temperature. (b) Simulated spectra generated by WinDNMR-Pro program.[90]

The pseudo-first-order rate constants calculated from the simulation program were concentration-dependent. It was found that the pseudo-first-order rate constants given by WinDNMR-Pro program have a good linear relationship with concentrations for each temperature. This suggested that the NHC ligand exchange proceeded a second-order mechanism and agreed with the proposed mechanism by Lin's group.[28] The second-order rate constants were calculated by dividing pseudo-first-order rate constants with concentrations and were used with the Eyring equation (eq. 4) to

construct Eyring plots to determine the parameters $\Delta H^{\ddagger}$ and $\Delta S^{\ddagger}$. Calculated activation free energies at 20 ºC for **61**, **62** and **63** are *ca*. 11.8, 10.5 and 10.9 kcal/mol, respectively.

While WinDNMR-Pro is convenient to use, simulation with another computer program MEXICO is more complicate and requires inputting more variables. However, MEXICO also provides opportunity to understand parameters used in the simulation of the dynamic NMR spectra. MEXICO is based on the theory of a *complex-valued* line position and transition probability.[93] Unlike other theories calculating lineshape in the frequency domain as used in a CW spectrometer, this theory calculates the effects of exchange in the time domain as they are actually measured on a pulse-Fourier-transform spectrometer and provides a rigorous description of the effect of dynamics on pulse experiments.[85,93,94] Similar to the estimation process with WinDNMR-Pro, the second-order rate constants were calculated by dividing pseudo-first-order rate given by MEXICO and were applied to Eyring eq. (eq. 4) to construct Eyring plots determining the parameters $\Delta H^{\ddagger}$ and $\Delta S^{\ddagger}$. Calculated activation free energies at 20 ºC for **61**, **62** and **63** are *ca*. 12.6, 11.2 and 11.5 kcal/mol, respectively.

Computational Studies of the NHC Ligand Exchange Process

To gain a better understanding of the mechanism for the ligand exchange process in (*N*-mesityl-*N′*-methylimidazolylidene)silver(I) halides **61**, **62**, **63**, a series of computational studies were carried out using Density Functional Theory (DFT)[95] as implemented in Gaussian 03/09.

Full geometry optimizations were performed on **61**, **62**, **63,** and the transition states to their ion pair species $[NHC_2Ag][AgX_2]$ (X = Cl, Br, and I: **61b**, **62b**, and **63b**, respectively), and the theoretical models of free NHC and free AgCl. All calculations were performed with the Gaussian 03 (G03)[96] or Gaussian 09 (G09)[97] suite of programs with the LANL2DZ (Los Alamos National Laboratory double-ζ)[98-100] basis set and Effective Core Potential (ECP) or the SDD (Stuttgart-Dresden)[101,102] basis set and ECP effects for silver atom and 6-311G(d,p) for all other elements (BSI and BSII, respectively). Geometry optimizations were performed using Density Functional Theory with either the B3LYP (Becke three-parameter hybrid exchange functional[103] and the Lee-Yang-Parr correlation functional[104]) or *m*PW1PW91 (Barone's Modified Perdew-Wang 1991 exchange functional and Perdew and Wang's 1991 correlation functional)[105] on all of the models. The SMD parameterized[106] PCM (Polarized Continuum Model) model was used to estimate solvation effects. Both SMD single point energy (SPE) calculations at the gas-phase optimized geometry and full geometry optimizations were performed.

Two mechanisms for NHC exchange were evaluated. First, a mechanism involving NHC-AgCl bond dissociation was considered. It was found that the dissociation energy is *ca.* 55 kcal/mol in the gas-phase and 43 kcal/mol in solution (CH_2Cl_2). While these results suggested that the NHC-AgCl bond is not a strong bond, the bond dissociation energy is much larger than that calculated from the coalescence studies. Second, the associative reaction pathway shown in Scheme 41 was calculated in solution (CH_2Cl_2) and the results are shown in Figure 31. The $\Delta G^{\ddagger}$ calculated for the

associative reaction path are 19.54, 17.47, and 12.54 kcal/mol for X = Cl, Br, and I, respectively. While the calculated $\Delta G^{\ddagger}$ are somewhat larger than the experimentally determined values (12.6, 11.2, and 11.5 kcal/mol) they are still within reason.

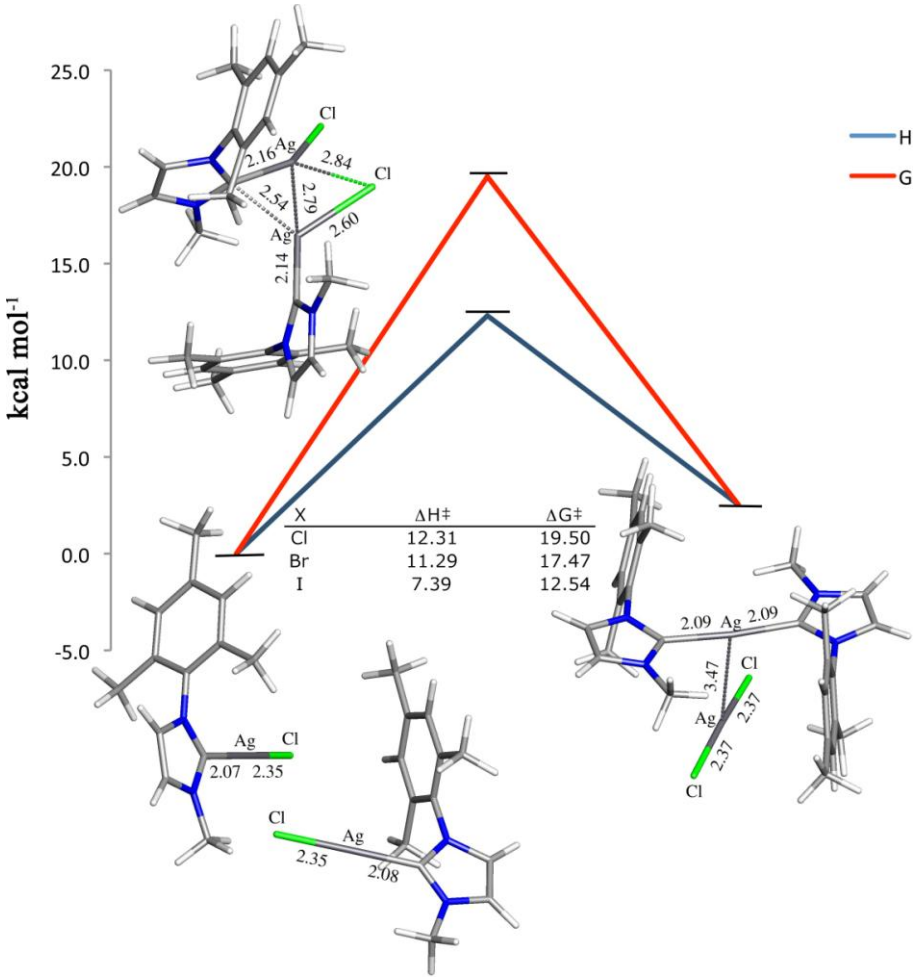

Figure 31. MPW1PW91/BSII results for the ligand exchange process of (*N*-mesityl-*N*′-methylimidazolylidene)silver halides.

Effects of Additional Phosphines to NHC-silver Halides

In Chapter III, it was found that the addition of triphenylphosphine facilitated the NHC ligand transfer from silver to ruthenium. This suggested that it would be interesting to study the effects of added phosphine ligands on the NHC exchange rate in NHC silver halide complexes.

In my initial study of the effect of the addition of phosphine, 0.7 equiv. of triphenylphosphine was added to a denzene-d_6 solution of (*N*-mesityl-*N*′-(2-(1-benzyl-1,2,3-triazol-4-yl)ethyl)imidazolylidene)silver(I) bromide **46** (eq. (8)). This addition of triphenylphosphine led to significant changes in the chemical shifts of key peaks for **46** both in ^{1}H and ^{13}C NMR spectra as shown in Figure 32.

The addition of triphenylphosphine to a CD_2Cl_2 solution of IMesAgCl **55** led to little or no change in the chemical shifts of the resonance for **55**. What appeared to be occurring instead was a change in the distribution of the neutral species **55a** and the ion pair **55b** (eq. (9)). This effect is seen in Figure 33. In these spectra, the peaks labeled "a" is due to the proton of the neutral species **55a** and the peak labeled "b" is due to the ion pair **55b**. Integration of these two components showed that the ratio of **55a**/**55b** changes in a linear fashion as the amount of triphenylphosphine is increased up until 1 equiv. of triphenylphosphine has been added (Figure 34). After 1 equiv. of triphenylphosphine had been added, the equilibrium between the neutral species and the ion pair had shifted such that > 95% of the silver species present was the ion pair.

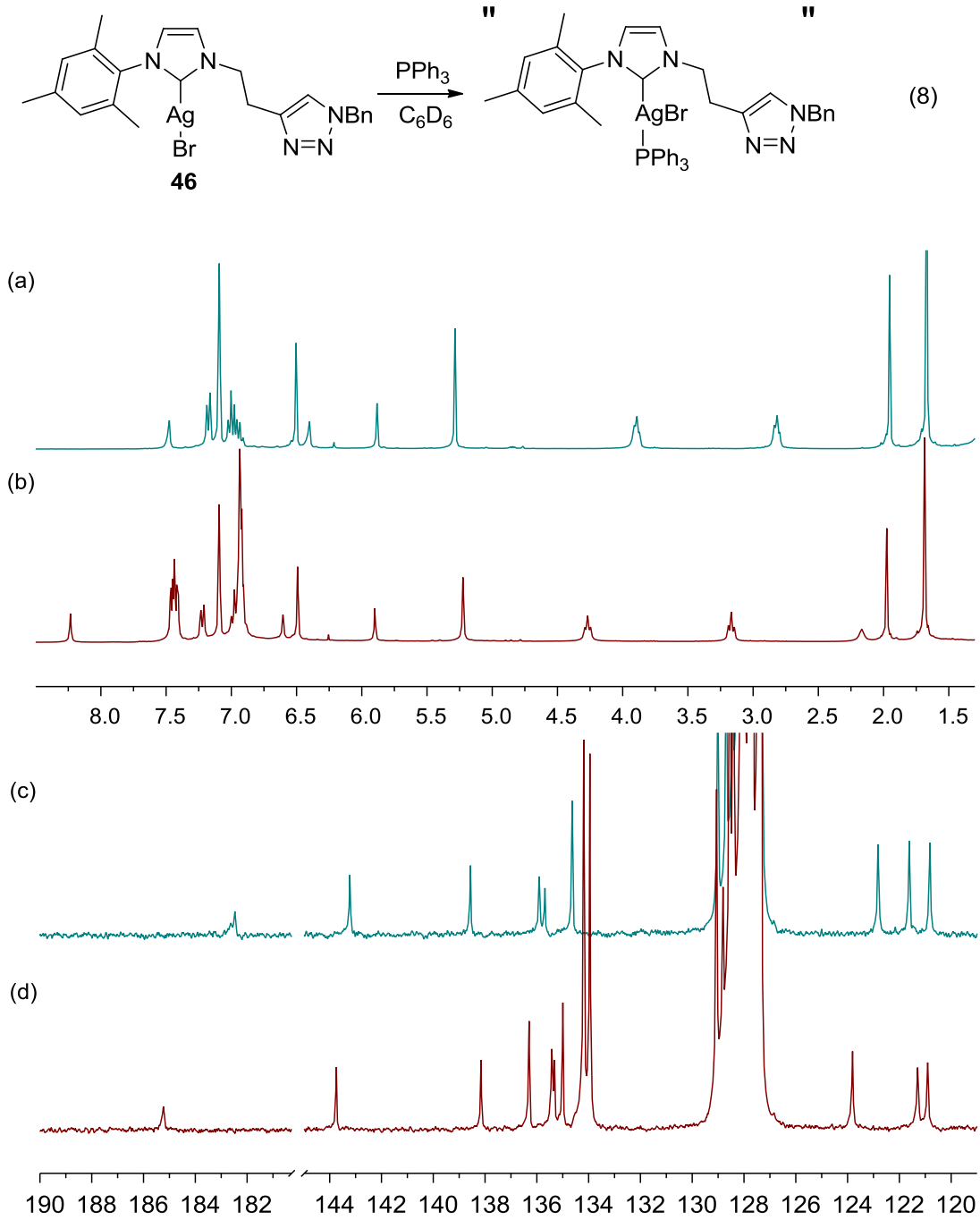

Figure 32. ^{1}H NMR spectra of **46** (a) before and (b) after the addition of 0.7 equiv. of triphenylphosphine and ^{13}C NMR spectra of **46** (c) before and (d) after the addition of 0.7 equiv. of triphenylphosphine.

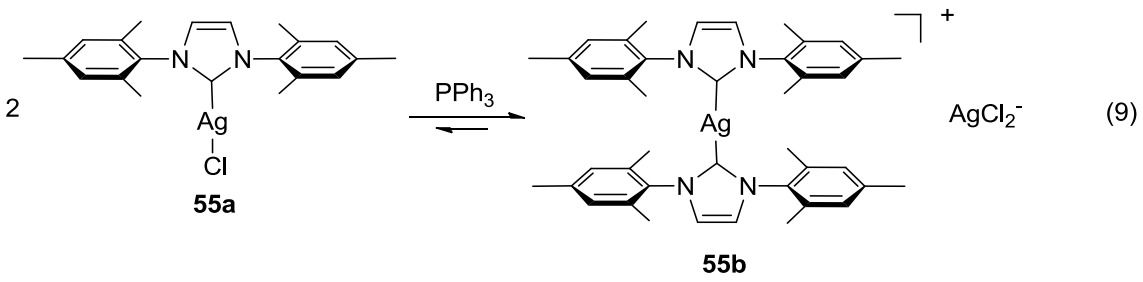

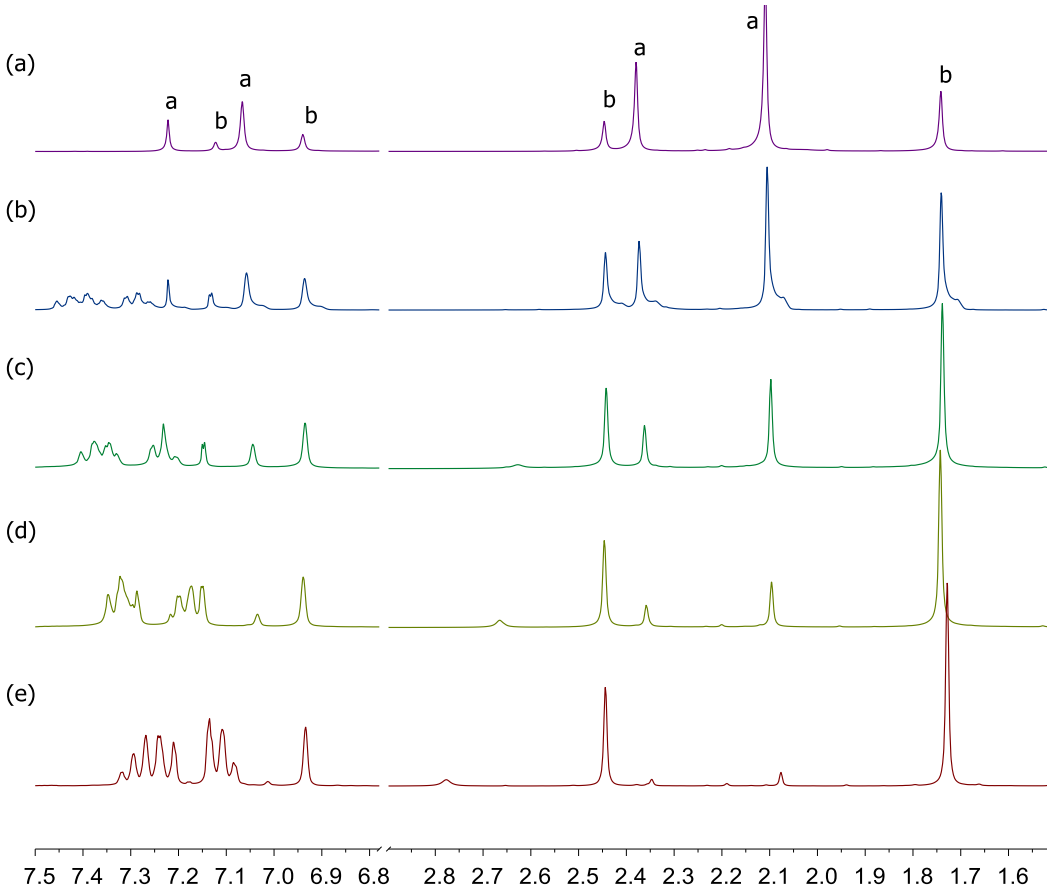

Figure 33. ^{1}H NMR spectra of **55** (a) before and after the addition of (b) 0.39, (c) 0.67, (d) 1.0 and (e) 1.8 equiv. of triphenylphosphine. Label "a" and "b" on the spectra indicate the neutral species **55a** and ion pair **55b**, respectively.

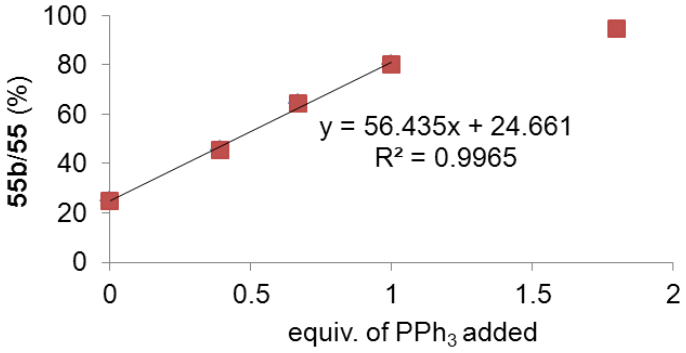

Figure 34. Based on the integration ratio on ^{1}H NMR spectra at 20 ºC, the amount of the ionic species [$IMes_2Ag$][$AgCl_2$] **55b** showed a good linear relationship with the additional amount of PPh_3 before 1 equiv. of PPh_3 was added.

At 0 ºC, when 0.39, 0.67, 1 and 1.8 equiv. of PPh_3 added, the ^{31}P NMR spectra of these solutions showed sharp singlet at 6.5, 5.9, 4.4 and 2.9 ppm, respectively. At -80 ºC, ^{31}P NMR spectra of these solutions contain one or more sets of doublet of doublets indicating formation of P-Ag bonds (Figure 35). With 0.39 equiv. of triphenylphosphine had been added, two sets of doublet of doublets were found. The major phosphorus species was a doublet of doublet centered at 6.7 ppm had ^{31}P-^{107}Ag and ^{31}P-^{109}Ag coupling constants 600 and 691 Hz. The minor component, which became the major component in the solution after addition of 0.67 - 1.8 equiv. of triphenylphosphine, was a doublet of doublets centered at 3.0 ppm with 276 and 318 Hz coupling constants.

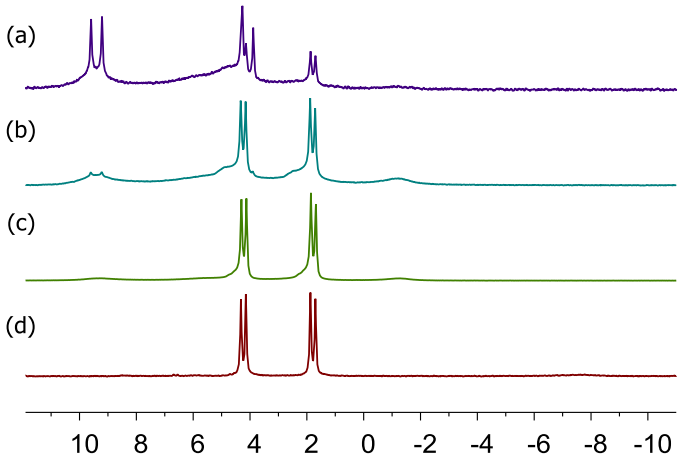

Figure 35. ^{31}P NMR spectra of a CD_2Cl_2 solution of **55** (a) before and after addition of (b) 0.39, (b) 0.67, (c) 1.0 and (d) 1.8 equiv. of triphenylphosphine at -80 ºC.

Studies of the effect of triphenylphosphine addition on the change of component distribution of IMesAgCl **55** showed that phosphine ligand coordination to silver can affect the structure of a silver complex and equilibrium involving (NHC)AgX neutral species and $(NHC)_2Ag^+$ AgX_2^- ion pairs. This suggested that triphenylphosphine could also affect the dynamics of NHC ligand exchange and the composition of (*N*-mesityl-*N*′-methylimidazolylidene)silver halide complexes studied above. Thus, I next examined the effects of triphenylphosphine addition to a 0.12 N solution of ^{13}C-labelled (*N*-mesityl-*N*′-methylimidazolylidene)silver iodide **63**. In these experiments, 0.2, 0.4, 0.9, 1.2, 1.6 and 3.0 equiv. of triphenylphosphine were added respectively. In this case, the neutral and ionic species **63a** and **63b** could not be distinguished by ^1H NMR at 21 ºC while VT ^{31}P and ^{13}C NMR spectroscopic studies of these solution did provide some interesting results which are discussed below.

VT ^{31}P NMR spectra of ^{13}C-labelled (*N*-mesityl-*N*′-methylimidazolylidene)silver iodide **63** solutions with added triphenylphosphine are shown in Figure 36. At 21 ºC, ^{31}P NMR spectra of these solutions showed sharp singlet at 4.1, 3.4 and 0.6 ppm when 0.9, 1.2, and 3.0 equiv. of triphenylphosphine were added. At -85 ºC, one or more sets of doublet of doublets were observed indicating the coordination of phosphine to silver and the formation of P-Ag bonds. Four sets of doublets of doublets were found in these spectra. With only 0.2 equiv. of triphenylphosphine was added, the major phosphorus species was a doublet of doublets centered at 6.8 ppm with ^{31}P-^{107}Ag and ^{31}P-^{109}Ag coupling constants 600 and 693 Hz. When 0.4 - 1.2 equiv. of triphenylphosphine added, this species was no longer detectable and the only species detected was a doublet of doublet centered at 3.0 ppm with ^{31}P-^{107}Ag and ^{31}P-^{109}Ag coupling constants of 276 and 319 Hz, respectively. These peaks and coupling constants are the same as the observed peaks seen in Figure 35 after addition of triphenylphosphine to **63**, suggesting the formation of similar products.

After addition of 3 equiv. of triphenylphosphine to a solution of **63**, a large singlet peak at δ -7.4 ppm in ^{31}P NMR was observed. This peak corresponds to free triphenylphosphine. In addition to this singlet, three sets of doublets of doublets were observed with integration ratio of 33:16:1. The larger doublet of doublets was the same as the peaks observed when 0.4 - 1.2 equiv. of triphenylphosphine was added. A lower concentration component centered at 5.6 ppm and had 223 and 257 Hz coupling constants. A very small set of doublet of doublets was found at -1.0 ppm with 261 and 302 Hz of coupling constants.

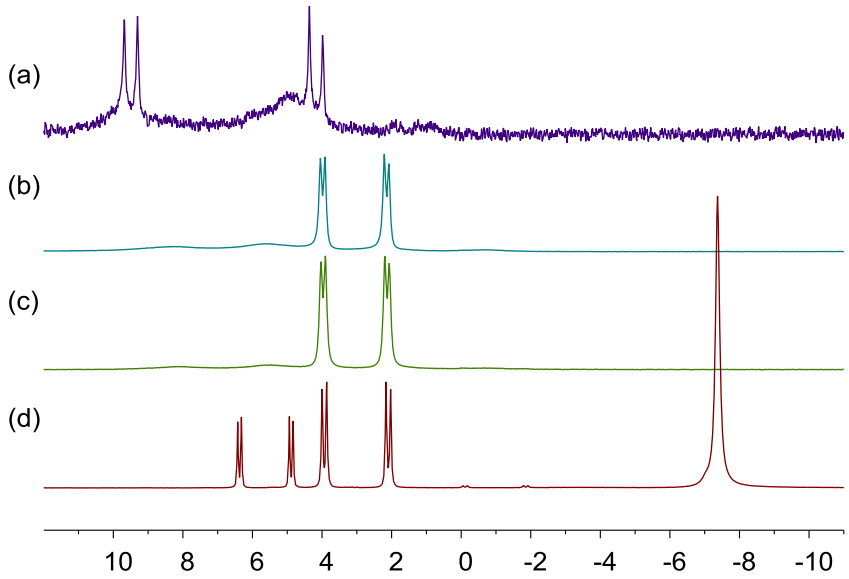

Figure 36. ^{31}P NMR spectra of the carbene carbons of **63** in CD_2Cl_2 solutions at -85 ºC after addition of (a) 0.2, (b) 0.9, (c) 1.2 and (d) 3.0 equiv. of triphenylphosphine.

VT ^{13}C NMR spectra of these solutions showed that the coalescence temperatures of **63** increased as the amount of triphenylphosphine increased (Figure 37). The -85 ºC ^{13}C NMR spectra are summarized in Figure 38, showing that the ratio of **63b**/**63a** increased as more triphenylphosphine added. As was for the case to **55**, the ratio **63b**/**63a** at -85 ºC appeared to be linearly correlatedwith the amount of triphenylphosphine added (Figure 39).

One thing should be noticed here: as discussed above, while the cations of **55b** and **63b** are the same, at -85 ºC ^{13}C NMR spectra, their coupling constants and chemical shift are indistinguishable. With current methods I knew, the actual anions in the solution could not be exactly identified. Therefore, the use of labeled "**55b**" and "**63b**" over here only refers to the $(NHC)_2Ag^+$ cations.

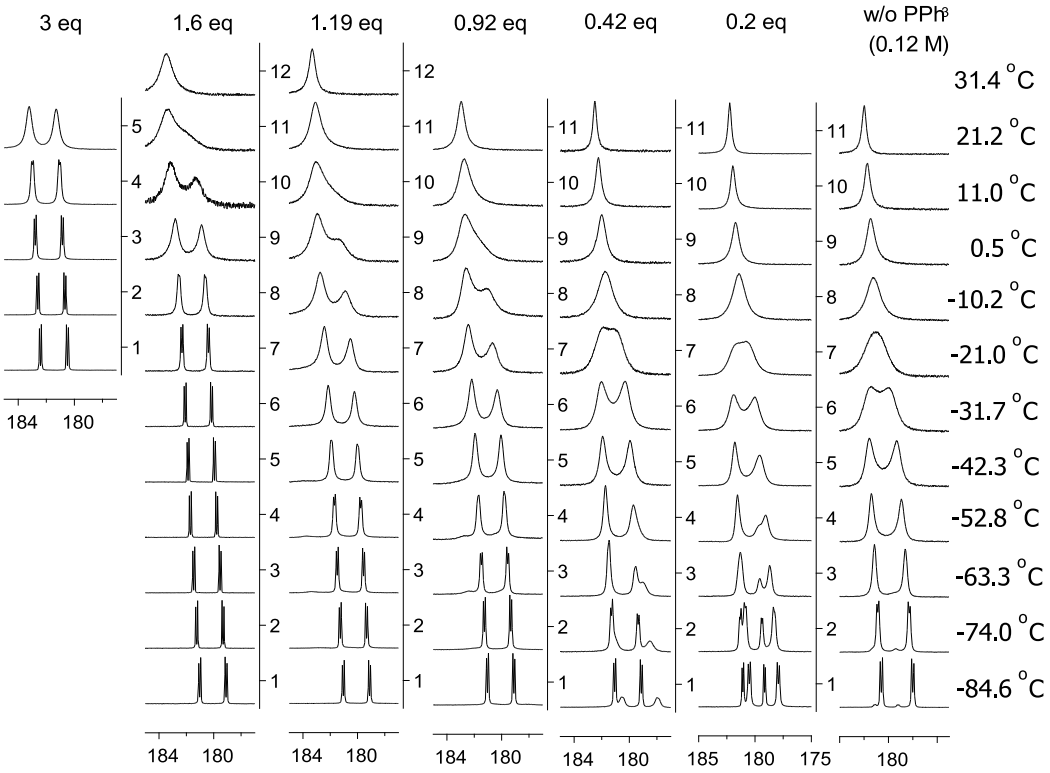

Figure 37. The coalescence temperatures of ^{13}C-labeled **63** increased as the amount of triphenylphosphine increased.

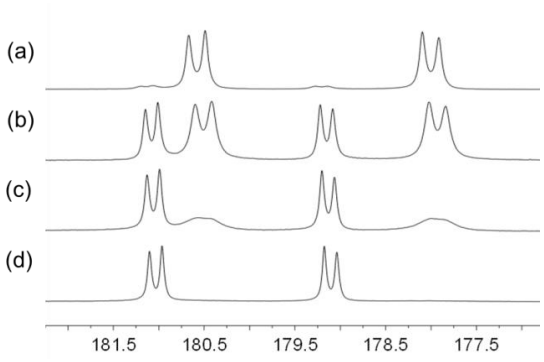

Figure 38. At -85 ºC, ^{13}C NMR spectra showed that the ratio **63b**/**63a** increased when the carbene carbons of (a) 0.0, (b) 0.2, (b) 0.4, (c) 0.9 and (d) 1.2 equiv. of triphenylphosphine was added to a CD_2Cl_2 solutions of **63**.

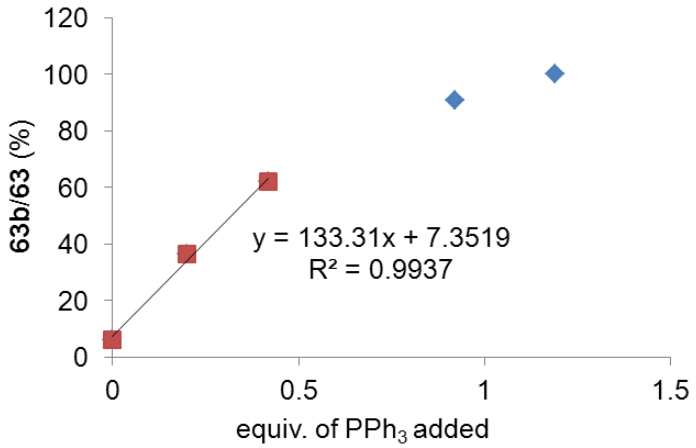

Figure 39. Based on the integration ratio on ^{13}C NMR spectra at -85 ºC, the amount of the ionic species **63b** showed a linear relationship with the additional amount of PPh_3 before 0.5 equiv. of PPh_3 was added.

The VT ^{31}P NMR spectra described above are similar to the spectra reported in the literature for triarylphosphine of silver halides complexes $(Ar_3P)_nAgX$ (n = 1 - 4) species: the more phosphine presented, the less the silver-phosphine coupling constants. A general trend of coupling constants in $(Ar_3P)_nAgX$ compounds is listed in Table 4.

Compared my ^{31}P spectra at -85 ºC or -80 ºC, the first formed species is more likely a silver-phosphine complex with sp hybridization on silver. The species with ^{31}P-^{107}Ag coupling constants *ca*. 276 and 261 Hz are more like $(Ar_3P)_3AgX$ species or may be $(Ar_3P)_2AgX_2^-$ while the species with ^{31}P-^{107}Ag coupling constant *ca*. 223 Hz should be a $[(Ar_3P)_4Ag]^+ X^-$ species. The solution behaviors in my cases are complicate, the possible products may form in the solutions and the corresponding formation mechanisms are showed in Scheme 42. In Scheme 42, the species with sp hybridization

on silver, *i.e.* the coordination number of 2, are colored with blue while species with sp^2 hybridization on silver are colored with red. The species with sp^3 hybridization on silver are colored by green.

Table 4. A general trend of coupling constants in $(Ar_3P)_nAgX$ compounds.

	Ag hybridization	^{31}P-^{107}Ag coupling constant
$(Ar_3P)AgX$	sp	440 - 610 Hz
$(Ar_3P)_2AgX$	sp^2	350 - 400 Hz
$(Ar_3P)_3AgX$	sp^3	250 - 330 Hz
$[(Ar_3P)_4Ag]^+ X^-$	sp^3	220 - 240 Hz
$[(Ar_3P)_2Ag]^+ Y^-$	sp	470 - 510 Hz
$[(Ar_3P)_3Ag]^+ Y^-$	sp^2	300 - 330 Hz
$[(Ar_3P)_4Ag]^+ Y^-$	sp^3	220 - 240 Hz

X = Cl, Br, I
Y = noncoordinated anions, such as BF_4^-, NO_3^-, PF_6^-
Ar = Ph, *o*-Me-C_6H_4, *m*-Me-C_6H_4, *p*-Me-C_6H_4

Both $(NHC)(PPh_3)Ag^+$ and $(PPh_3)AgX$ are possible candidate for the first formed silver-phosphine complex with sp hybridization on silver. The -85 ºC ^{13}C NMR spectra (Figure 38) showed that the first form species is more like $(NHC)_2Ag^+$. However, without knowing the extract spectra of $(NHC)(PPh_3)Ag^+$, the possibility of $(NHC)(PPh_3)Ag^+$ cannot be ruled out. In addition, if $(NHC)(PPh_3)Ag^+$ is the species, the increasing amount of ionic species carbene peak ratio on ^{13}C NMR spectra should be the same as the phosphine added. If $(PPh_3)AgX$ is the species, the silver source should be AgX_2^-. With the consuming of AgX_2^-, the Le Châtelier's principle will drive the equilibrium between (NHC)AgX and $(NHC)_2Ag^+$ AgX_2^- to the formation of ion pair.

Because consuming one AgX_2^- will produce two carbene in one $(NHC)_2Ag^+$, the increasing rate of ionic carbene peak on ^{13}C NMR spectra will be twice of the phosphine added. Based on the ^{13}C NMR spectra (Figure 38), when 0.2 equiv. of phosphine was added, 40% of the carbene carbon presented at the position of ionic species. Therefore, it is believed that when 0.2 equiv. of triphenylphosphine was added, $(PPh_3)AgX$ and 0.2 equiv. of $(NHC)_2Ag^+$ were generated in the solution.

On -85 ºC ^{13}C NMR spectra, only two species were found. In the previous discussion, these two species should be (NHC)AgX and $(NHC)_2Ag^+$. In consequence, the formation of $(NHC)_x(PPh_3)_yAgX$ and $(NHC)_x(PPh_3)_yAg^+$ (x = 1, 2 and y = 1, 2, 3) will be rule out. The possible silver-phosphine complexes left here are $(PPh_3)_mAg+$, $(PPh_3)_mAgX$, and $(PPh_3)_mAgX_2^-$.

With the discussion above, the species with ^{31}P-^{107}Ag coupling constants *ca*. 276 and 261 Hz be $(PPh_3)_3AgX$ or $(PPh_3)_2AgX_2^-$ while the species with *ca*. 223 Hz of ^{31}P-^{107}Ag coupling constant should be a $[(Ar_3P)_4Ag]^+ X^-$ species. Considering the amount of phosphine added, the predominant silver-phosphine complex with 0.2 - 3.0 equiv. of phosphine added should be $(PPh_3)_2AgX_2^-$ and the species with very low intensity when 3.0 equiv. of phosphine was added to the solution should be $(PPh_3)_3AgX$. The final conclusion of these discussions is summarized in Scheme 43.

Scheme 42. When triphenylphosphine was added to an NHCAgX solution, many possible products can form.

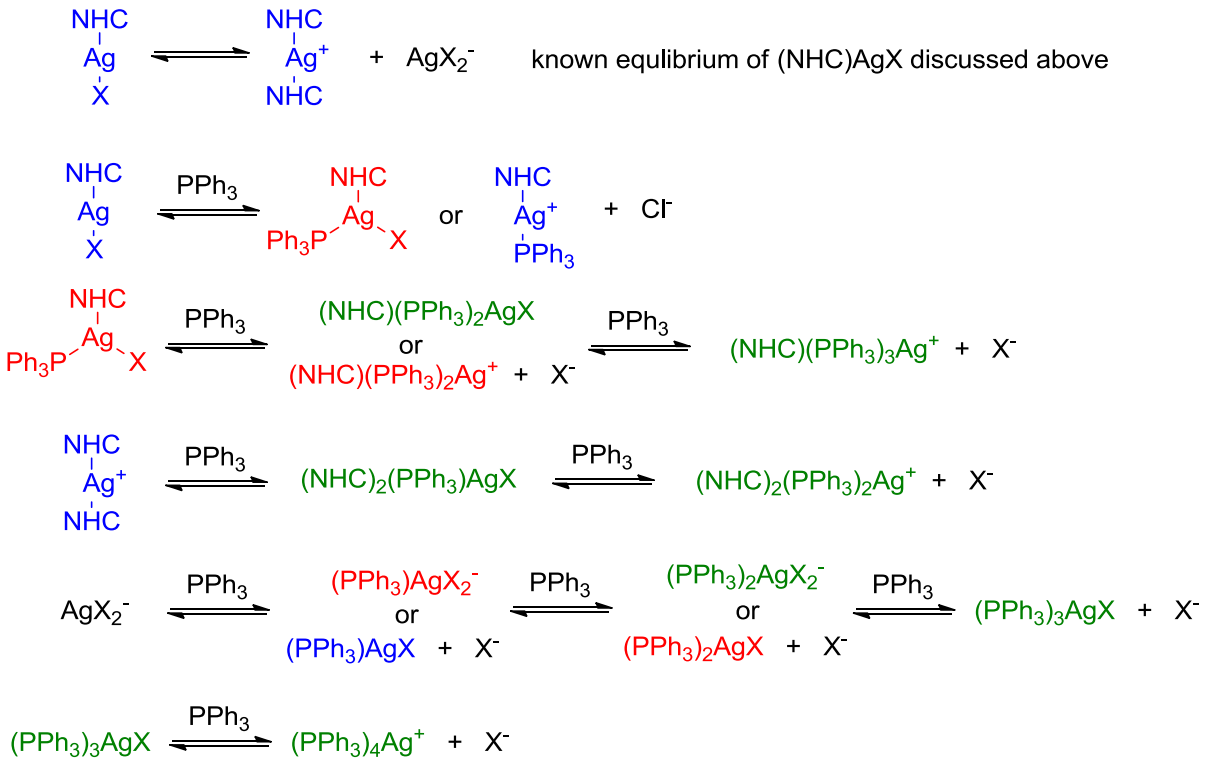

Scheme 43. Proposed mechanism of species presented in solutions when triphenylphosphine was added to an NHCAgX solution.

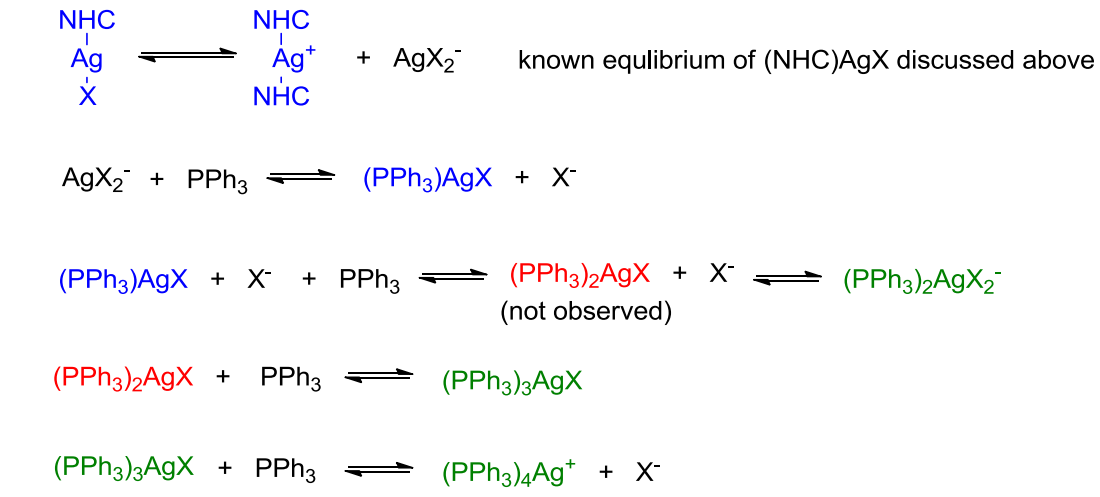

Conclusion

^{13}C-labeled (*N*-mesityl-*N'*-methyllimidazolylidene)silver halides have been prepared and VT ^{13}C NMR spectroscopy was used to study the NHC ligand exchange processes for these complexes. Using ^{13}C labeled derivatives in this study improved the s/n ratio and made it possible to obtain spectra at various concentrations and also showed the presence of low concentrations of ion pair complexes that are in equilibrium with a neutral NHC silver halide complex. The concentration-dependent coalescence temperature suggested that an associative process was involved in the exchange. The effects of bridging anions and phosphine additives were also examined. A modified mechanism based on DFT calculations is proposed to explain such an exchange process.

The effect of added phosphine on the NMR spectra of ^{13}C-labeled (*N*-mesityl-*N'*-methyllimidazolylidene)silver iodide complexes was also studied using VT ^{1}H, ^{13}C, and ^{31}P NMR spectroscopy. These studies showed that phosphine addition both altered the exchange rates for NHC ligands and affected the nature of the species present in solution. Based on literature data, the effects of phosphine addition are proposed to result from formation of phosphine-silver complexes.

CHAPTER V

CONCLUSIONS

Research presented in this dissertation included studies of both fundamental and applied chemistry of NHC-metal complexes. Chapters II and III of this dissertation described the utility of polymers as phase tags for the separation and recycling of NHC-metal catalysts. The polymer-supported ligands, catalysts, and sequestrants showed comparable reactivity to their low molecular weight counterparts. Due to the nature of the polymers used, these polymer-supported compounds showed different solubility properties. Using these materials provides simple methods to separate deeply colored, metal-containing by-products from the reaction mixtures.

In Chapter IV, ^{13}C-labeling technique was used to label the NHC-silver complexes' carbene carbons which usually have a low signal-to-noise ratio in ^{13}C NMR spectroscopy. This method facilitated studies of the solution behaviors of low concentration materials in a short time. With this technique, I was able to detect the minor components of equilibrium mixtures of NHC-silver complexes even when the minor component is *ca.* 5% of the total amount. Also, the concentration-dependence of the NHC ligand exchange in silver complexes was studied. The NHC ligand exchange behaviors of NHC-silver(I) complexes were carefully examined and many exchange-affecting factors were evaluated. This investigation is useful for the future study of transmetallation, a common method used to prepare other NHC-metal complexes.

CHAPTER VI

EXPERIMENTAL SECTION

Materials

Polyisobutylene was a gift from BASF (Glissopal® 1000 and 1300). The polyethylene oligomers (UNILIN® 550) were a gift from Baker-Hughes Baker Petrolite. All other reagents and solvents were purchased from commercial sources and used without further purification unless otherwise specified.

Instrumentation

^{1}H NMR spectra were obtained on Varian Inova 300, 400, or 500 MHz spectrometers operating at 300, 400, and 500 MHz, respectively. ^{13}C NMR spectra were measured on these spectrometers operating at 75, 100, and 125 MHz. Chemical shifts of ^{1}H and ^{13}C NMR spectra are reported in parts per million (δ) relative to residual proton resonances in the deuterated solvents ($CDCl_3$, CD_2Cl_2, or C_6D_6). ^{31}P NMR spectra were recorded on spectrometers operating at Varian Inova 300 or 400 MHz spectrometers operating at 122 and 164 MHz, respectively. Chemical shifts of ^{31}P NMR spectra were reported in ppm and were referenced to external 85% H_3PO_4 aqueous solution at room. Coupling constants (*J* values) were reported as Hertz (Hz) and spin multiplicities are indicated by the following symbols: s (singlet), d (doublet), dd (doublet of doublets), t (triplet), q (quartet), br (broad), and m (multiplet). Temperatures recorded for VT NMR experiments were calibrated with 100% MeOH. Integrations of the chemically different protons on pendant groups on PIB-bound intermediates reflect the normal accuracy associated with integration in ^{1}H NMR spectroscopy. The large signal due to the PIB-

protons in the 1-2 ppm region of the ^{1}H NMR spectrum of these PIB-bound products can also be integrated. A typical value for the polymers we use is 180/1 since the PIB used has a M_n of ca. 1300. However, since samples of PIB vary in M_n and since the normal ca. 5-10% errors in integration are exaggerated in NMR analyses of a very large (e.g. a 180 proton signal in this case) and a very small signal (e.g. a 1 proton signal), these integrations in the ^{1}H NMR spectra are not listed below.

ICP-MS (inductively coupled plasma mass spectroscopy) data were obtained using a Perkin Elmer ELAN® DRC II instrument with argon as carrier gas and 1% HNO3 aqueous solution as a matrix. X-ray diffraction patterns were recorded on Bruker single-crystal APEXii CCD Diffractometers with three-circle D8 Goniometer, molybdenum X-ray radiator, and Kryoflex Cyrosystem low temperature attachment operated at 110 K. Melting points were measured by Stanford Research Systems OptiMelt apparatus and uncorrected.

Elemental analysis of Ag, I, Cl was analyed using a Cameca SX50 electron microprobe equipped with four wavelength-dispersive spectrometers (WDS). A WDS spectrometer is a monochromator which consists of a rotatable, oriented diffraction crystal coupled with a proportional gas-filled ionization detector in a geometric relationship following Bragg's Law. WDS was used rather than EDS because of the former's better resolution, detection limits, accuracy and reproducibility. Analyses were carried out at an accelerating voltage of 15 KV at a beam current of 10 nA and a beam diameter of 20μm using PET diffracting crystals. The sample was prepared by pressing several milligrams of the powdered material between two highly polished (0.25 μm)

stainless steel cylinders to yield a thin mm diameter smooth surfaced pellet that was then transferred onto a conductive carbon tape. The pellet was coated with approx. 150Å of spec pure carbon to prevent charge buildup under the electron beam. During analysis, the sample stage was moved repetitively between ten adjacent points at 2 second intervals to obtain more representative sampling of the pellet surface and to minimize any possible thermal damage to the sample. The following standards were used: Ag_2S for Ag, RbI for I, and NaCl for Cl. All analyses were processed through the Cameca PAP (Pouchot and Pichoir) full-quantitative ZAF type matrix correction program. In order to more properly correct for interelement matrix effects, carbon was calculated by difference to sum the analyses to 100% by weight. BSE (back-scattered electron) imaging was used to examine the surface for homogeneity. BSE examination yields an image where the brightness is directly proportional to mean atomic number.

Computational calculations were performed with the Gaussian 03 (G03) or Gaussian 09 suite of programs on a supercomputer composed with a cluster of 3 64-core Altix 450 machines with Itanium2 montecito dual core cpus housed in two tall racks and connected via gigabit ethernet.

Synthesis and Experimental Procedures

Hydroxy-terminated polyisobutylene: In a 250-mL round-bottomed flask, equipped with a magnetic stir bar and a rubber septum, the vinyl-terminated PIB (39 g, 39 mmol) was dissolved in 50 mL of hexanes. Then a 2.0 M solution of $BH_3{\cdot}SMe_2$ (7.7 mL, 15.4 mmol) in THF was slowly added. After 18 h, the reaction mixture was cooled to 0 ºC and 12 mL of a 4 N aqueous NaOH solution and 100 mL of water were added to the

hydroboration product. Then 7 mL of a 30% H_2O_2 solution was slowly added and the mixture was stirred overnight at room temperature. At this point, the two phases were separated and the organic phase was washed with H_2O (3 x 50 mL) and brine (50 mL), and then dried over $MgSO_4$. After filtration, the solvents were removed under reduced pressure and the product was dried under vacuum for 24 h, a total yield of 40 g of product was obtained. ^{1}H NMR (300 MHz, $CDCl_3$), δ: 3.48 (dd, *J* = 5.4, 10.2 Hz, 1H), 3.31 (dd, *J* = 7.5, 10.2 Hz, 1H), 1.46-0.75 (PIB protons).

Polyisobutyl mesylate: In a 250-mL round-bottomed flask, equipped with a magnetic stir bar a rubber septum, the hydroxy-terminated polyisobutylene (10 g, 9.8 mmol) and methanesulfonyl chloride (2.3 mL, 29 mmol) were dissolved in 100 mL of CH_2Cl_2 and cooled to 0 ºC. Then Et_3N (4.3 mL, 31 mmol) was added dropwise. The reaction mixture was allowed to stir for 3 h after warming to room temperature. The solvent was removed under reduced pressure to yield a crude viscous oil. This oil was dissolved in 300 mL of hexane and this hexane solution was extracted and washed with water (3 x 100 mL), dried over $MgSO_4$ and filtered. The solvent was removed under reduced pressure to yield 10.5 g (98%) of product. ^{1}H NMR (300 MHz, $CDCl_3$), δ: 4.06 (dd, *J* = 5.4, 9.3 Hz, 1H), 3.88 (dd, *J* = 7.5, 9.3 Hz, 1H), 2.96 (s, 3H), 1.95 (m, 2H), 1.39–0.88 (PIB protons).

***N*-Methyl-*N′*-polyisobutylimidazolium iodide:** In a 50-mL round-bottomed flask, equipped with a magnetic stir bar and a rubber septum, polyisobutyl mesylate (1.21 g, 1.1 mmol), *N*-methylimidazole (0.49 g, 5.9 mmol) and sodium iodide (0.32 g, 2.2 mmol) was mixed with 15 mL of toluene and 10 mL of DMF. After refluxing for 2 d, the

reaction mixture was cooled to room temperature. At this point, the upper phase of the two-phase mixture that formed was separated and washed with water (3 x 50 mL) and dried over $MgSO_4$. After filtration, the solvents were removed under reduced pressure to yield a crude product which contained the excess *N*-methylimidazole and the desired product. This mixture was further purified by column chromatography (elution first with CH_2Cl_2 and then with 9:1 solution of CH_2Cl_2 and methanol) to yield 0.7 g (59%) of product. ^{1}H NMR (300 MHz, $CDCl_3$), δ: 10.59 (s, 1H), 7.18 (s, 2H), 4.3-4.0 (br, 5H), 2.4-0.8 (PIB protons). ^{13}C NMR (75 MHz, $CDCl_3$), δ: 138.1, 123.1, 121.7, multiple poorly resolved peaks between 60-58, 49.7, multiple poorly resolved peaks between 40-30.

2,6-Diisopropyl-4-(polyisobutyl)aniline: In a 100-mL pressure vessel, a mixture of 2,6-diisopropylaniline (23 g, 130 mmol), polyisobutylene (10 g, 10 mmol), and aluminum trichloride (4.0 g, 30 mmol) was stirred in a sand bath at 200 °C. After 3 days, the deep purple solution was cooled to approximately 100 °C and added to 200 mL of hexane. After cooling to room temperature, the mixture was filtered and washed with water (3 x 150 mL) and CH_3CN (3 x150 mL). The solvent was removed under reduced pressure to yield a crude product which contained the desired product and unreacted starting materials. This mixture was purified by column chromatography (eluted first with hexane and then with CH_2Cl_2). Solvent removal afforded the product as a light yellow viscous liquid (7.5 g, 63% yield). ^{1}H NMR (300 MHz, $CDCl_3$), δ: 7.03 (s, 2H), 3.60 (s, 2H), 2.96 (m, 2H), 1.77 (s, 2H), 1.6-0.8 (PIB protons).

***N,N′*-Dis(2,6-diisopropyl-4-polyisobutylphenyl)ethylenediimine:** In a 100-mL round-bottomed flask, equipped with a magnetic stir bar and a rubber septum, a mixture of 2,6-diisopropyl-4-(polyisobutyl)aniline (6.6 g, 5.6 mmol), and a catalytic amount of formic acid in 20 mL of hexane was prepared. To this stirring solution, a solution of glyoxal (0.41 g of a 40% aqueous solution, 2.8 mmol) in 5 mL of isopropanol was added. The reaction mixture initially turned cloudy to a clear yellow solution after 5 min. The reaction mixture was allowed to stir for 20 h. At this point, the bright yellow solution was dried with Na_2SO_4 and the solvent was removed under reduced pressure, affording a dark yellow viscous liquid (6.5 g, 99% yield). ^{1}H NMR (300 MHz, $CDCl_3$), δ: 8.10 (s, 2H), 7.17 (s, 4H), 2.97 (m, 4H), 1.83 (s, 2H), 1.6-0.8 (PIB protons). ^{13}C NMR (125 MHz, $CDCl_3$), δ: 163.9, 146.4, 145.6, 136.0, 121.6, multiple poorly resolved peaks between 60-58 and 40-30, 18.9.

1,3-Bis(2,6-diisopropyl-4-(polyisobutyl)phenyl)imidazolium chloride: In a 100-mL round-bottomed flask, equipped with a magnetic stir bar and a rubber septum, *N,N'*-bis(2,6-diisopropyl-4-polyisobutylphenyl)ethylenediimine (6.3 g, 2.6 mmol) was dissolved in 25 mL of THF. Chloromethyl ethyl ether (0.25 g, 2.6 mmol) was added and the mixture was heated to 40 °C for 20 h. The solvent was removed under reduced pressure and the residue was purified by column chromatography (eluted first with CH_2Cl_2 and then with 9:1 solution of CH_2Cl_2 and methanol). Solvent removal afforded the product as a light brown viscous liquid (2.0 g, 31% yield). ^{1}H NMR (300 MHz, $CDCl_3$), δ: 8.63 (s, 1H), 8.41 (s, 2H), 7.33 (s, 4H), 2.46 (m, 4H), 1.90 (s, 6H), 1.6-0.8

(PIB protons). ^{13}C NMR (125 MHz, $CDCl_3$), δ: 154.4, 144.0, 137.9, 127.8, 127.2, 122.2, multiple poorly resolved peaks between 60-58 and 40-30, 18.9.

(1,3-Bis(2,6-diisopropyl-4-(polyisobutyl)phenyl)imidazoylidene)silver(I) chloride: In a 25-mL round-bottomed flask, equipped with a magnetic stir bar and a rubber septum, 1,3-bis(2,6-diisopropyl-4-(polyisobutyl)phenyl)imidazolium chloride **8** (0.86 g, 0.40 mmol) was dissolved in 6 mL of hexane. Silver oxide (0.058 g, 0.25 mmol) was added and the mixture was fluxed for 24 h. After cooling to room temperature, the reaction mixture was filtered through celite to remove excess Ag_2O and the celite was washed with hexane. The solvent was removed from the combined hexane solution under reduced pressure, affording 0.8534 g (95%) of a viscous oil product. ^1H NMR (500 MHz, $CDCl_3$), δ: 7.26 (s, 4H), 7.11 (s, 2H), 2.58-2.46 (m, 4H), 1.84 (s, 6H), 1.6-0.8 (PIB protons). ^{13}C NMR (125 MHz, $CDCl_3$), δ: 184.7 (dd, $J13_C$-107_{Ag} = 236 Hz, $J13_C$-109_{Ag} = 271 Hz), 152.2, 144.2, 131.9, 123.6, 122.1, multiple poorly resolved peaks between 60-58 and 40-30, 28.7, 24.8, 24.0.

(1,3-Bis(2,6-diisopropyl-4-(polyisobutyl)phenyl)imidazoylidene)(allyl)palladium (II) chloride: To a 25-mL round-bottomed flask, equipped with a magnetic stir bar and a rubber septum was added $(allylPdCl)_2$ (12.4 mg, 0.34 mmol) along with a solution of 1,3-bis(2,6-diisopropyl-4-(polyisobutyl)phenyl)imidazol-2-ylidene silver(I) chloride **9** (0.8534 g, 0.38 mmol) in 5 mL of CH_2Cl_2. After 12 h, the reaction mixture was filtered through celite and the celite was washed with hexane. The solvent was removed from the combined hexane solutions under reduced pressure to yield 0.85 g (96%) of a brown residue of product as a viscous oil. ^1H NMR (500 MHz, $CDCl_3$), δ: 7.23 (s, 4H), 7.06 (s,

2H), 4.85-4.7 (m, 1H), 3.87 (d, *J* = 6.8 Hz, 1H), 3.13-3.00 (m, 4H), 2.90-2.78 (m, 2H), 2.69 (d, *J* = 13.3 Hz, 1H), 1.84 (s, 6H), 1.75-0.7 (PIB protons). ^{13}C NMR (125 MHz, $CDCl_3$), δ: 186.2, 151.1, 144.9, 144.7, 133.1, 124.3, 121.7, 114.1, 72.3, multiple poorly resolved peaks between 60-58, 49.2, multiple poorly resolved peaks between 40-30, 28.5, 28.4, 26.7, 25.9, 23.0, 22.9.

Bis(*N*-methyl-*N′*-polyisobutylimidazoylidene)palladium(II) iodide: *N*-Methyl-*N*'-polyisobutylimidazolium iodide **5** (0.52 g, 0.48 mmol) and sodium iodide (0.47 g, 3.1 mmol) were dissolved in 10 mL of THF in a 50-mL round-bottomed flask, equipped with a magnetic stir bar and a rubber septum. This THF solution was cooled to -78 ºC and potassium *t*ert-butoxide (62.3 mg, 0.55 mmol) was added. After stirring at -78 ºC for 40 min, a solution of bis(benzonitrile)dichloropalladium(II) (82.4 mg, 0.22 mmol) in 3 mL of THF was added. The mixture was allowed to stir at -78 ºC for 30 min and then warmed to room temperature. After stirring at room temperature for another 14 h, the solvent was removed under reduced pressure. The residue was dissolved in 20 mL of hexane and washed with 90% ethanol (3 x 15 mL). The hexane phase was concentrated and purified by column chromatography (hexane first and then CH_2Cl_2) to yield 0.35 g (58%) of an orange viscous liquid. ^{1}H NMR (300 MHz, $CDCl_3$): 6.88 (s, 2H), 6.85 (s, 2H), 4.6-4.3 (br, 2H), 4.3-4.1 (br, 6H), 4.1-3.9 (br, 2H), 2.8-2.4 (br, 2H), 2-0.8 (PIB protons).

General Procedure for Aryl Amination with Catalyst 10 and Recycling

In a 10-mL Schlenk flask, equipped with a magnetic stir bar and a rubber septum, a mixture of 4-bromotoluene (87 mg, 0.50 mmol), morpholine (61 mg, 0.70 mmol),

potassium *tert*-butoxide (84 mg, 0.75 mmol), and the catalyst **10** (13 mg, 0.005 mmol) were dissolved in 2 mL of heptane. After 20 min at 80 ºC, the reaction was complete in the first cycle of an aryl amination using **10**. At this point, 3 mL of CH_3CN was added to the reaction mixture. After vigorous stirring, the mixture was allowed to settle and the two phases separated. The CH_3CN layer containing the product was removed and fresh substrates and base were added to the heptane phase to start a new catalytic cycle.

General Procedure for Heck Reaction with Catalyst 10 and Recycling

A substrate solution containing 4-iodoacetophenone (8.1906 g, 33.3 mmol) and *n*-butyl acrylate (4.8603 g, 37.9 mmol) dissolved in 51.4 g of heptane-saturated DMF was prepared and added to a 10-mL Schlenk flask equipped with a magnetic stir bar and a rubber septum, that contained catalyst **10** (11 mg, 4.2 μmol) dissolved in 1 mL of decane. After addition of Et_3N (0.1 g, 1 mmol), the resulting mixture was stirred at 65 ºC for 10 h. The reaction mixture was cooled to room temperature and became two phases. The bottom phase was removed using a syringe. Fresh substrate solution and Et_3N (0.05 g, 0.46 mmol) were added to the remaining heptane phase to start the second cycle and the recovered polar phase was analyzed for product by ^1H NMR spectroscopy.

General Procedure for Heck Reaction with Catalyst 11 and Recycling

In a 10-mL Schlenk flask, equipped with a magnetic stir bar and a rubber septum, catalyst **11** (12 mg, 4.8 μmol) was dissolved in 1 mL of heptane. 4-Iodoacetophenone (0.123 g, 0.5 mmol), *n*-butyl acrylate (0.077 g, 0.6 mmol) and 1 mL of heptane-saturated DMF were added followed by 0.2 mL of Et_3N. The resulting mixture was stirred at 75 ºC for 2 d. After cooling to room temperature, the solution became biphasic. The

bottom phase was removed using a syringe. Fresh substrates and base were added to the remaining heptane solution in the flask to start the second cycle.

General Procedure for Microwave-assisted Heck Reaction with Catalyst 11 and Recycling

In a microwave reaction tube, the palladium catalyst **11** (29.3 mg, 11.6 μmol) was dissolved in 2 mL of heptane in a microwave reaction tube. Then 2 g of a substrate solution (prepared using 4-iodoacetophenone (8.1906 g, 33.3 mmol) and *n*-butyl acrylate (4.8603 g, 37.9 mmol) in 51.4 g of heptane-saturated DMF) and 0.4 mL of Et_3N were added to the solution of **11**. The reaction mixture was heated at 130 ºC for 30 min in a microwave reactor. On cooling to room temperature the reaction mixture became biphasic. The two phases were separated and fresh substrate solution and Et_3N were added to the top phase to start the 2^{nd} cycle and the bottom polar phase was analyzed for product by ^1H NMR spectroscopy.

General Procedure for Sample Digestion and Sample Preparation for ICP-MS Analysis

All solvent was removed from the product-containing DMF-rich phase of a catalytic reaction. Then 2 mL of concentrated nitric acid was added to this residue at 25 ºC and the resulting mixture was heated in a sand bath at 132 ºC for 48 h. Another 2 mL of concentrated nitric acid was added and the mixture was heated at 132 ºC for a further 55 h. At this point, 2 mL of concentrated sulfuric acid was added and the sample was heated at 132 ºC a further 48 h. At this point, the solution was cooled to room temperature and diluted with 1% aqueous HNO_3 and the diluted solution was analyzed by ICP-MS.

Ethyl *N*-mesitylformimidate: In a 50-mL round-bottomed flask with stir bar, 2,4,6-trimethylaniline (12.1835 g, 90.1 mmol) and triethyl orthoformate (15.6291 g, 147 mmol) were mixed together and connected to distillation equipment. The solution was stirred in a sand bath regulated at 150 ºC. After 10 h., the reaction mixture was cooled to room temperature. At this point, some white solid precipitated. 5 mL of hexane was then added to the mixture and the mixture was filtered. Concentrating the filtrate at 70 ºC at reduced pressure for 3 h gave 16.5831 g (87 mmol, 96.6 %) of oil. ^{1}H NMR (300 MHz, $CDCl_3$): δ 7.44 (s, 1H), 6.83 (s, 2H), 4.37 (q, *J* = 7.2 Hz, 2H), 2.34 (s, 3H), 2.08 (s, 6H), and 1.40 (t, *J* = 7.2 Hz, 3H). ^{13}C NMR (125.5 MHz, $CDCl_3$): δ 150.9, 143.1, 132.4, 128.7, 128.5, 61.9, 20.7, 18.4, and 14.3.

***N*-Mesityl-*N*'-(prop-2-ynyl)formimidamide:** In a 10-mL round-bottomed flask with stir bar, ethyl *N*-2,4,6-trimethylphenylformimidate (2.0876 g, 10.9 mmol) and propargyl amine (643.5 mg, 11.7 mmol) were mixed together. The reaction mixture turned cloudy after stirring at room temperature for 2 days. The suspension was stirred for two more days to make the reaction complete. Hexane was added to the reaction mixture and the solid was collected by vacuum filtration. The solid was washed with hexane. After standing for 30 min, crystals formed in the bottom of the solution phase. The crystals were combined with solid to give 1.3 g (60 %) product. ^{1}H NMR (500 MHz, $CDCl_3$): δ 7.31 (s, 1H), 6.82 (s, 2H), 4.16 (br, 2H), 2.27 (t, *J* = 2.5 Hz, 1H), 2.22 (s, 3H), and 2.10 (s, 6H). ^{13}C NMR (125.5 MHz, $CDCl_3$): δ multiple peaks between 151-126, 80.6, 71.4, 32.1 (br), 20.5, and 18.1. mp = 79 ºC (decompose).

***N*-Mesitylethane-1,2-diamine:** In a 10-mL round-bottomed flask with stir bar and reflux condenser, 2,4,6-trimethylaniline (6.5981 g, 48.8 mmol), 2-bromoethylamine hydrobromide (4.0949 g, 20.0 mmol), and 10 mL of toluene was mixed together. The mixture was stirred in an oil bath regulated at 120 ºC for 4 h. At this point, the solid was collected by vacuum filteration and washed with two 150-mL portions of chloroform. The solid was combined and treated with 50 mL of 8 M sodium hydroxide solution, 100 mL of distillated water, and 150 mL of CH_2Cl_2. After shaken for 10 min, the solid dissolved. The CH_2Cl_2 layer was separated and the aqueous solution was extracted with 150 mL of CH_2Cl_2 twice. The CH_2Cl_2 solutions were combined and dried with $MgSO_4$. Removing the solvent by vacuum distillation gave a colorless liquid 3.55 g (99.7 %). ^{1}H NMR (500 MHz, $CDCl_3$): δ 6.80 (5, 2H), 2.96 (t, J = 5.5 Hz, 2H), 2.88 (t, J = 5.5 Hz, 2H), 2.27 (s, 3H), and 2.24 (s, 6H). ^{13}C NMR (125 MHz, $CDCl_3$): δ 143.7, 131.5, 130.0, 129.6, 51.5, 42.8, 20.8, and 18.6.

***N*-Mesityl-4,5-dihydroimidazole hydrobromide: Method A:** In a 10-mL round-bottomed flask with stir bar and reflux condenser, *N*-mesitylformimidate (0.5728 g , 3.00 mmol), 2-bromoethylamine hydrobromide (0.6174 g, 3.01 mmol), sodium carbonate (0.6703 g, 6.3 mmol), and 3 mL of 1,2-dimethoxyethane were mixed together and refluxed for 1 day. The solid was removed and washed with CH_2Cl_2. The solutions were combined and concentrated by vacuum distillation to give 0.4822 g (60 %) of a white solid. **Method B:** In a 10-mL round-bottomed flask with stir bar and reflux condenser, diisopropylethylamine (309.6 mg, 2.4 mmol) was added to a solution of *N*-mesitylethane-1,2-diaminium dibromide (254.6 mg, 0.748 mmol) and of triethyl

orthoformate (236.4 mg, 1.595 mmol) in 2 mL of acetonitrile. After staying in a sand bath regulated at 90 ºC for 20 min, the mixture became a homogeneous solution. After refluxing overnight, the solution was cooled to room temperature and the solvent was removed bt vacuum distillation. Then 30 mL of ethyl acetate was added to the residue to yield brownish precipitate and a yellow solution. The solid was collected, washed with 20 mL of ethyl acetate and dried to give 0.32 g (89 %) of a solid which was a mixture of dihydroimidazolium bromide and diisopropylethylamine hydrobromide. ^{1}H NMR (300 MHz, $CDCl_3$): δ 8.25 (s, 1H), 6.93 (s, 2H), 4.33 (t, J = 10.9 Hz, 2H), 4.10 (t, J = 10.9 Hz, 2H), 2.27 (s, 3H), and 2.24 (s, 6H). ^{13}C NMR (75 MHz, $CDCl_3$): δ 158.4, 140.4, 135.1, 130.1, 129.9, 50.9, 45.3, 20.9, and 17.8.

1-Benzyl-4-(2-bromoethyl)-1,2,3-triazole: In a 10-mL round-bottomed flask, equipped with a magnetic stir bar and a rubber septum, a mixture of benzyl azide (0.279 g, 2.10 mmol), 4-bromobut-1-yne (0.282 g, 2.12 mmol) and tris(triphenylphosphine)copper(I) bromide (0.012 g, 12.9 μmol) was dissolved in 2 mL of dichloromethane. The reaction mixture was allowed to stir for 12 h. at room temperature. At this point, Amberlite IRC-50 was added and the resulting suspension was shaken for 1 h. to remove copper salt. After filtration, the solvent was removed by vacuum distillation yielding an orange oil (0.60 g, > 99%). ^{1}H NMR (300 MHz, $CDCl_3$), δ: 7.45-7.35 (m, 3H), 7.3-7.23 (m, 2H), 5.53 (s, 2H), 3.65 (t, J = 6.6 Hz, 2H), and 3.28 (t, J = 6.6 Hz, 2H). ^{13}C NMR (75 MHz, $CDCl_3$): δ 145.2, 134.6, 129.0, 128.6, 127.8, 121.6, 54.0, 31.4, and 29.3.

***N*-Mesityl-*N′*-(2-(1-benzyl-1,2,3-triazol-4-yl)ethyl)imidazolium bromide:** In a 10-mL round-bottomed flask, equipped with a magnetic stir bar and a rubber septum, a mixture

of *N*-mestyleimidazole (0.313 g, 1.66 mmol) and 1-benzyl-4-(2-bromoethyl)-1,2,3-triazole (0.445 g, 1.67 mmol) was dissolved in 2 mL of dimethoxyethane. The reaction mixture was allowed to reflux for 24 h. After cooling to room temperature, the solution was centrifuged, a biphasic mixture formed. Removing the upper layer of dimethoxyethane solution and drying afforded an orange viscous liquid (0.59 g, 79% yield). ^{1}H NMR (500 MHz, $CDCl_3$), δ: 9.65 (s, 1H), 8.07 (s, 1H), 8.06 (s, 1H), 7.23-7.17 (br, 5H), 7.01 (s, 1H), 6.85 (s, 2H), 5.38 (s, 2H), 4.94 (t, *J* = 6.6 Hz, 2H), 3.39 (t, *J* = 6.6 Hz, 2H), 2.23 (s, 3H), and 1.80 (s, 6H). ^{13}C NMR (125 MHz, $CDCl_3$): δ 142.4, 140.8, 137.2, 137.1, 134.6, 134.0, 130.3, 129.5, 128.7, 128.3, 127.9, 123.6, 122.7, 53.8, 49.0, 26.5, 20.8, and 17.1.

(*N*-Mesityl-*N′*-(2-(1-benzyl-1,2,3-triazol-4-yl)ethyl)imidazolylidene)silver(I) bromide: To a 25-mL round-bottomed flask, equipped with a magnetic stirbar and rubber septum, was added a solution of *N*-mesityl-*N′*-(2-(1-benzyl-1,2,3-triazol-4-yl)ethyl)imidazolium bromide (0.23 g, 0.51 mmol) in CH_2Cl_2 (2 mL) and silver oxide (81 mg, 0.35 mmol). The flask was covered with aluminum foil and the reaction mixture was allowed to stir under nitrogen for 18 h. At this point, the stirring was ceased and the reaction mixture was filtered through celite and the resulting solid was washed twice with 1 mL of CH_2Cl_2. The CH_2Cl_2 solutions were combined and the solvent was removed under reduced pressure to yield a yellowish solid (0.27 g, 96%). ^{1}H NMR (400 MHz, CD_2Cl_2, rt) δ: 7.28 (s, 1H), 7.00 (s, 2H), 6.98 (s, 1H), 3.91 (d, $J(^{13}C\text{-}^{1}H)$ = 4.8 Hz, 3H), 2.35 (s, 3H) and 1.96 (s, 6H). ^{13}C NMR (100 MHz, CD_2Cl_2, rt)

δ: 181.4, 139.4, 135.5, 134.9, 129.2, 122.8, 122.5, 38.8 (d, $J(^{13}C\text{-}^{13}C)$ = 11.2 Hz), 20.9 and 17.5.

Polyisobutyl vinyl ether: In a pressure tube equipped with a magnetic stir bar, hydroxy-terminated polyisobutylene (5.06 g, 3.8 mmol) was dissolved in ethyl vinyl ether (13 g, 181 mmol) and 13 mL of THF. (1,10-phenanthroline)palladium acetate (44.5 mg, 0.116 mmol) was suspended in 2 mL of ethyl vinyl ether and added. The resulting mixture was stirred in a 70 ºC sand bath for 3 d. After cooling to room temperature, the reaction mixture was filtered through a short column of active carbon and the active carbon was washed with 10 mL of hexane. Removal of the solvent by vacuum distillation afforded a colorless viscous oil (4.4 g, 86%). ^{1}H NMR (300 MHz, C_6D_6), δ: 6.48 (dd, *J* = 6.7, 14.3 Hz, 1H), 4.20 (d, *J* = 14.3 Hz, 1H), 3.97 (d, *J* = 6.7 Hz, 1H), 3.41 (dd, *J* = 5.2, 9.3 Hz, 1H), 3.28 (m, 1H), 2.0-0.75 (PIB protons). ^{13}C NMR (75 MHz, C_6D_6), δ: 152.8, 86.5, 74.7, multiple poorly resolved peaks between 61-58, 50.3, multiple poorly resolved peaks between 39-29, and 20.9.

Polyethylene vinyl ether: In a pressure tube equipped with a magnetic stir bar was added hydroxy-terminated polyethylene (0.63 g, 1.1 mmol), ethyl vinyl ether (11 g, 153 mmol), 7 mL of tolunene and 7 mL of DMF. (1,10-phenanthroline)palladium acetate (44.5 mg, 0.116 mmol) was suspended in 2 mL of ethyl vinyl ether and added. The resulting mixture was stirred in a 70 ºC sand bath for 3 d. After cooling to room temperature, the reaction mixture was filtered and washed with 10 mL of toluene. Drying the solvent in vacuum for 12 h afforded a yellowish powder (0.6 g, 95%). ^{1}H NMR (500 MHz, C_6D_6), δ: 6.43 (dd, *J* = 6.9, 14.3 Hz, 1H), 4.20 (dd, *J* = 1.5, 14.3 Hz,

1H), 3.97 (dd, *J* = 1.5, 6.9 Hz, 1H), 3.50 (t, *J* = 6.5 Hz, 2H), 1.7-1.1 (PE protons) and 0.91 (t, *J* = 6.7 Hz, 3H). ^{13}C NMR (75 MHz, C_6D_6), δ: 152.8, 86.5, 74.7, multiple poorly resolved peaks between 61-58, 50.3, multiple poorly resolved peaks between 39-29, and 20.9.

(*N*,*N*′-Bis(2,6-dimethyl-4-(polyisobutyl)phenyl)imidazoylidene)silver(I) chloride: A 0.4268 g (0.185 mmol) sample of 1 *N*,*N*′-bis(2,6-dimethyl-4-(polyisobutyl)phenyl) imidazolium chloride and 30.8 mg (0.133 mmol) of Ag_2O were dissolved in 4 mL of dichloromethane. The reaction was reflux for 16 h. After the reaction was cooled to room temperature, it was filtered through celite to remove excess Ag_2O. The solution was centrifuged at 5 ºC to separate the finer silver salt. Solvent was removed under reduced pressure to yield an orange residue. The yield was quantitative (0.4667 g). ^{1}H NMR (300 MHz, $CDCl_3$), δ: 7.15 (s, 4H), 7.09 (s, 2H), 2.09 (s, 12H), and 1.9-0.7 (PIB protons). ^{13}C NMR (125 MHz, $CDCl_3$), δ: 182.875 (dd, $J(^{13}C\text{-}^{107}Ag)$ = 236.6 Hz, $J(^{13}C\text{-}^{109}Ag)$ = 271.6 Hz), 152.39, 134.92, 133.76, 126.71, 122.68, multiple poorly resolved peaks between 61-57, multiple poorly resolved peaks between 40-30, and 18.36.

***N*,*N*′-Bis((1-polyisobutyl-1,2,3-triazol-4-yl)methyl)imidazolium bromide:** A 0.606 g (2.69 mmol) sample of *N*,*N*′-bis(prop-2-ynyl)imidazolium bromide, 17 mg (0.17 mmol) of CuCl, and 6.17 g (5.92 mmol) of azide-terminated polyisobutylene[1] were dissolved in 105 mL of dichloromethane and 20 mL of methanol. The solution was stirred at room temperature for 24 h. After the reaction was completed, 1.19 g of EDTA and 20 mL of water was added and stirred at room temperature for 24 h. Dichloromethane layer was separated and remove under reduced pressure, and dissolved in 100 mL of hexane and

washed with methanol until the methanol layer became colorless. The hexane was removed under reduced pressure. After the purification by column chromatography (eluted first with and then with 9:1/dichloromethane:methanol), the product was an orange vicious residue. The yield was 82% (5.12 g). ^{1}H NMR (500 MHz, $CDCl_3$), δ: 10.85 (b, 1H), 8.21 (s, 2H), 7.44 (s, 2H), 5.61 (s, 4H), 4.22 (dd, *J* = 7.4, 13.5 Hz, 2H), 4.03 (dd, *J* = 6, 13.5 Hz, 2H), 2.13 (m, 2H), and 1.7-0.6 (PIB protons). ^{13}C NMR (125 MHz, $CDCl_3$), δ: 139.64, 136.64, 125.59, 123.07, multiple poorly resolved peaks between 60-57 and 39-28, and 20.55.

(*N*,*N*′-Bis(2-(1-*n*-octadecyl-1,2,3-triazol-4-yl)methyl)imidazolylidene)silver(I) bromide: 158.4 mg (0.194 mmol) of *N*,*N*′-bis((1-octadecyl-1,2,3-triazol-4-yl)ethyl)imidazolium bromide and 33.8 mg (0.146 mmol) of Ag_2O was dissolved in 10 mL of dichloromethane. The solution was stirred at 49 ºC for 24 h. The solution was filtered through celite to remove excess silver oxide and the solid was washed by dichloromethane. The solution was dried with sodium sulfate and solvents were removed under reduced pressure to yield an orange viscous residue. The yield was 94 % (0.1688 g). ^{1}H NMR (300 MHz, $CDCl_3$), δ: 7.794 (s, 2H), 7.216 (s, 2H), 5.365 (s, 4H), 4.299 (t, *J* = 7.5 Hz, 4H), 1.866 (m, 4H), 1.11- 1.35 (m, 60H), 0.85 (t, *J* = 6.6 Hz, 2H). ^{13}C NMR ($CDCl_3$), δ: 181.67, 142.43, 123.40, 121.58, 50.55, 46.69, 31.89, multiple poorly resolved peaks between 28-31, 22.66, 26.48, and 14.10. HRMS (ESI): Calc. for $[M - Br]^+$ (^{107}Ag isotope): 841.5713. Found: 841.6153.

(*N*,*N*′-Bis((1-polyisobutyl-1,2,3-triazol-4-yl)methyl)imidazolylidene)silver(I) bromide: A 0.32 g (0.138 mmol) sample of *N*,*N*′-bis((1-polyisobutyl-1,2,3-triazol-4-

yl)methyl)imidazolium bromide and 17.4 mg (0.075 mmol) of Ag_2O were dissolved in 3 mL of dichloromethane. The solution was stirred at 49 ºC for 24 h. The solution was filtered to remove excess silver oxide and the solid was washed by dichloromethane. The solution was dried with sodium sulfate and solvents were removed under reduced pressure to yield an orange viscous residue. The yield was 93 % (0.313 g). ^{1}H NMR (300 MHz, $CDCl_3$), δ: 7.68 (s, 2H), 7.22 (s, 2H), 5.30 (s, 4H), 4.21 (dd, *J* = 7.4, 13.5 Hz, 2H), 4.02 (dd, *J* = 6, 13.5 Hz, 2H), 2.10 (m, 2H), and 0.6-1.8 (PIB protons). ^{13}C NMR (125 MHz, $CDCl_3$), δ: 181.16, 142.14, 123.90, 121.55, multiple poorly resolved peaks between 28-39 and 57-60, and 20.68.

^{13}C-Labeled *N*-mesitylimidazole: To a 25 mL round-bottomed flask, equipped with a magnetic stirbar and rubber septum, was added glacial acetic acid (1.83 g, 30.5 mmol), 20% aqueous ^{13}C-labelled formaldehyde (1.1 g, 7.11 mmol) and 40% aqueous glyoxal (1.04 g, 7.17 mmol). The reaction vessel was then flushed with dry nitrogen and then the flask was placed on an oil bath regulated at 70 ºC. A mixture of glacial acetic acid (1.82 g, 30.3 mmol), ammonium acetate (0.546 g, 7.1 mmol), water (0.16 g), and mesitylamine (0.89 g, 6.6 mmol) was added dropwise over a period of about 20 min with a glass syringe. The reaction mixture was stirred for 19 h at 70 ºC. At this point, the reaction mixture was allowed to cool to room temperature and added dropwise into a saturated $NaHCO_3$ aqueous solution (60 mL). The mixture was allowd to stir for 1 h at room temperature. The precipitate was with filtered, washed with 20 mL of water to yield a brown solid, which was purified by column chromatography with silica gel (hexane then ethyl acetate) to yield 0.83 g (67%) as a yellow solid. ^{1}H NMR (400 MHz,

$CDCl_3$, rt) δ: 7.46 (d, $J13_{C}$-1_{H} = 200 Hz, 1H), 7.23 (d, *J* = 7 Hz, 1H), 6.95 (s, 2H), 6.89 (d, *J* = 7 Hz, 1H), 2.32 (s, 3H) and 1.97 (s, 6H). ^{13}C NMR (100 MHz, $CDCl_3$, rt) δ: large peak at 137.27, multiple small peaks between 140-132, 129.02, 120.12, 21.00 and 17.30. The extent of ^{13}C labeling in this common intermediate for NHC ligand synthesis was determined by integrating the signal for the doublet due to ^{13}C-^{1}H coupling for the proton signal on C2 of the *N*-mesitylimidazole versus the singlet for the ^{12}C-containing *N*-mesitylimidazole. This integration showed that the extent of labeling was 92%.

^{13}C-Labeled *N*-mesityl-*N′*-methylimidazolium chloride: To a pressure tube equipped with a magnetic stir bar was added ^{13}C-labelled *N*-mesitylimidazole (0.192 g, 1.03 mmol), 1.0 M solution of methyl bromide in *t*-butyl methyl ether (5 mL, 5 mmol) and acetonitrile (5 mL). The reaction mixture was allowed to stir in a sand bath regulated at 120 ºC for 4 d. After cooling to room temperature, the solvent was removed under reduced pressure to yield a white solid. Analysis of this solid with ^{1}H NMR spectroscopy showed the reaction conversion was 75%. The solid was dissolved in 0.2 mL of acetonitrile and added to 10 mL of hexanes. Filtration of the mixture afforded a white solid (0.122 g, 50 %). ^{1}H NMR (500 MHz, $CDCl_3$, rt) δ: 10.56 (d, *J*(^{13}C-^{1}H) = 224 Hz, 1H), 7.64 (br, 1H), 7.11 (br, 1H), 6.98 (s, 2H), 4.36 (s, 3H), 2.32 (s, 3H) and 2.05 (s, 6H). ^{13}C-NMR (100 MHz, $CDCl_3$, rt) δ: large peak at 139.2, small peaks at 141.3, 134.2, 129.8, 123.7, 122.9, 37.3, 21.1 and 17.6.

^{13}C-Labeled *N*-mesityl-*N′*-methylimidazolium bromide: To a pressure tube equipped with a magnetic stir bar was added ^{13}C-labelled *N*-mesitylimidazole (0.183 g, 0.98 mmol), 2.0 M solution of methyl chloride in *t*-butyl methyl ether (2 mL, 4 mmol) and

acetonitrile (2.5 mL). The reaction mixture was allowed to stir in a sand bath regulated at 60 ºC for 20 d. After cooling to room temperature, the solvent was removed under reduced pressure until 0.5 mL of solution. When the solution was added to 10 mL of hexanes and a white precipitate formed. Filtration of the mixture afforded a yellowish solid (0.188 g, 68 %). ^{1}H-NMR (400 MHz, $CDCl_3$, rt) δ: 10.43 (d, $J(^{13}C\text{-}^{1}H)$ = 214 Hz, 1H), 7.62 (m, 1H), 7.11 (m, 1H), 6.98 (s, 2H), 4.38 (d, $J(^{13}C\text{-}^{1}H)$ = 4.3 Hz), 2.32 (s, 3H) and 2.07 (s, 6H). ^{13}C-NMR (100 MHz, $CDCl_3$, rt) δ: large peak at 138.8, multiple small peaks between 146-132, 130.5, 129.9, 123.8, 122.8, 37.5, 21.1 and 17.7.

^{13}C-Labeled *N*-mesityl-*N′*-methylimidazolium iodide: To a 25 mL round-bottomed flask equipped with a magnetic stirbar and rubber septum was added ^{13}C-labelled *N*-mesitylimidazole (0.107 g, 0.57 mmol), methyl iodide (0.12 g, 0.85 mmol) and dichloromethane (2 mL). The reaction mixture was allowed to stir at room temperature for 18 h. At this point, the solvent was removed under reduced pressure to yield 0.16 g (86 %) as a yellow oil. ^{1}H NMR (400 MHz, $CDCl_3$, rt) δ: 9.90 (d, $J(^{13}C\text{-}^{1}H)$ = 224 Hz, 1H), 7.85 (s, 1H), 7.16 (s, 1H), 6.97 (s, 2H), 4.34 (s, 3H), 2.31 (s, 3H) and 2.06 (s, 6H). ^{13}C NMR (100 MHz, $CDCl_3$, rt) δ: large peak at 137.35, multiple small peaks between 142-128, 124.72, 123.06, 37.90, 21.04 and 17.89.

^{13}C-Labelled (*N*-mesityl-*N′*-methylimidazolylidene)silver(I) chloride: To a 10 mL round-bottomed flask, equipped with a magnetic stirbar and rubber septum, was added a solution of ^{13}C-labelled *N*-mesityl-*N′*-methylimidazolium chloride (56 mg, 0.24 mmol) in acetonitrile (2 mL) and silver oxide (28 mg, 0.12 mmol). The flask was covered with aluminum foil and the reaction mixture was allowed to stir under nitrogen for 18 h. At

this point, the stirring was ceased and the reaction mixture was filtered through celite and the resulting solid was washed twice with 1 mL of acetonitrile. The acetonitrile solutions were combined and the solvent was removed under reduced pressure to yield a white solid (65 mg, 79%). ^{1}H NMR (400 MHz, CD_2Cl_2, rt) δ: 7.21 (m, 1H), 7.00 (s, 2H), 6.97 (m, 1H), 3.91 (m, 3H), 2.35 (s, 3H) and 1.97 (s, 6H). ^{13}C NMR (100 MHz, CD_2Cl_2, rt) δ: 182.1, 140.0, 137.9, 135.4, 129.7, 123.3, 122.8, 39.3 (d, $J(^{13}C\text{-}^{13}C)$ = 11.2 Hz), 21.4 and 18.0.

^{13}C-Labelled (*N*-mesityl-*N′*-methylimidazolylidene)silver(I) bromide: To a 10 mL round-bottomed flask, equipped with a magnetic stirbar and rubber septum, was added a solution of ^{13}C-labelled *N*-mesityl-*N′*-methylimidazolium bromide (84 mg, 0.30 mmol) in acetonitrile (2 mL) and silver oxide (0.056 g, 0.30 mmol). The flask was covered with aluminum foil and the reaction mixture was allowed to stir under nitrogen for 18 h. At this point, the stirring was ceased and the reaction mixture was filtered through celite and the resulting solid was washed twice with 1 mL of acetonitrile. The acetonitrile solutions were combined and the solvent was removed under reduced pressure to yield a yellowish solid (111 mg, 95%). ^{1}H NMR (400 MHz, CD_2Cl_2, rt) δ: 7.23 (dd, *J* = 1.7, 2.5 Hz, 1H), 6.99 (s, 2H), 6.97 (dd, *J* = 1.7, 2.5 Hz, 1H), 3.89 (d, $J(^{13}C\text{-}^{1}H)$ = 4.9 Hz, 3H), 2.36 (s, 3H) and 1.93 (s, 6H). ^{13}C NMR (100 MHz, CD_2Cl_2, rt) δ: 182.9, 140.0, 137.9, 135.4, 129.7, 123.3, 122.9, 39.2 (d, $J(^{13}C\text{-}^{1}H)$ = 11.1 Hz), 21.4 and 18.0.

^{13}C-Labelled (*N*-mesityl-*N′*-methylimidazolylidene)silver(I) iodide: To a 25 mL round-bottomed flask, equipped with a magnetic stirbar and rubber septum, was added a solution of ^{13}C-labelled *N*-mesityl-*N′*-methylimidazolium iodide (0.10 g, 0.30 mmol) in

acetonitrile (2 mL) and silver oxide (56 mg, 0.48 mmol). The flask was covered with aluminum foil and the reaction mixture was allowed to stir under nitrogen for 18 h. At this point, the stirring was stopped and the reaction mixture was filtered through celite and the resulting solid was washed twice with 1 mL of acetonitrile. The acetonitrile solutions were combined and the solvents were removed under reduced pressure to yield a yellowish solid (0.12 g, 90%). ^{1}H NMR (400 MHz, CD_2Cl_2, rt) δ: 7.28 (s, 1H), 7.00 (s, 2H), 6.98 (s, 1H), 3.91 (d, $J(^{13}C\text{-}^{1}H)$ = 4.8 Hz, 3H), 2.35 (s, 3H) and 1.96 (s, 6H). ^{13}C NMR (100 MHz, CD_2Cl_2, rt) δ: 181.4, 139.4, 135.5, 134.9, 129.2, 122.8, 122.5, 38.8 (d, $J(^{13}C\text{-}^{13}C)$ = 11.2 Hz), 20.9 and 17.5.

REFERENCES

(1) Díez-González, S.; Nolan, S. P. *Coord. Chem. Rev.* **2007**, *251*, 874-883.

(2) Clavier, H.; Nolan, S. P. *Annu. Rep. Prog. Chem., Sect. B* **2007**, *103*, 193-222.

(3) Nolan, S. P. *N-Heterocyclic Carbenes in Synthesis*; Wiley-VCH, 2006.

(4) Enders, D.; Niemeier, O.; Henseler, A. *Chem. Rev.* **2007**, *107*, 5606-5655.

(5) Marion, N.; Díez-González, S.; Nolan, S. P. *Angew. Chem. Int. Ed.* **2007**, *46*, 2988-3000.

(6) Zhao, L.; Zhang, C.; Zhuo, L.; Zhang, Y.; Ying, J. Y. *J. Am. Chem. Soc.* **2008**, *130*, 12586-12587.

(7) Moss, G. P.; Smith, P. A. S.; Tavernier, D. *Pure Appl. Chem.* **1995**, *67*, 1307-1375.

(8) Tomioka, H. *Pure and Appl. Chem.* **2003**, *75*, 1041-1047.

(9) Bourissou, D.; Guerret, O.; Gabbaï, F. P.; Bertrand, G. *Chem. Rev.* **2000**, *100*, 39-92.

(10) Sulzbach, H. M.; Bolton, E.; Lenoir, D.; Schleyer, P. v R.; Schaefer III, H. F. *J. Am. Chem. Soc.* **1996**, *118*, 9908-9914.

(11) Heinemann, C.; Müller, T.; Apeloig, Y.; Schwarz, H. *J. Am. Chem. Soc.* **1996**, *118*, 2023-2038.

(12) Herrmann, W. A.; Köcher, C. *Angew. Chem. Int. Ed.* **1997**, *36*, 2162-2187.

(13) Arduengo, A. J., III; Dias, H. V. R.; Dixon, D. A.; Harlow, R. L.; Klooster, W. T.; Koetzle, T. F. *J. Am. Chem. Soc.* **1994**, *116*, 6812-6822.

(14) Díez-González, S. *N-Heterocyclic Carbenes: From Laboratory Curiosities to Efficient Synthetic Tools*; Royal Society of Chemistry, 2010.

(15) Perry, M. C.; Burgess, K. *Tetrahedron: Asymmetry* **2003**, *14*, 951-961.

(16) Wanzlick, H. W. *Angew. Chem. Int. Ed.* **1962**, *1*, 75-80.

(17) Öfele, K. *J. Organomet. Chem.* **1968**, *12*, P42-P43.

(18) Wanzlick, H.-W.; Schönherr, H.-J. *Angew. Chem. Int. Ed.* **1968**, *7*, 141-142.

(19) Cardin, D. J.; Çetinkaya, B.; Lappert, M. F. *Chem. Rev.* **1972**, *72*, 545-574.

(20) Arduengo, A. J., III; Harlow, R. L.; Kline, M. *J. Am. Chem. Soc.* **1991**, *113*, 361-363.

(21) Herrmann, W. A.; Elison, M.; Fisher, J.; Köcher, C.; Artus, G. R. J. *Angew. Chem. Int. Ed.* **1995**, *34*, 2371-2374.

(22) Öfele, K.; Herrmann, W. A.; Mihalios, D.; M., E.; Herdtweck, E.; Scherer, W.; Mink, J. *J. Organomet. Chem.* **1993**, *459*, 177-184.

(23) Herrmann, W. A.; Mihalios, D.; Öfele, K.; Kiprof, P.; Belmedjahed, F. *Chem. Ber.* **1992**, *125*, 1795-1799.

(24) Arnold, P. L.; Casely, I. J. *Chem. Rev.* **2009**, *109*, 3599-3611.

(25) Bianchini, C.; Masi, D.; Romerosa, A.; Zanobini, F.; Peruzzini, M. *Organometallics* **1999**, *18*, 2376-2386.

(26) Herrmann, W. A. *Angew. Chem. Int. Ed.* **2002**, *41*, 1290-1309.

(27) Peris, E. *Top. Organomet. Chem.* **2007**, *21*, 83-116.

(28) Wang, H. M. J.; Lin, I. J. B. *Organometallics* **1998**, *17*, 972-975.

(29) Glorius, F. *Top. Organomet. Chem.* **2007**, *21*, 1-20.

(30) Kuhn, K. M.; Grubbs, R. H. *Org. Lett.* **2008**, *10*, 2075-2077.

(31) Schwarz, J.; Böhn, V. P. W.; Gardiner, M. G.; Grosche, M.; Herrmann, W. A.; Hieringer, W.; Raudaschl-Sieber, G. *Chem. Eur. J.* **2000**, *6*, 1773-1780.

(32) Schürer, S. C.; Gessler, S.; Buschmann, N.; Blechert, S. *Angew. Chem. Int. Ed.* **2000**, *39*, 3898-3901.

(33) Bergbreiter, D. E.; Tian, J. *Tetrahedron Lett.* **2007**, *48*, 4499-4503.

(34) Li, J.; Sung, S.; Tian, J.; Bergbreiter, D. E. *Tetrahedron* **2005**, *61*, 12081-12092.

(35) Bergbreiter, D. E.; Li, J. *Chem. Commun.* **2004**, 42-43.

(36) Bergbreiter, D. E.; Sung, S. D.; Li, J.; Ortiz, D.; Hamilton, P. N. *Org. Process Res. Dev.* **2004**, *8*, 461-468.

(37) Bergbreiter, D. E.; Frels, J. D.; Li, C. *Macromol. Symp.* **2003**, *204*, 113-140.

(38) Bergbreiter, D. E. *Chem. Rev.* **2002**, *102*, 3345-3384.

(39) Osburn, P. L.; Bergbreiter, D. E. *Prog. Polym. Sci.* **2001**, *26*, 2015-2081.

(40) Bergbreiter, D. E.; Yang, Y.-C. *J. Org. Chem.* **2010**, *75*, 873-878.

(41) Hongfa, C.; Tian, J.; Bazzi, H. S.; Bergbreiter, D. E. *Org. Lett.* **2007**, *9*, 3259-3261.

(42) Hongfa, C.; Su, H.-L.; Bazzi, H. S.; Bergbreiter, D. E. *Org. Lett.* **2009**, *11*, 665-667.

(43) Keith, J. A.; Henry, P. M. *Angew. Chem. Int. Ed.* **2009**, *48*, 9038-9049.

(44) Keith, J. A.; Nielsen, R. J.; Oxgaard, J.; Goddard, W. A., III *J. Am. Chem. Soc.* **2007**, *129*, 12342-12343.

(45) Smidt, J.; Hafner, W.; Jira, R.; Sedlmeier, J.; Sieber, R.; Rüttinger, R.; Kojer, H. *Angew. Chem.* **1959**, *71*, 176-182.

(46) Marion, N.; Navarro, O.; Mei, J.; Stevens, E. D.; Scott, N. M.; Nolan, S. P. *J. Am. Chem. Soc.* **2006**, *128*, 4101-4111.

(47) Rouhi, A. M. *Chem. Eng. News* **2002**, *80*, 34-38.

(48) Galderon, N.; Chen, H. Y.; Scott, K. W. *Tetrahedron Lett.* **1967**, *8*, 3327-3329.

(49) Hérisson, P. J.-L.; Chauvin, Y. *Makromol. Chem.* **1970**, *141*, 161-176.

(50) Grubbs, R. H. *Handbook of Metathesis*; Wiley-VCH, 2003.

(51) Nguyen, S. T.; Johnson, L. K.; Grubbs, R. H.; Ziller, J. W. *J. Am. Chem. Soc.* **1992**, *114*, 3974-3975.

(52) Nguyen, S. T.; Grubbs, R. H.; Ziller, J. W. *J. Am. Chem. Soc.* **1993**, *115*, 9858-9859.

(53) Weskamp, T.; Schattenmann, W. C.; Spiegler, M.; Herrmann, W. A. *Angew. Chem. Int. Ed.* **1998**, *37*, 2490-2493.

(54) Weskamp, T.; Kohl, F. J.; Hieringer, W.; Gleich, D.; Herrmann, W. A. *Angew. Chem. Int. Ed.* **1999**, *38*, 2416-2419.

(55) Briot, A.; Bujard, M.; Gouverneur, V.; Nolan, S. P.; Mioskowski, C. *Org. Lett.* **2000**, *2*, 1517-1519.

(56) Scholl, M.; Ding, S.; Lee, C. W.; Grubbs, R. H. *Org. Lett.* **1999**, *1*, 953-956.

(57) Sanford, M. S.; Love, J. A.; Grubbs, R. H. *Organometallics* **2001**, *20*, 5314-5318.

(58) Love, J. A.; Morgan, J. P.; Trnka, T. M.; Grubbs, R. H. *Angew. Chem. Int. Ed.* **2002**, *41*, 4035-4037.

(59) Schrodi, Y.; Pederson, R. L. *Aldrich. Acta* **2007**, *40*, 45-52.

(60) Kingsbury, J. S.; Harrity, J. P. a; Bonitatebus, P. J.; Hoveyda, A. H. *J. Am. Chem. Soc.* **1999**, *121*, 791-799.

(61) Garber, S. B.; Kingsbury, J. S.; Gray, B. L.; Hoveyda, A. H. *J. Am. Chem. Soc.* **2000**, *122*, 8168-8179.

(62) Arduengo, A. J., III; Gentry, F. P., Jr.; Taverkere, P. K.; Simmons III, H. E. *US Patent 6,177,575 B1* **2001**.

(63) Flynn, D. L.; Devraj, R. V.; Parlow, J. J. *Curr. Opin. Drug Discov. Devel* **1998**, *1*, 41-51.

(64) Bergbreiter, D. E. *Curr. Opin. Drug Discov. Devel* **2001**, *4*, 736-744.

(65) Westhus, M.; Gonthier, E.; Brohm, D.; Breinbauer, R. *Tetrahedron Lett.* **2004**, *45*, 3141-3142.

(66) Wurm, F.; König, H. M.; Hilf, S.; Kilbinger, A. F. M. *J. Am. Chem. Soc.* **2008**, *130*, 5876-5877.

(67) Sanford, M. S.; Love, J. a; Grubbs, R. H. *J. Am. Chem. Soc.* **2001**, *123*, 6543-6554.

(68) Díez-González, S.; Marion, N.; Nolan, S. P. *Chem. Rev.* **2009**, *109*, 3612-3676.

(69) Garrison, J. C.; Youngs, W. J. *Chem. Rev.* **2005**, *105*, 3978-4008.

(70) Tapu, D.; Dixon, D. A.; Roe, C. *Chem. Rev.* **2009**, *109*, 3385-3407.

(71) Lin, J. C. Y.; Huang, R. T. W.; Lee, C. S.; Bhattacharyya, A.; Hwang, W. S.; Lin, I. J. B. *Chem. Rev.* **2009**, *109*, 3561-3598.

(72) Powell, A. B.; Bielawski, C. W.; Cowley, A. H. *J. Am. Chem. Soc.* **2010**, *132*, 10184-10194.

(73) Ploeg, A. F. M. J. van der; Koten, G. van; Spek, A. L. *Inorg. Chem.* **1979**, *18*, 1052-1060.

(74) Ilie, A.; Raț, C. I.; Scheutzow, S.; Kiske, C.; Lux, K.; Klapötke, T. M.; Silvestru, C.; Karaghiosoff, K. *Inorg. Chem.* **2011**, *50*, 2675-2684.

(75) Bergbreiter, D. E.; Lynch, T. J. *J. Org. Chem.* **1981**, *46*, 727-733.

(76) Bergbreiter, D. E.; Lynch, T. J.; Shimazu, S. *Organometallics* **1983**, *2*, 1354-1359.

(77) Ramnial, T.; Abernethy, C. D.; Spicer, M. D.; Mckenzie, I. D.; Gay, I. D.; Clyburne, J. A. C. *Inorg. Chem.* **2003**, *42*, 1391-1393.

(78) Frémont, P. de; Scott, N. M.; Stevens, E. D.; Ramnial, T.; Lightbody, O. C.; Macdonald, C. L. B.; Clyburne, J. A. C.; Abernethy, C. D.; Nolan, S. P. *Organometallics* **2005**, *24*, 6301-6309.

(79) Lin, I. J. B.; Vasam, C. S. *Coord. Chem. Rev.* **2007**, *251*, 642-670.

(80) Hintermair, U.; Englert, U.; Leitner, W. *Organometallics* **2011**, *30*, 3726-3731.

(81) Iglesias, M.; Beetstra, D. J.; Knight, J. C.; Ooi, L.-L.; Stasch, A.; Coles, S.; Male, L.; Hursthouse, M. B.; Cavell, K. J.; Dervisi, A.; Fallis, I. A. *Organometallics* **2008**, *27*, 3279-3289.

(82) Kaplan, J. L. *NMR of Chemically Exchanging Systems*; Academic Press: New York, 1980.

(83) Sandstrom, J. *Dynamic NMR Spectroscopy*; Academic Press: London, 1983.

(84) Jackman, L. M.; Cotton, F. A. *Dynamic Nuclear Magnetic Resonance Spectroscopy*; Academic Press: New York, 1975.

(85) Bain, A. D.; Rex, D. M.; Smith, R. N. *Magn. Reson. Chem.* **2001**, *39*, 122-126.

(86) Binsch, G. *J. Am. Chem. Soc.* **1969**, *91*, 1304-1309.

(87) Dumont, R. S.; Hazendonk, P.; Bain, A. *J. Chem. Phys.* **2000**, *113*, 3270-3281.

(88) Szalay, Z.; Rohonczy, J. *J. Magn. Reson.* **2008**, *191*, 56-65.

(89) Siegert, U.; Hahn, H.; Lang, H. *Inorg. Chim. Acta* **2010**, *363*, 944-948.

(90) Reich, H. J. *J. Chem. Educ.* **1995**, *72*, 1086.

(91) Reich, H. J.; Goldenberg, W. S.; Gudmundsson, B. Ö.; Sanders, A. W.; Kulicke, K. J.; Simon, K.; Guzei, I. a *J. Am. Chem. Soc.* **2001**, *123*, 8067-8079.

(92) Kulasekharan, R.; Jayaraj, N.; Porel, M.; Choudhury, R.; Sundaresan, A. K.; Parthasarathy, A.; Ottaviani, M. F.; Jockusch, S.; Turro, N. J.; Ramamurthy, V. *Langmuir* **2010**, *26*, 6943-6953.

(93) Bain, A. D.; Duns, G. J. *Can. J. Chem.* **1996**, *74*, 819-824.

(94) Bain, A. D.; Duns, G. J. *J. Magn. Reson. A* **1995**, *112*, 258-260.

(95) Parr, R. G.; Weitao, Y. *Density-Functional Theory of Atoms and Molecules*; Oxford University Press, NY, 1994.

(96) Gaussian 03, Revision C.02, Frisch, M. J.; Trucks, G. W.; Schlegel, H. B.; Scuseria, G. E.; Robb, M. A.; Cheeseman, J. R.; Montgomery, Jr., J. A.; Vreven, T.; Kudin, K. N.; Burant, J. C.; Millam, J. M.; Iyengar, S. S.; Tomasi, J.; Barone, V.; Mennucci, B., J. A. ; Gaussian, Inc., Wallingford CT, 2004.

(97) Gaussian 09, Revision A.1, Frisch, M. J.; Trucks, G. W.; Schlegel, H. B.; Scuseria, G. E.; Robb, M. A.; Cheeseman, J. R.; Scalmani, G.; Barone, V.; Mennucci, B.; Petersson, G. A.; Nakatsuji, H.; Caricato, M.; Li, X.; Hratchian, H. P.; Izmaylov, A. F.; Blo, D. J. Gaussian, Inc., Wallingford CT, 2009.

(98) Hay, P. J.; Wadt, W. R. *J. Chem. Phys.* **1985**, *82*, 270-283.

(99) Wadt, W. R.; Hay, P. J. *J. Chem. Phys.* **1985**, *82*, 284-298.

(100) Hay, P. J.; Wadt, W. R. *J. Chem. Phys.* **1985**, *82*, 299-310.

(101) Andrae, D.; Häußermann, U.; Dolg, M.; Stoll, H.; Preuß, H. *Theor. Chim. Acta* **1990**, 123-141.

(102) Martin, J. M. L.; Sundermann, A. *J. Chem. Phys.* **2001**, *114*, 3408-3420.

(103) Becke, A. D. *J. Chem. Phys.* **1993**, *98*, 5648-5652.

(104) Lee, C.; Yang, W.; Parr, R. G. *Phys. Rev. B* **1988**, *37*, 785-789.

(105) Adamo, C.; Barone, V. *J. Chem. Phys.* **1998**, *108*, 664-675.

(106) Marenich, A. V.; Cramer, C. J.; Truhlar, D. G. *J. Phys. Chem. B* **2009**, *113*, 6378-6396.

VITA

Name:	Haw-Lih Su
Address:	Department of Chemistry, Texas A&M University P.O. Box 30012, College Station, TX 77842-3012
Email Address:	hawlih@gmail.com
Education:	B.S., Chemistry, National Tsing Hua University, Taiwan, 2000 M.S., Chemistry, National Tsing Hua University, Taiwan, 2002 Ph.D., Chemistry, Texas A&M University, 2011